DISSERTATIONES
NEUROSCIENTIAE
UNIVERSITATIS
TARTUENSIS
40

MARIA PIIRSALU

Effects of inflammation and diet on the metabolic profile and selected genetic parameters of Bl6 and 129Sv mouse lines

DISSERTATIONES NEUROSCIENTIAE UNIVERSITATIS TARTUENSIS
40

DISSERTATIONES NEUROSCIENTIAE UNIVERSITATIS TARTUENSIS
40

MARIA PIIRSALU

Effects of inflammation and diet on the metabolic profile and selected genetic parameters of Bl6 and 129Sv mouse lines

UNIVERSITY OF TARTU
Press

Department of Physiology, Institute of Biomedicine and Translational Medicine, University of Tartu, Tartu, Estonia.

The dissertation was accepted for the commencement of the degree of Doctor of Philosophy in Neurosciences on March 17, 2023, by the council for the Curriculum of Neurosciences.

Supervisors: Eero Vasar, MD, PhD, Professor
Department of Physiology, Institute of Biomedicine and Translational Medicine, University of Tartu, Tartu, Estonia

Kersti Lilleväli, PhD, Associate Professor
Department of Physiology, Institute of Biomedicine and Translational Medicine, University of Tartu, Tartu, Estonia

Mihkel Zilmer, PhD, Professor
Department of Biochemistry, Institute of Biomedicine and Translational Medicine, University of Tartu, Tartu, Estonia

Reviewers: Martti Laan, MD, PhD, Associate Professor
Department of Biomedicine, Institute of Biomedicine and Translational Medicine, University of Tartu, Tartu, Estonia

Monika Jürgenson, PhD, Research Fellow
Department of Pharmacology, Institute of Biomedicine and Translational Medicine, University of Tartu, Tartu, Estonia

Opponent: Marie Agnete Larsen, MD, PhD, Associate Professor
Department of Biomedicine,
University of Aarhus, Aarhus, Denmark

Commencement: April 18th, 2023

This study was supported by research grants IUT20-41 and PRG685 from the Estonian Research Council. This research was also supported by the European Union through the European Regional Development Fund (Project No. 2014-2020.4.01.15-0012).

ISSN 1736-2792 (print)
ISBN 978-9916-27-158-2 (print)
ISSN 2806-2418 (pdf)
ISBN 978-9916-27-159-9 (pdf)

University of Tartu Press
www.tyk.ee

CONTENTS

ABBREVIATIONS

129Sv	129S6/SvEvTac
AAA	aromatic amino acids
ACE	Angiotensin Converting Enzyme 1
Ac-Orn	acetyl-ornithine
ADMA	asymmetric dimethylarginine
Ala	alanine
alpha-AAA	alpha-aminoadipic acid
APC(s)	antigen-presenting cell(s)
AUC	area under the curve
BBB	blood brain barrier
BCAA	branched-chain amino acid
Bl6	C57BL/6NTac
C0	free carnitine
C2	acetylcarnitine
C3	propionylcarnitine
C4-	mixture of butyryl- and isobutyrylcarnitine
C5-	mixture of isovalerylcarnitine and 2-methybutyrylcarnitine
CD11b	cluster of differentiation molecule 11b
CD206	mannose receptor
Cit	citrulline
CNS	central nervous system
CO2	carbon dioxide
CPT-1 ratio	ratio of LCACs to free carnitine
CRT-1 ratio	ratio of SCACs to free carnitine
CVO	circumventricular organ
CX3CR1	CX3C chemokine receptor 1/fractalkine receptor
DIO	diet-induced obesity
Disc1	disrupted-in-schizophrenia-1 gene
ER	endoplasmic reticulum
FIA	flow injection analysis
Fpr3	formyl peptide receptor 3 gene
GLM	general linear model
Gly	glycine
GPL(s)	glycerophospholipid(s)
HFD	high-fat diet
His	histidine
HPLC	high performance liquid chromatography
Ile	isoleucine
LBP	LPS binding protein
LCAC(s)	long-chain acylcarnitine(s)
LC-MS	liquid chromatography techniques
Leu	leucine

Lmp2	immunoproteasome subunit 2
LPS	lipopolysaccharide
lysoPC(s)	lysophosphatidylcholine(s)
MCAC(s)	Medium-chain acylcarnitine(s)
Met	methionine
MFI	mean fluorescence intensity
MHC-II	major histocompatibility complex class II
MHC-I	major histocompatibility complex class I
MUFA(s)	monounsaturated fatty acid(s)
NMDA	N-methyl-D-aspartate
Nnt	nicotinamide nucleotide transhydrogenase gene
OPC	oligodendrocyte progenitor cell
PBS	phosphate-buffered saline
PC(s)	phosphatidylcholine(s)
PC aa	phosphatidylcholine diacyl
PC ae	phosphatidylcholine acyl-alkyl
Phe	Phenylalanine
Pro	proline
PUFA(s)	polyunsaturated fatty acid(s)
ROS	reactive oxygen species
SCAC(s)	short-chain acylcarnitine(s)
SDMA	symmetric dimethylarginine
Ser	serine
SFA	saturated fatty acid
SM(s)	sphingomyelin(s)
T2D	type 2 diabetes
t4-OH-Pro	trans-4-hydroxyproline
Tap1	transporter associated with antigen processing subunit 1
Tap2	transporter associated with antigen processing subunit 2
TapBP	Tapasin
Thr	threonine
TLR4	toll-like receptor 4
Tyr	tyrosine
UFA(s)	unsaturated fatty acid(s)
Val	valine
ΔBT	body temperature change
ΔBW	body weight change
β2m	beta 2 microglobulin

LIST OF ORIGINAL PUBLICATIONS

I. **Piirsalu, Maria**, Egon Taalberg, Kersti Lilleväli, Li Tian, Mihkel Zilmer, and Eero Vasar. 2020. "Treatment With Lipopolysaccharide Induces Distinct Changes in Metabolite Profile and Body Weight in 129Sv and Bl6 Mouse Strains." Frontiers in Pharmacology 11: 371. https://doi.org/10.3389/fphar.2020.00371.

II. **Piirsalu, Maria**, Keerthana Chithanathan, Mohan Jayaram, Tanel Visnapuu, Kersti Lilleväli, Mihkel Zilmer, and Eero Vasar. 2022. "Lipopolysaccharide-Induced Strain-Specific Differences in Neuro-inflammation and MHC-I Pathway Regulation in the Brains of Bl6 and 129Sv Mice." Cells 11 (6): 1032. https://doi.org/10.3390/cells11061032.

III. **Piirsalu, Maria**, Egon Taalberg, Mohan Jayaram, Kersti Lilleväli, Mihkel Zilmer, and Eero Vasar. 2022. "Impact of a High-Fat Diet on the Metabolomics Profile of 129S6 and C57BL6 Mouse Strains." International Journal of Molecular Sciences 23 (19): 11682. https://doi.org/10.3390/ijms231911682.

Author's contribution to the publications:

I. The author participated in designing the study, performed behavioral experiments, carried out statistical analysis, wrote the manuscript and handled the correspondence.

II. The author participated in designing the study, performed behavioral, gene and protein expression experiments, carried out statistical analysis, wrote the manuscript and handled the correspondence.

III. The author participated in designing the study, performed behavioral experiments, carried out statistical analysis, wrote the manuscript and handled the correspondence.

INTRODUCTION

Mice share many physiological and genetic characteristics with humans and have therefore become an unavoidably important component for drug development and for modeling human diseases. A drug candidate or treatment must pass extensive preclinical efficacy and safety testing before it can be approved for human clinical trials. For this reason, inbred mouse strains are essential to medicine and biological research. However, these mice have lost the polymorphisms in their genome due to inbreeding and are homozygous in the vast majority of alleles. The genetic variation between different strains of mice means that they differ significantly at the molecular and cellular levels. These differences in turn result in a specific behavioral phenotype for each strain. It is therefore crucial to gain new insight about strain-specific variations since genetic differences among strains frequently lead to differential responses in models of human diseases. New knowledge will help scientists better understand how to choose the best suited model for a particular scientific question, which is essential for efficient data interpretation.

In this dissertation, I will compare mice from two inbred genetic backgrounds: C57BL/6NTac (Bl6) and 129S6/SvEvTac (129Sv). These mice are among one of the most widely utilized mouse strains in biomedical and transgenic research and are the gold standard for creating transgenic mouse models. From previous research we know that Bl6 mice actively cope with stressful situations, whereas the responding strategy of the 129Sv line is inherently passive.

In our study, we aimed to explore the possible differences of these strains in coping with endotoxemia and dietary influences. First, we demonstrate that systemic administration of lipopolysaccharide (LPS), the activator of innate immune response, causes a stronger hypometabolic state in the Bl6 strain but enhances the production of proinflammatory metabolites in 129Sv mice. We demonstrate that LPS administration leads to changes in polyamine metabolism in Bl6 mice but not in 129Sv mice. More precisely, LPS increases the biosynthesis of putrescine in Bl6 mice, which has been shown to possess neuroprotective activity in the central nervous system (CNS). This led us next to further investigate the possible different outcomes of LPS-induced inflammatory response in the CNS of Bl6 and 129Sv mice. We demonstrate that microglia of 129Sv mice have increased inflammatory status in response to activation by LPS, not seen in Bl6 mice. However, we did see that under baseline conditions, microglia of Bl6 mice seem to be in a higher immune-alert state. Gene and protein expression analysis revealed that LPS administration induced a significantly stronger upregulation of MHC-I-pathway related components in the brain of Bl6 compared to 129Sv mice. Additionally, correlation analysis highlighted the olfactory bulb region of Bl6 mice and the frontal cortex of 129Sv mice as brain regions most affected by LPS in these strains. Based on these results, we hypothesize that the brain of Bl6 mice, particularly the

olfactory bulb region, exists in a more immunocompetent state compared to that of 129Sv mice. Since several studies have indicated that consumption of high-fat foods may induce systemic inflammation, we finally aimed to investigate the impact of genetic background on the metabolic response to high-fat diet (HFD) in these strains. We found that 9 weeks of HFD induced a significant body weight gain in 129Sv, but not in Bl6 mice. Besides that, 129Sv mice displayed anxiety-like behavior in the open field test. Metabolite profiling revealed that 129Sv mice had higher levels of circulating branched-chain amino acids (BCAA-s), which were even more amplified by HFD. HFD also induced a decrease in glycine, spermidine, and t4-OH-proline levels in 129Sv mice. Although acylcarnitines dominated in baseline conditions in the 129Sv strain, this strain experienced significantly stronger acylcarnitine-reducing effects of HFD. Moreover, 129Sv mice had higher levels of lipids in baseline conditions, but HFD caused more pronounced alterations in lipid profile in Bl6 mice. Thus, our results indicate that the Bl6 line is better adapted to abundant fat intake.

This thesis has provided a deeper insight into the coping strategies of the Bl6 and 129Sv mouse lines, which should be considered when designing and interpreting studies with mouse models, especially immunological studies. Our work adds to the growing body of research showing that Bl6 and 129Sv mice display vastly distinct adaptation capacities, regardless of the nature of stressful challenges.

REVIEW OF THE LITERATURE

1. Bl6 and 129Sv inbred mouse strains

An inbred mouse strain is a result of at least 20 consecutive generations of brother-sister matings and as a result, these mice are essentially genetic clones of one another. With the use of the same inbred strain, genetic variability can be removed as a confounding factor. Most studies with transgenic mouse models use inbred mouse strains, of which the two most common are Bl6 and 129Sv. The standard approach for generating transgenic mouse models combines these two strains. Typically, genetically modified mice are created using embryonic stem cells from 129Sv mouse substrains, whereas Bl6 is the most widely used background strain in biomedical research (Hedrich 2004; Yoshiki & Moriwaki 2006). The growing popularity of Bl6 mice as a preclinical model may affect the validity and translatability of many scientific findings. The simultaneous use of 129Sv, neglected in many cases, helps to overcome the obstacles inherent in the use of only the Bl6 strain. For translational research, it is critical that animal models are accurately characterized and validated as models of human disease. Although there does not exist an ideal biological model for heterogeneous disorders, it is evident from the literature that some mouse strains are more suitable than others for studying particular behavioral characteristics associated with pathophysiology (Crawley et al., 1997). In mice, and especially in genetically modified models, special considerations must be made because these modifications are influenced by the genetics of the background strain, husbandry, and experimental conditions. Thus, it is very important to understand the translational value of these different mouse lines and to find out for which studies of human pathology one or the other line may be appropriate for. In general, it is advisable to compare at least two mouse strains to determine the effects of genetic background (Silva et al., 1997). In the experimental population, mixing the genetic background may also result in controlled genetic variation more similar to the highly heterogeneous human population.

Bl6 and 129Sv mouse strains differ significantly from one another in a number of ways. It is well-established that Bl6 mice have greater locomotor activity and increased exploratory behavior, whereas 129Sv mice display reduced locomotor and exploratory activity as well as increased anxiety-like behavior (Võikar et al., 2001; Abramov et al., 2008; Heinla et al., 2014). Previous research has shown that Bl6 mice have an active coping strategy (attempting to escape stressors) when faced with stressful situations, in contrast to the more passive coping strategy (helplessness to deal with stressors) of the 129Sv strain, which is even more amplified in environmental enrichment conditions (Abramov et al., 2008; Heinla et al., 2014; Varul et al., 2021). Besides that, there are numerous other physiological and behavioral differences between 129Sv and Bl6. Bl6 mice are more aggressive, exhibit significant preference for alcohol and demonstrate extensive barbering behavior (Belknap et al., 1993; Middaugh et al., 1999; Sarna et al., 2000; Heinla et al., 2014). When compared to Bl6

mice, the 129Sv strain's pain sensitivity is significantly reduced (Võikar et al., 2004; Abramov et al., 2008). While the exposure of mice to cat odor induces anxiety-like responses in Bl6 mice, it does not stimulate such responses in the 129Sv strain (Raud et al., 2007). They also exhibit different reactions to amphetamine administration: when compared to 129Sv, acute treatment with amphetamine causes stronger motor stimulation in Bl6 mice, which is accompanied with the augmented dopamine efflux in the striatum (Chen et al 2007). One of the major reasons 129Sv and Bl6 mice differ in their basal dopamine system activity, is the frameshift mutation in the disrupted-in-schizophrenia-1 (*Disc1*) gene in 129Sv mice, which causes alterations in dopamine homeostasis and affects cognitive abilities (Mukaida et al., 1996; Koike et al., 2006; Trossbach et al., 2016).

Bl6 and 129Sv are also widely used in immunological studies. Several studies have demonstrated that they show different immune responses and have different susceptibility to infectious diseases. For instance, 129Sv mice infected with the influenza virus exhibit hyper-induction of proinflammatory cytokines and mice tend to die from infection. On the other hand, the proinflammatory cytokine response in the Bl6 strain is mild, and mice manage to cope effectively with the infection (Davidson et al., 2014).

Previous studies, including our own, seem to suggest that 129Sv mice are a more appropriate model for studying anxiety-, depressive-, and psychosis-like conditions. Nevertheless, translating preclinical findings from mice to psychiatric disorders in humans is a difficult task. Although no mouse can ever fully model all aspects of complex, heterogeneous psychiatric disorders, they are inevitably an important component in characterizing various aspects of these disorders. Many psychiatric disorders are associated with behavioral and cognitive endophenotypes that can be modeled and studied in mice (Seong et al., 2002). It is known that some strains of mice are more suitable than others for studying specific behavioral traits associated with psychiatric disorders. Inflammation, along with metabolic syndrome, is a common feature of psychiatric disorders and antipsychotic medication use. With this in mind, the aim of our study was to increase knowledge about the coping strategies of Bl6 and 129Sv mice, focusing on two inflammatory triggers – bacterial lipopolysaccharide and high-fat diet.

2. Inflammation and bacterial lipopolysaccharide

Inflammation-induced animal models are essential for developing new therapeutic treatments and testing potential drug candidates that target inflammation. However, they are also useful for studying the inflammatory mechanisms of various CNS diseases such as Alzheimer's, Parkinson's, Huntington's, and amyotrophic lateral sclerosis, as well as psychiatric disorders such as depression and schizophrenia, where chronic inflammation plays a key role in pathophysiology of the disease (Batista et al., 2019; Feng et al., 2020).

Due to genetic mutations and polymorphisms, different inbred mouse strains differ greatly in their immune responses. As previously mentioned, recent work has demonstrated that 129Sv are more vulnerable to influenza and infected mice have increased lung damage, morbidity and mortality compared to Bl6 mice (Davidson et al., 2014). Susceptibility to herpes simplex virus type 1 also varies between mouse strain: 129Sv mice are more susceptible to the herpes virus, whereas Bl6 mice seem to be resistant (Cantin et al. 1999; Lundberg et al. 2003). In addition, 129Sv mice carry a nonfunctional formyl peptide receptor 3 (*Fpr3*) gene variant that belongs to the group of genes that are upregulated in immune cells after LPS exposure and thus likely contribute to immune defense against bacteria (Stempel et al. 2016). Immune responses even differ between Bl6 substrains. Compared with the C57BL/6N substrain, C57BL/6J mice are more susceptible to certain bacterial infections and exhibit deficient neutrophil recruitment to sites of inflammation, which has been linked to a missense mutation in *Nlrp12* in C57BL/6J mice (Ulland et al. 2016).

The induction of inflammation can be achieved in several ways, and LPS has become an important tool for this purpose. LPS is a major component of the outer membrane of Gram-negative bacteria and serves as an early warning signal of bacterial infection. As an endotoxin, it is a potent innate immune activator that is recognized by toll-like receptor 4 (TLR4). In case of infection, LPS is extracted from bacterial membranes and bound to LPS binding protein (LBP), which transfers LPS to TLR4 by interacting with CD14. The interaction between LPS and TLR4 leads to the activation of several signaling components, including NF-κB and IRF3, and the production of proinflammatory cytokines (Chow et al., 1999; Raetz and Whitfield, 2002; Park and Lee, 2013).

Peripheral LPS administration has been widely used in immunological studies to stimulate innate immunity and activate neuroimmune and neuroendocrine systems. Systemic administration of LPS triggers inflammatory processes that have a negative impact on the brain and result in sickness and depressive-like behavior in rodents. Low doses of LPS induces neuroinflammation without penetrating the blood brain barrier (BBB) and most effects of peripherally administered LPS are mediated through LPS receptors located outside the brain (Banks et al., 2015). Thus, LPS can activate neuroimmune pathways and processes without triggering or depending on BBB disruption. However, it is possible that LPS enters the CNS by bypassing this barrier at sites with a weaker BBB, such as the circumventricular organs (CVOs) (Rivest, 2003). Nonetheless, it is commonly accepted that peripherally administered LPS first activates cells in the liver to produce TNFα, which distributes in the blood and enters the brain via TNFα receptors, where it stimulates the synthesis of additional TNFα and initiates a cascade of cytokines to induce activation of glia (mainly microglia) in the brain, leading to neuroinflammation (Qin et al., 2007).

Activation of microglia is a pathophysiological hallmark of CNS disorders. Microglia are the brain's resident immune cells that regularly scan their residing microenvironment and act as the first line of defense against pathogens or injury in the CNS. Upon activation, microglia regulate the expression of several

molecules, including major histocompatibility complex class II (MHC-II), CX3C chemokine receptor 1 (CX3CR1), cluster of differentiation molecule 11b (CD11b) and mannose receptor (CD206), all of which are investigated in this study. In addition, previous studies have demonstrated that LPS-activated microglia mediate oligodendrocyte progenitor cell (OPC) death (Pang et al., 2010), with that in mind, we also investigated the effect of LPS administration on OPCs.

3. High-fat diet

Inflammation has also been linked to the development of metabolic disorders such as type 2 diabetes (T2D), fatty liver disease, and cardiovascular disease. A high-fat diet (HFD) is commonly used in rodents to study the effects of dietary changes on the onset and progression of insulin resistance and obesity. It is well known that a long-term feeding of HFD is associated with low-grade systemic inflammation induced by reactive oxygen species (Hotamisligil, 2006). HFD recruits macrophages to adipose tissue and induces the expression of proinflammatory cytokines including TNF-α, IL-1, and IL-6 (Kanda et al., 2006). In the case of psychiatric disorders such as schizophrenia spectrum disorders, major depressive disorder, and bipolar disorder, the development of obesity and metabolic syndrome in patients occurs in parallel with the development of the disease, reducing the effectiveness of treatment and complicating the further course of the disease.

Animal models of diet-induced obesity (DIO) have become very useful to analyze the etiology of obesity *in vivo*. However, the phenotypes of DIO mice are known to vary, and many factors can influence the development of obesity, including specific environment, experimental setup, diet (caloric value, composition, fat source), and animals involved (age, sex, strain). The genetic background of mice is one of the most important factors that influences susceptibility to DIO. Different strains of mice have been shown to have different susceptibility to HFD-induced obesity, glucose intolerance, and insulin resistance. For example, BALB/c mice have been shown to exhibit some protection against these detrimental effects (Montgomery et al., 2013). The response to HFD may even differ between different substrains. For example, among the various genetic differences identified between the C57BL/6J and C57BL/6N substrains, deletion of the nicotinamide nucleotide transhydrogenase (*Nnt*) gene has been the subject of numerous studies. Nnt is a mitochondrial enzyme that regulates mitochondrial NADPH levels and redox balance and is thought to be one of the reasons that C57BL/6J mice develop glucose intolerance and impaired insulin secretion under HFD (Attané et al., 2016). In the context of diet-induced non-alcoholic/alcoholic fatty liver disease, 129Sv mice have been shown to have a higher susceptibility to developing a disease-like phenotype compared to Bl6 mice (Fengler et al. 2016).

4. Targeted metabolomics approach

Metabolomics is a rapidly growing field of life sciences that has recently found wide application in many different areas, including molecular epidemiology, biomarker discovery and identification, drug development, and personalized healthcare. Metabolomics aims to identify and quantify the totality of small (< 1500 Da) molecule intermediates and products of metabolism in biofluids, tissues and cellular extracts.

In this work, we used a targeted metabolomics approach. Targeted metabolomics deals with specific classes of metabolites such as amino acids, peptides, organic acids, lipids, nucleotides, etc. and allows their absolute and precise quantification. We chose the targeted metabolomics approach in our work because characterization of the metabolic changes that occur is key to understanding the differences in the molecular mechanisms underlying the metabolic disturbances caused by immunological and dietary interventions in Bl6 and 129Sv mouse lines. The applied targeted analysis with the AbsoluteIDQ p180 kit allows for the identification of 186 metabolites in 5 compound classes: acylcarnitines, amino acids, biogenic amines, hexoses, and phospho- and sphingolipids.

4.1. Acylcarnitines

Acylcarnitines are biological intermediates that play an important role in energy production. They are essential for oxidative catabolism of long-chain fatty acids by transporting them across the mitochondrial membrane from the cytosol into the mitochondrial matrix for β-oxidation and energy production. Several studies have reported alterations of acylcarnitine profile in pathological conditions including T2D (Adams et al., 2009), cardiovascular diseases (Makrecka-Kuka et al., 2017), and first episode psychosis (Kriisa et al., 2017). A recent study showed that 129Sv mice have significantly higher blood plasma levels of short-chain acylcarnitines (SCACs) C4- and C5- compared to Bl6 mice (Narvik et al., 2018). Acylcarnitine C5- in mouse blood is a mixture of isovalerylcarnitine and 2-methylbutyrylcarnitine and elevated C5- levels in 129Sv mice are due to the accumulation of isovalerylcarnitine. This is caused by a splice site mutation in the *lvd* gene that results in a deficiency of isovaleryl-CoA dehydrogenase (Leandro et al., 2019).

4.2. Amino acids and their derivatives biogenic amines

Amino acids and biogenic amines are involved in a wide range of biochemical processes and pathways. They are building blocks for proteins and precursors for a variety of fundamental cellular biochemical reactions ranging from the synthesis of purines, pyrimidines, nucleotides and urea to the formation of metabolites of the citric acid cycle. Branched-chain amino acids (BCAAs) and alpha-aminoadipic acid (alpha-AAA) are potential modulators of glucose homeostasis and are elevated in individuals with metabolic syndrome (Wang et

al., 2011; Wang et al., 2013; McCormack et al., 2013). Recently, however, alpha-AAA has been found to have protective properties against obesity and T2D (Xu et al., 2019). BCAAs are associated with the synthesis of fatty acids and thus with insulin resistance and T2D. In obese and diabetic individuals, plasma BCAA levels correlate directly with insulin levels. Elevated levels of the amino acids taurine and glycine have also been shown to be a risk indicator for the development of T2D (Merino et al., 2018). In addition, taurine is also part of the biomarker signature of first episode psychosis (Koido et al., 2016). Recently, it was shown that the levels of biogenic amines acetyl-ornithine (Ac-Orn), alpha-AAA, and carnosine were significantly higher in Bl6 compared to 129Sv mice (Narvik et al., 2018). Alpha-AAA is a component of the lysine metabolic pathway and a marker of oxidative stress (Yuan et al., 2011; Zeitoun-Ghandour et al., 2011). Studies in rodents have shown that alpha-AAA inhibits the synthesis of kynurenic acid, which is a neuroactive metabolite and antagonist of glutamatergic N-methyl-D-aspartate (NMDA) and AMPA/kainate and alpha-7 nicotinic receptors (Tuboly et al., 2015). Higher levels of alpha-AAA in Bl6 mice have been shown to be the result of a defect in the *Dhtkd1* gene, which has been identified as a primary regulator of alpha-AAA, and defects in this gene lead to accumulation of alpha-AAA (Wu et al., 1995; Leandro et al., 2019). Carnosine is a dipeptide (beta-alanyl-L-histidine) that is abundant in excitable tissues such as muscle and brain, can scavenge free radicals, and has neuroprotective properties (Klebanov et al., 1998; Bae et al., 2013).

4.3. Phospholipids

Lipids are an important source and store of energy for metabolism. Phospholipids comprise two main categories: glycerophospholipids (GPLs) and sphingolipids (sphingomyelins, SMs). Prominent members of the GPL family are phosphatidylcholines (PCs), which are the main precursors of lysophosphatidylcholines (lysoPCs). LysoPCs are formed when one of the fatty acyl groups in PCs is removed by phospholipase. GPLs and SMs are components of membrane bilayers that form a physical barrier against pathogens as a first line of defense and contain cell surface receptors such as Toll-like receptor 4 (TLR 4), which plays a key role in LPS-mediated signal transduction. Thus, PCs are involved in the early stages of the inflammatory cascade. LysoPCs play a role in modulating the immune response through immune cell activation and transport. These functions have been linked to inflammatory diseases such as diabetes, obesity, atherosclerosis, cancer, and rheumatoid arthritis (Cas et al., 2020). Recent evidence suggests that several GPLs and SMs are also potential biomarkers for cardiovascular disease (Paapstel et al., 2018) and first episode psychosis (Leppik et al., 2019).

4.4. Hexoses

Targeted metabolomics analysis with the AbsoluteIDQ p180 kit does not distinguish between hexoses and measures the sum of all hexoses present in a sample, which is 90-95% glucose. Impaired glucose uptake is a hallmark of T2D and metabolic syndrome and is characterized by insulin deficiency or resistance to its action.

5. Concluding remarks

Previous studies have shown that considerable metabolic heterogeneity exists between Bl6 and 129Sv mouse strains. Metabolites C4-, C5-, and SM (OH) C22:2 are significantly higher in 129Sv mice, whereas carnosine, alpha-AAA, Ac-Orn, and LysoPC a C16:1 are part of the metabolic signature of Bl6 mice (Narvik et al., 2018). Two metabolites that clearly stand out are carnosine and alpha-AAA. Carnosine has antioxidant properties and has been shown to act as a scavenger of reactive oxygen species (ROS), sugars, polyunsaturated fatty acids (PUFAs), and proteins (Guiotto et al., 2005; Dawson et al., 2002; Rajanikant et al., 2007). Alpha-AAA has been found to have protective properties against obesity and T2D (Xu et al., 2019). In addition, 129Sv strains carry a 25-base pair frameshift deletion within exon 6 of the *Disc1* gene, resulting in misassembly of the full-length protein. Both human studies and animal models suggest that the *Disc1* gene is a strong susceptibility factor for mental illness, possibly related to dopamine impairment. Inflammation is known to play an important role in the development and maintenance of various psychiatric disorders. In addition, patients with mental illnesses have an increased prevalence of metabolic syndrome.

With this in mind, we aimed to investigate the coping mechanisms of Bl6 and 129Sv mice, with particular emphasis on inflammation and the development of metabolic syndrome. To investigate the possible differences in coping with inflammation, we first administered mice LPS, the activator of the innate immune response. We examined the effect of LPS on locomotor activity, body temperature and weight, metabolic profile, and neuroinflammation parameters. Second, we aimed to investigate the influence of genetic background on the metabolic response to HFD in these strains. We examined the effects of a 9-week HFD on locomotor activity, body weight, and metabolomics profile.

Considering the above differences, we hypothesize that Bl6 mice may be partially protected from the detrimental effects of LPS and HFD, whereas 129Sv might exhibit stronger response to LPS and HFD.

AIMS OF THE STUDY

The general aim of this dissertation was to provide a deeper insight into the coping strategies of two common inbred mouse strains: Bl6 and 129Sv, focusing on two inflammatory triggers – LPS and HFD.

Specific aims of present dissertation were:

1. To characterize behavioral and metabolic profiles of Bl6 and 129Sv mice after acute systemic administration of LPS.
2. To investigate microglia activation and overall severity of neuroinflammation in Bl6 and 129Sv mice in response to acute systemic LPS administration.
3. To investigate the body weight change, behavior, and metabolic profile in Bl6 and 129Sv strains in response to HFD.

MATERIAL AND METHODS

In this thesis, *in vivo* experiments were performed with laboratory animals. A series of tests were performed to evaluate the effects of peripheral LPS administration and diet on different variables. This involved different techniques including measurement of locomotor activity in phenotyper cages, targeted metabolomics assay, gene and protein expression analyses, and flow cytometric analyses (Figure 1).

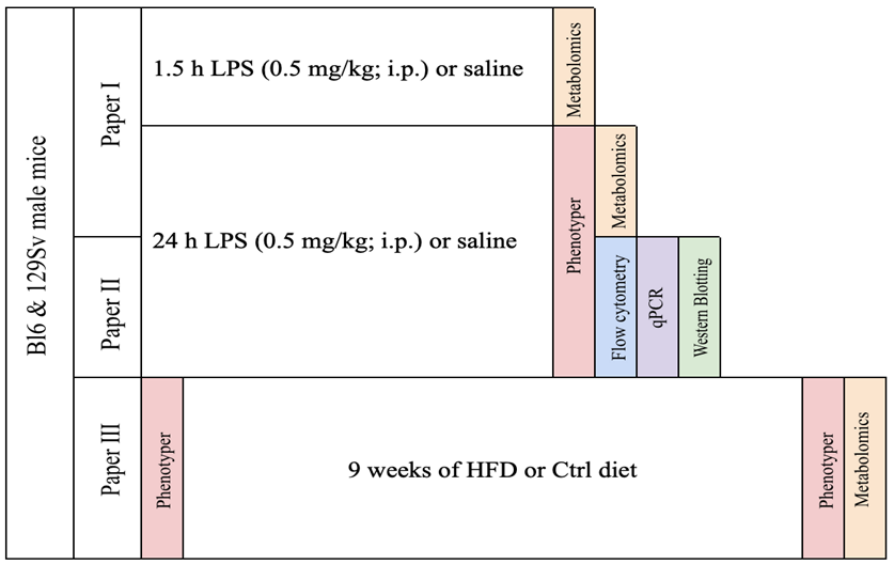

Figure 1. Scheme of treatments and techniques used in publications.

1. Mice (Paper I, II, III)

In papers I, II and III male mice (4-5-month-old) from two inbred strains: C57BL/6NTac and 129S6/SvEvTac were used. The number of animals used in experiments varied in the papers (paper I: Bl6 n = 56 and 129Sv n = 56; paper II: Bl6 n = 58 and 129Sv n = 58; paper III: Bl6 n = 28 and 129Sv n = 30).

All mice were maintained in a conventional animal facility in the Laboratory Animal Center at University of Tartu at constant ambient temperature of 22± 2°C, with 45-65% humidity and a 12h light-dark cycle (lights off at 19:00). All mice received a standard chow diet (V1534-300 rat/mice universal maintenance diet; Ssniff Spezialiäten GmbH, Soest, Germany) and water *ad libitum* until further dietary interventions or death. All animal experiments were performed upon approval of the European Communities Directive (2010/63/EU) with permit (No. 141, 17 April 2019) from the Estonian National Board of Animal Experiments.

2. LPS treatment (Paper I, II)

LPS (derived from E. coli serotype 0111:B4; Sigma-Aldrich, St. Louis, MO, USA) was dissolved in 0.9% NaCl (saline). Mice were randomly assigned to receive one intraperitoneal (i.p.) injection of 0.5 mg/kg LPS or 0.9% NaCl (saline). The LPS dose was chosen based on the results of a pilot study, aimed at finding the lowest dose sufficient to elicit behavioral effects without being lethal to the animals. Mice from each strain were divided into two subgroups comprising 1.5 (paper I) and 24-hour (paper I and II) LPS treatment time points. These timepoints were chosen based on the literature showing that 1.5 h after LPS administration, the expression of several inflammatory cytokines is increased (e.g., TNFα, IL-1β, IL-6, etc.), which then rapidly decrease and reach baseline levels after 24 h (Lalić et al., 2018). 24 h after LPS administration, the expression of important cytokines (e.g., CXCL9) increases and microglial activation occurs (Lalić et al., 2018; Catorce et al., 2016).

3. Mouse diets (Paper III)

In paper III mice were fed either standard chow diet (V1534-300 rat/mice universal maintenance diet; Ssniff Spezialiäten GmbH, Soest, Germany) or high-fat diet (HFD) chow (D12451, 45 kJ% fat (lard); Ssniff Spezialiäten GmbH, Soest, Germany) for 9 weeks. Diet compositions are shown in Table 1. Diet and duration were chosen based on the experiments previously carried out in our laboratory (Kaare et al., 2021).

Table 1. Composition of the standard chow and HFD.

	Control Diet (3.230 kcal/kg)	**High-Fat Diet (4.615 kcal/kg)**
Fat (kJ%)	9	45
Protein (kJ%)	24	20
Carbohydrate (kJ%)	67	35
Crude Nutrients [%]		
Crude protein (N × 6.25)	19.0	22.0
Crude fat	3.3	23.6
Crude fiber	4.9	5.7
Crude ash	6.4	5.3
Starch	35.2	6.8
Sugar	5.3	21.1
N free extracts	54.2	40.0

Food and water intake were recorded weekly during the 9-week study period. Food and water consumption were measured by subtracting the mass (g) or volume (ml) of remaining food and water from the initial food and water mass or volume provided to each cage weekly. For analysis, food and water consumption data were corrected for the number of animals per cage.

4. Measurement of body weight and temperature (Papers I, II, III)

In papers I and II, body weight was measured before and 24 hours after injection of LPS and saline. In paper III, all mice were weighed weekly starting from the first day of dietary intervention and body weight was tracked for 9 weeks throughout the study period. In addition, at the end of the dietary intervention at week 9, the body weight of Bl6 and 129Sv mice was measured before and after the phenotyper experiment.

Body temperature was determined in the LPS studies in papers I and II. Baseline temperature was measured with a rectal thermometer (TSE Technical and Scientific Equipment GmbH, Berlin, Germany) before administration of LPS or saline. At 1.5 h and 24 h after the administration of LPS and saline, the measurement of body temperature was repeated.

5. Locomotor activity in phenotyper cages (Papers I, II, III)

The locomotor activity of mice was monitored in PhenoTyper® (EthoVision 3.0, Noldus Information Technology, Wageningen, The Netherlands) cages. One phenotyper trial comprised a 24-h period during which mice were individually housed in 30 cm × 30 cm × 35 cm plexiglass cages with sawdust bedding, similar to home cage. Mice had free access to food and water throughout the experimental period and were maintained on a 12:12 h light-dark cycle. In papers I and II, mice were placed in the phenotyper cages immediately after LPS administration and observed for 24 hours. In paper III, phenotyper tests were performed at week 1 (on the first day of the dietary intervention) and week 9 (at the end of the dietary intervention). Animal movements were continuously recorded with a video tracking system. Each cage was equipped with a top unit with an integrated infrared-sensitive camera and infrared LED lights to allow tracking in the dark phase. In papers I, II and III the open-field arena was virtually divided into central and peripheral zones, with the central zone defined as half of the total area. In paper III, the food and water zone was additionally included. The total distance traveled and the time spent in the center and in the food and water zone were measured.

6. Metabolomic studies (Papers I, III)

In paper I, the measurement of metabolites was performed with a separate group of animals than the experimental group for locomotor activity, and the mice were taken directly from their home cages. In paper III, we performed the metabolomic study with the same group of animals that had previously been subjected to the phenotyper tests.

6.1. Sample collection

Mice were euthanized by decapitation, and trunk blood was collected into EDTA-coated microcentrifuge tubes and stored on ice. All tubes were centrifuged at 2000× *g* for 15 min at 4 °C. Plasma supernatant was separated and stored at −80 °C until further analysis.

6.2. Measurement of metabolites

The AbsoluteIDQ™ p180 kit (BIOCRATES Life Sciences AG, Innsbruck, Austria) was used to determine plasma levels of 186 different compounds. Samples were measured using QTRAP 4500 mass spectrometry (Sciex, Framingham, MA, USA) in combination with high performance liquid chromatography (HPLC) (Agilent 1260 series, Agilent Technologies, Waldbronn, Germany). The first step of sample preparation was performed on the AbsoluteIDQ kit plate included in the test kit with 96 wells for holding the zero sample, three samples of phosphate-buffered saline (PBS), seven calibration standards, and at least three quality controls. Plasma samples were thawed and centrifuged at 4°C for 5 minutes at 2,750 × g. To all wells, except the well in position A1, 10 µl of the internal standard mixture was added. Then, 10 µl of the calibration standards, PBS, quality controls, and plasma samples were added to each well. To each well, 50 µl of a 5% solution of phenyl isothiocyanate in pyridine/ethanol/water (1:1:1, v/v/v) was added for amino acid derivatization.

After 20 min of incubation, the plate was dried at room temperature under dry air flow and all compounds were extracted into solution with 300 µl of 5 mM ammonium acetate in methanol. After 30 min of shaking, the plate was centrifuged and the extract was filtered through a filter membrane into the 96-well capture plate below. From the capture plate, 50 µl of the solution was transferred to another 96-well plate and diluted with 250 µl of 40% (v/v) methanol in water for liquid chromatography techniques (LC-MS). For flow injection analysis (FIA), 20 µl of the solution was transferred to another 96-well plate and diluted with 380 µl of FIA mobile phase solvent prepared by diluting Biocrates Solvent I supplied with the kit in 290 ml of HPLC methanol.

Amino acids and biogenic amines in the samples were measured using the LC-MS techniques. Acylcarnitines (Cx:y), hexoses, sphingolipids [SMx:y or SM (OH)x:y], glycerophospholipids [lysophosphatidylcholines (lysoPCx:y) and phosphatidylcholines (PCaa x:y and PC ae x:y)] were measured by FIA tandem mass spectrometry. Multiple reaction monitoring was used for both analytical

methods. Concentrations of metabolites were automatically calculated in μM by MetIDQ™ software (BIOCRATES Life Sciences AG).

7. Gene and protein expression analysis in mouse brain areas (Paper II)

7.1. Gene expression of MHC-I-related genes by RT-qPCR (Paper II)

24 h after LPS administration, mice were euthanized by decapitation, brains were removed, and the olfactory bulbs, prefrontal cortex, hypothalamus, hippocampus, midbrain, and cerebellum were dissected. Total RNA from aforementioned brain regions was extracted using Trizol® reagent (Invitrogen, Waltham, MA, USA) according to the manufacturer's protocol. RNA was reverse transcribed (2 μg) using random hexamers (Applied Biosystems, Foster City, CA, USA) and SuperScript™ III Reverse Transcriptase (Invitrogen, USA). Real-time qPCR was performed using 5x HOT FIREPol® EvaGreen® qPCR Supermix (Solis BioDyne, Tartu, Estonia) and corresponding primers (TAG Copenhagen, Copenhagen, Denmark; Table 2) on a QuantStudio 12 K Flex Real-Time PCR Detection System (Applied Biosystems, USA) according to the manufacturer's instructions.

Table 2. List of DNA primer sequences used in RT-qPCR gene expression analysis.

Gene		Sequence (5'-3')	Product length (bp)
Hprt	Forward Reverse	5'-GCAGTACAGCCCCAAAATGG-3' 5'-AACAAAGTCTGGCCTGTATCCAA-3'	85 bp
β2m	Forward Reverse	5'-TGGTCTTTCTGGTGCTTGTC-3' 5'-TATGTTCGGCTTCCCATTCTCC-3'	107 bp
Tap1	Forward Reverse	5'-CTTGGATGATGCCACCAGTG-3' 5'-AGAAGAACCGTCCGAGAAGC-3'	99 bp
Tap2	Forward Reverse	5'-GCGCCATCTTTTTCATGTGC-3' 5′-AAGGTCTTGGCGCAACAAAG-3'	143 bp
Lmp2	Forward Reverse	5'-ATGGGAGGGATGCTAATTCGAC-3' 5'-ATGGCATCTGTGGTGAAACG-3'	134 bp
Tapbp	Forward Reverse	5'-CAGCTACCTCCAGTCACTGC-3' 5'-GCCCTGAGAAGCCTGCCA-3'	124 bp
Ace	Forward Reverse	5'-TCGCTACAACTTCGACTGGT-3' 5'-GAACTGGAACTGCAGCACAA-3'	163 bp

7.2. Protein extraction and Western blot analysis (Paper II)

Total protein fraction was extracted from hippocampus and olfactory bulb. Samples were sonicated in ice-cold RIPA lysis buffer (Thermo Scientific, Waltham, MA, USA) containing 1× protease inhibitor (78430, Thermo Scientific) and centrifuged at 14,000× *g* for 10 min at 4 °C. Protein concentrations were determined using the BCA protein assay kit (23225, Thermo Scientific). Equal amounts of protein (20 µg) from each sample were separated on a NuPAGE Bis–Tris gel using the XCELL SureLock System (Invitrogen, USA). The protein was then transferred to a nitrocellulose membrane and the membranes were blocked and incubated overnight at 4 °C with primary antibodies (Table 3). Immunoblots were then incubated with goat anti-rabbit (A11369, Invitrogen, USA) or goat anti-mouse (A-21057, Invitrogen, USA) fluorescent conjugated secondary antibodies for 1 h at room temperature, followed by visualization with LI-COR Odyssey CLx system (LI-COR Biotechnologies, Lincoln, NE, USA). B-actin was used as a loading control.

Table 3. List of antibodies used for Western blotting.

Protein	Host	Dilution	Company	Catalog No
Beta 2 microglobulin (β2m)	Rabbit	1:10000	Abcam	ab75853
Tapasin (TapBP)	Rabbit	1:1000	Abcam	ab196764
Angiotensin Converting Enzyme 1 (ACE)	Rabbit	1:10000	Abcam	ab254222
B-actin	Mouse	1:10000	Santa Cruz Biotechnology	sc-47778

8. Flow Cytometry (Paper II)

After 24 hours of LPS/saline exposure, mice were euthanized by an overdose of carbon dioxide (CO_2), after which the hippocampus and cerebellum were dissected. The dissected brain regions were carefully homogenized in FC buffer (ice-cold PBS + 1% fetal calf serum) through 70 µm cell strainers (BD Falcon). Isolated cells were blocked with 10% rat serum in ice-cold PBS for 1 h. Brain cells were stained with 0.5 µL anti-mouse CD11b-BV421 (#101251, BioLegend, San Diego, CA, USA), CD45-BV650 (#103151, BioLegend, San Diego, CA, USA), O4- PE (#130-117-357, Miltenyi Biotec, Bergisch Gladbach, Germany), CX3CR1-A488 (#149021, BioLegend San Diego, CA, USA) for 1 h at 4 °C. Cells were washed and resuspended in 0.5 mL PBS. Samples were acquired with a 5-laser LSR Fortessa (BD Biosciences, San Jose, CA, USA) cytometer and analyzed using Kaluza v1.2 software (Beckman Coulter, Indianapolis, IN, USA).

9. Statistical analysis

Results are given as mean values ± SD in paper I and as mean values ± SEM in papers II and III. Statistical analyzes were performed using GraphPad Prism 8 and 9 software (GraphPad, San Diego, CA, USA) and TIBCO StatisticaTM version 13.3.0. The Shapiro-Wilk test was applied to assess the normality of the data distribution. To normalize the distribution of locomotor and metabolic data, the values were log transformed before data analysis (log_{10} in paper I and II; log_2 in paper III). In papers I and II, decreases in body weight (ΔBW) and temperature (ΔBT) are expressed as a change of the initial weight and temperature, respectively (ΔBW = [final weight – initial weight]/initial weight (x 100%); ΔBT = [final temperature – initial temperature]/ initial temperature (x 100%)). Statistical significance was determined by using two-way ANOVA (strain × treatment or strain × diet) or repeated-measures ANOVA (time × treatment or time × diet) followed by Bonferroni post hoc test. All differences were considered statistically significant at $p \leq 0.05$. In addition, general linear model (GLM) analysis with backward elimination was performed in papers I and III to analyze the metabolomics data. For this, unpaired t-tests and Bonferroni correction for multiple testing were used (in paper I: $p \leq 0.0002$; in paper III: $p \leq 0.00027$). Significant markers that exceeded the Bonferroni threshold were included in the GLM analysis. Association analyses were performed using Pearson correlation.

10. Ethics

All animal experiments were performed in accordance with the European Communities Directive (2010/63/EU) and with the approval (No. 141, April 17, 2019) of the Estonian National Board of Animal Experiments.

RESULTS

1. LPS-induced differences in metabolite profile (Paper I)

1.1. Locomotor Activity, body temperature and weight Changes

Bl6 and 129Sv mice were administered a single intraperitoneal injection of LPS (0.5 mg/kg), and locomotor activity was recorded for 24 hours. Both strains showed significant LPS-induced suppression of their motor response during the 24-hour period in the whole arena (treatment – $F_{(1,23)} = 49.19$, $p < 0.0001$; Figures 2A-C). In addition, LPS-exposed mice traveled significantly shorter distances in the central zone compared to control mice (treatment – $F_{(1,23)} = 28.30$, $p < 0.0001$; Figure 2D). However, when the 24-h cycle was divided into lights-on and lights-off periods, LPS-induced suppression of locomotor activity in the center of the arena was significant only during the dark period (treatment – $F_{(1,23)} = 29.99$, $p < 0.0001$; Figures 2E, F).

The difference in motor activity between Bl6 and 129Sv mice was detected within 2 hours after the start of the phenotyper trial. The motor activity of saline-treated 129Sv mice was significantly lower than that of saline-treated Bl6 animals [strain $F_{(1,23)} = 4.96$, $p = 0.04$; treatment $F_{(1,23)} = 13.87$, $p = 0.001$; Figure 2G]. However, this difference was no longer apparent from the third hour onward (Figure 2H). This observation could be due to a higher anxiety-like behavior of 129Sv at the beginning of the behavioral testing, indicating passive adaptation.

The change in body temperature (ΔT) of Bl6 and 129Sv mice was evaluated 1.5 and 24 hours after administration of saline and LPS. Body temperature measurements were conducted with mice housed in their home cage environment. Groups were compared using two-way ANOVA (time × treatment) followed by Bonferroni post-hoc test. A significant effect of time ($F_{(1, 35)} = 13.01$ $p = 0.00096$) and treatment ($F_{(1, 35)} = 6.39$ $p = 0.016$) was observed in 129Sv. Comparison of the groups showed that the ΔT of the LPS-treated mice was slightly lower compared to that of saline-treated control mice in both strains, although no statistically significant difference was observed between the LPS and saline groups. However, there was a significant difference between the 1.5-hour and 24-hour LPS response in 129Sv. 24 hours after LPS administration, the ΔT of 129Sv was significantly higher compared to 1.5-hour LPS treatment, indicating different LPS-induced thermoregulation at the 1.5- and 24-hour time points. In contrast, the ΔT of Bl6 mice was similar at 1.5 and 24 hours after LPS administration (Figure 2I).

Two-way ANOVA (strain × treatment) showed a significant difference in 24-h change in body weight (ΔBW) between LPS- and saline-treated mice in both strains. Administration of LPS resulted in a highly significant loss of body weight in both strains (treatment: $F_{(1,36)} = 175.8$, $p < 0.0001$; strain: $F_{(1,36)} = 20.18$, $p < 0.0001$; strain × treatment: $F_{(1,36)} = 3.80$, $p = 0.06$). However, the LPS-induced loss of body weight was much more pronounced in Bl6, as they

lost 12.1 ± 0.68% of body weight during the 24-h period, while the decrease in 129Sv was only 7.6 ± 0.51% of initial body weight (Table 4).

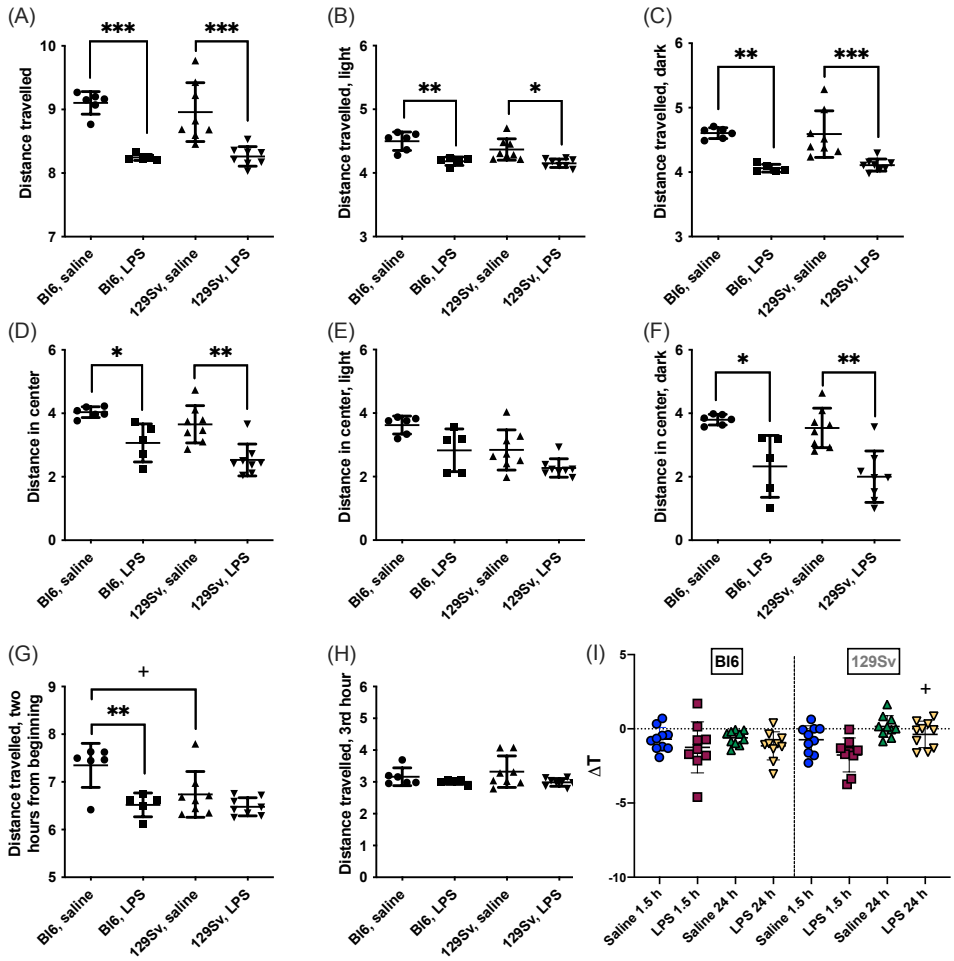

Figure 2. Locomotor activity (log_{10} values, data expressed as mean ± SD) of Bl6 and 129Sv mice in the 24 h LPS challenge. (A) Total distance traveled in 24 h period. (B) Total distance traveled in lights-on period. (C) Total distance traveled in lights-off period. Center distance traveled in 24-h cycle (D), lights-on (E) and lights-off (F) periods. Distance traveled 2 h from the beginning (G) and on the third hour (H). * significant difference between LPS and saline administration groups (Bonferroni's multiple comparisons): *$p \leq 0.05$, **$p \leq 0.01$, ***$p \leq 0.001$; + significant difference between Bl6 and 129Sv mice in saline administration groups, +$p \leq 0.05$. (I) Body temperature (ΔT) changes 1.5 and 24 h after 0.5 mg/kg LPS administration in Bl6 and 129Sv. Two-way ANOVA followed by Bonferroni post hoc test: + a significant difference between 129Sv 1.5 and 24 h LPS treatment groups: +$p < 0.05$.

Table 4. Body weight change (BW) and weight loss % change of the initial weight (weight2 − weight1/weight1 × 100%) 24 h after 0.5 mg/kg LPS administration. Values are represented as mean SD. Two-way ANOVA followed by Bonferroni post hoc test: * a significant difference between saline and LPS treatment: ****$p < 0.0001$; + a significant difference between Bl6 and 129Sv mice of the same treatment group: +++$p < 0.001$.

	Saline Bl6 (Mean ± SD)	**LPS Bl6 (Mean ± SD)**	**Saline 129Sv (Mean ± SD)**	**LPS 129Sv (Mean ± SD)**	**Two-way ANOVA *p*-value**		
					Strain	**Treatment**	**Strain x Treatment**
24 h ΔBW (g)	-0.50 ± 0.73	-3.44 ± 0.73****	-0.01 ± 0.40	-2.2 ± 0.52****+++	<0.0001	<0.0001	0.06
24 h ΔBW (%)	-1.7 ± 2.49	-12.1 ± 2.16	-0.08 ± 1.43	-7.6 ± 1.62			

1.2. Basal differences in metabolic profile between Bl6 and 129Sv

To determine basal differences in metabolic profiles between Bl6 and 129Sv, saline-treated control animals were compared using paired t-tests and Bonferroni correction (p-value less than or equal to 0.0002) and general linear model (GLM) multivariate analysis.

Six metabolites survived Bonferroni correction in both the 1.5- and 24-hour saline treatment groups. These metabolites included biogenic amines Ac-Orn, alpha-AAA and carnosine, which dominated in Bl6 mice and SCAC (C5-), sphingolipid SM (OH) C22:2, and the ratio of C5- to carnitine (C5-/C0), which dominated in 129Sv mice (Supplementary Figure 1, paper I). In addition, 24-h saline-treated Bl6 mice had higher serotonin and lower C4- levels in blood compared to 129Sv. This difference was absent in the groups treated with saline for 1.5 hours, as serotonin levels were higher and plasma C4- levels were lower in the blood of 129Sv, probably indicating acute stress-induced changes.

GLM analysis confirmed a significant main effect [1.5 h saline: $F_{(10,9)} = 58.37$, $p < 0.0001$; 24 h saline: $F_{(10,4)} = 87.08$, $p = 0.0003$] of mouse strain on the concentrations of the various metabolites. In both the 1.5- and 24-h saline treatment groups, metabolite levels differed significantly between Bl6 and 129Sv, including C5-, biogenic amines (Ac-Orn, alpha-AAA, carnosine), LysoPCa C16:1 and SM (OH) C22:2 (all $p \leq 0.0001$). In addition, there was a significant difference in the blood levels of PC aa C34:3 ($p = 0.001$), PC ae C38:4 ($p = 0.005$), hexoses ($p = 0.005$), and LysoPC a C20:3 ($p = 0.009$) in the 1.5-hour group and of PC ae C40:6 ($p = 0.0003$), PC ae C36:2 ($p = 0.004$), SM (OH) C14:1 ($p = 0.004$) and PC ae C38:2 ($p = 0.008$) in the 24-hour group (Supplementary Table 3, paper I).

1.3. LPS Induced Alterations of Metabolic Profile in Bl6

To determine differences between saline and LPS administration, Bl6 and 129Sv strains were first analyzed separately using two-way ANOVA [treatment (saline or LPS) × time (1.5 h or 24 h LPS challenge)]. After statistically significant ANOVA results, Bonferroni post-hoc analysis was performed.

Administration of LPS resulted in altered concentrations of 87 metabolites and their ratios in the Bl6 strain. 21 of them were altered early in the 1.5-h LPS challenge, 58 were altered later in the 24-h LPS challenge, and eight of them were altered at both time points. The detailed results are presented in Supplementary Table 1 of paper I.

Metabolites that were decreased both 1.5 hours and 24 hours after LPS treatment were SCACs (C3, C4-), amino acids citrulline and tyrosine (Tyr), biogenic amines (Ac-Orn, putrescine), and the ratio between Tyr and phenylalanine (Phe). Putrescine was decreased 1.5 hours after LPS treatment; however, 24 hours after LPS treatment, it was significantly increased compared to saline-treated controls (Figure 3F). Accordingly, the spermidine/putrescine ratio exhibited a significant increase 1.5 hours after LPS treatment and a significant decrease 24 hours after LPS treatment.

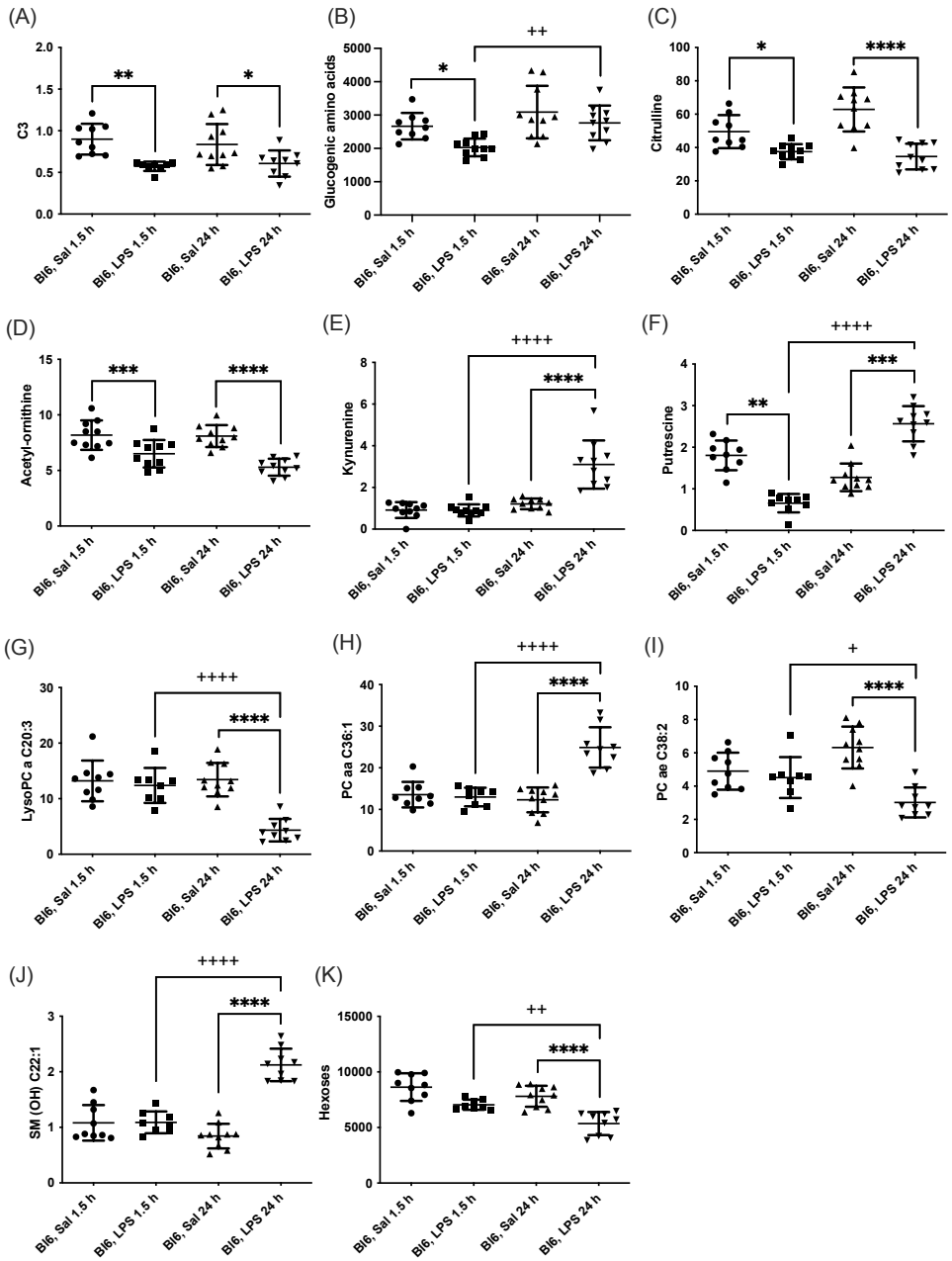

Figure 3. LPS treatment-induced changes in concentrations of (A) C3, (B) glucogenic amino acids, (C) citrulline, (D) Ac-Orn, (E) kynurenine, (F) putrescine, (G) lysophosphatidylcholines (C20:3), (H) phosphatidylcholine diacyls (C36:1), (I) phosphatidylcholine acyl-alkyls (C38:2), (J) sphingolipids (OH C22:1) and (K) hexoses in Bl6 mice after 1.5 and 24 h from administration. Data was analyzed by two-way ANOVA followed by the Bonferroni post hoc test. *significant *p*-value between saline and LPS treatment; +significant *p*-value between 1.5 h and 24 h LPS treatments. *$p \leq 0.05$, **$p \leq 0.01$, ***$p \leq 0.001$, ****$p \leq 0.0001$, ++$p \leq 0.01$, ++++$p \leq 0.0001$.

1.5-h LPS administration resulted in a significant decrease in acylcarnitines (C3:1, C4:1, C5-, C5:1, C6:1, C12-DC, C14:2-OH; Figure 3A), amino acids (alanine (Ala), glycine (Gly), histidine (His), Phe, methionine (Met), proline (Pro), serine (Ser), threonine (Thr), and valine (Val)), biogenic amine alpha-AAA, as well as in the sum of aromatic amino acids (AAA) and the sum of glucogenic amino acids (Figure 3B). In contrast, the ratio of Gly/Ser was increased.

24-h LPS challenge induced significant changes in several metabolites compared with saline-treated animals, including a decrease in serotonin, LysoPC acyls (LysoPC a C16:1, LysoPC a C17:0, LysoPC a C18:1, LysoPC a C18:2, LysoPC a C20:3, LysoPC a C20:4), PC acyl-alkyls (PC ae C36:2, PC ae C38:2, PC ae C38:3, PC ae C38:5), hexoses, and in the ratio between Leu/kynurenine, serotonin/kynurenine, LysoPC a C16:1/LysoPC a C16:0, and LysoPC a C18:2/LysoPC a C18:1. On the other hand, a significant increase was observed in LCACs (C16, C16:1, C18, C18:1, and C18:2), biogenic amines (asymmetric dimethylarginine (ADMA), symmetric dimethylarginine (SDMA), kynurenine, PC diacyls (PC aa C32:3, PC aa C34:1, PC aa C34:2, PC aa C36:1, PC aa C38:4, PC aa C38:6, PC aa C40:5, PC aa C40:6, PC aa C42:4) and in the ratio of SCACs to free carnitine (CRT-1), LCACs to free carnitine (CPT-1), C5-/C0, Arg/ citrulline, kynurenine/Trp, kynurenine/alpha-AAA, and LysoPC a C20:4/LysoPC a C20:3. One of the most significant alterations was the increase in 12 out of 15 circulating sphingolipids. Most significant results are highlighted in Figure 3.

1.3.1. GLM analysis of LPS-induced alterations in Bl6

Paired t-tests with Bonferroni correction (p-value less than or equal to 0.0002) were used to first sort out significant differences in metabolite levels. Then, GLM analysis was performed to confirm the differences between LPS and saline treatment groups in the 1.5 and 24 h LPS challenge.

The final GLM model demonstrated a significant main effect of 1.5 h LPS treatment [$F_{(9,6)} = 5.01$, $p = 0.03$] on metabolite levels. Significant shifts in the model included SCAC C3 ($p < 0.0001$), Ala ($p = 0.0001$), Gly ($p = 0.001$), His ($p = 0.0004$), Phe ($p = 0.001$), Pro ($p < 0.0001$), Ser ($p < 0.0001$), Tyr ($p = 0.002$), and the biogenic amine Ac-Orn ($p = 0.001$). The most significant effect was observed between the 1.5 hour LPS treatment and the decrease in C3, Ala, Pro, and Ser (Table 5).

The GLM model of 24-h LPS treatment demonstrated a robust main effect of treatment [$F_{(17,1)}= 221092$, $p = 0.0017$] on selected metabolite levels. The final model retained BW change, citrulline, biogenic amines kynurenine and putrescine, GPLs (LysoPC a C16:1, LysoPC a C20:3, LysoPC a C20:4, PC aa C36:1, PC aa C40:6, PC ae C38:2), sphingolipids [SM (OH) C22:1, SM (OH) C22:2, SM C16:0, SM C24:0, SM C24:1], and hexoses (all p-values < 0.0001; Supplementary Table 4, paper I). Citrulline, LysoPC acyls, PC diacyls, and hexoses were significantly downregulated after the 24-h LPS challenge. On the other hand, kynurenine, putrescine, PC ae C38:2, and sphingolipids were significantly upregulated (Table 6).

Table 5. Effect of LPS treatment after 1.5 h on metabolite levels among Bl6 mice. Statistically significant regression coefficients (ß), confidence intervals (CI) and *t*- and *p*-values (derived from GLM analysis) of $\log_{10}$-transformed metabolite levels.

Bl6 1.5 h LPS				
Metabolites	**Beta (ß)**	**ß (95 % Cl)**	***t*-value**	***p*-value**
Propionylcarnitine (C3)	-0.84	-1.15, -0.52	-5.68	<0.0001
Alanine (Ala)	-0.81	-1.15, -0.47	-5.16	0.0001
Glycine (Gly)	-0.74	-1.12, -0.35	-4.08	0.001
Histidine (His)	-0.78	-1.14, -0.41	-4.59	0.0004
Phenylalanine (Phe)	-0.73	-1.12, -0.33	-3.96	0.001
Proline (Pro)	-0.86	-1.15, -0.56	-6.20	<0.0001
Serine (Ser)	-0.86	-1.15, -0.56	-6.20	<0.0001
Tyrosine (Tyr)	-0.72	-1.12, -0.32	-3.92	0.002
Acetylornithine (Ac-Orn)	-0.73	-1.12, -0.34	-4.01	0.001

Table 6. Effect of LPS treatment after 24 h on metabolite levels among Bl6 mice. Statistically significant regression coefficients (ß), confidence intervals (CI) and *t*- and *p*-values (derived from GLM analysis) of $\log_{10}$-transformed metabolite levels.

Bl6 24 h LPS				
Metabolites	**Beta (ß)**	**ß (95 % Cl)**	***t*-value**	***p*-value**
Δ body weight	-0.90	-1.12, -0.68	-8.64	<0.0001
Citrulline (Cit)	-0.83	-1.11, -0.54	-6.05	<0.0001
Acetylornithine (Ac-Orn)	-0.86	-1.12, -0.60	-6.90	<0.0001
Kynurenine	0.87	0.62, 1.12	7.23	<0.0001
Putrescine	0.88	0.64, 1.12	7.80	<0.0001
lysoPC a C16:1	-0.88	-1.12, -0.64	-7.64	<0.0001
lysoPC a C20:3	-0.88	-1.12, -0.64	-7.61	<0.0001
lysoPC a C20:4	-0.81	-1.11, -0.52	-5.78	<0.0001
PC aa C36:1	0.85	0.57, 1.12	6.56	<0.0001
PC aa C40:6	0.85	0.58, 1.12	6.68	<0.0001
PC ae C38:2	-0.85	-1.12, -0.59	-6.74	<0.0001
SM (OH) C22:1	0.92	0.72, 1.12	9.58	<0.0001
SM (OH) C22:2	0.89	0.66, 1.12	8.05	<0.0001
SM C16:0	0.94	0.76, 1.12	11.02	<0.0001
SM C24:0	0.85	0.57, 1.12	6.53	<0.0001
SM C24:1	0.95	0.80, 1.11	12.84	<0.0001
Hexoses (H1)	-0.78	-1.10, -0.45	-5.06	<0.0001

1.4. LPS Induced Alterations of Metabolic Profile in 129Sv

The pattern of altered levels of metabolites in 129Sv differed from that of Bl6. The 1.5 h LPS challenge caused less alterations in 129Sv than seen in Bl6. 1.5 h after LPS administration merely 9 altered levels of metabolites and their ratios were identified, including decrease in SCACs (C2, C3, C4-, C5-), citrulline, ratios of C3/C3, C5-/0, Tyr/Phe and increase in PC diacyl PC aa C42:0. Detailed results are presented in Supplementary Table 2 of paper I.

24 h after LPS administration large-scale alterations were observed in the metabolic profile, including 71 altered levels of metabolites and their ratios. Citrulline was the only amino acid significantly reduced in 129Sv. Accordingly, the ratio Arg/citrulline was elevated. Similarly to Bl6 mice, 129Sv exhibited significant decrease of SCAC (C3) and increase in LCACs (C12, C14:1, C14:1-OH, C14:2, C14:2-OH, C16, C16-OH, C16:1, C16:1-OH, C16:2, C16:2-OH, C18, C18:1, C18:1-OH, C18:2). However, the number of altered LCACs was more extended from that seen in Bl6 mice. Moreover, the sum of hydroxylated LCACs was significantly elevated. Similar to Bl6 strain, ratios of acylcarnities to free carnitine (CRT-1 and CPT-1) were significantly elevated. Among 129Sv mice, 24 h LPS treatment caused a significant change in the levels of biogenic amines serotonin and kynurenine. The level of serotonin was significantly reduced, whereas the value of kynurenine was elevated. Furthermore, the ratio kynurenine/Trp was elevated, whereas the ratio serotonin/Trp was reduced. Moreover, the ratio kynurenine/alpha-AAA was significantly elevated. From 90 circulating glycerophospholipids (GPLs) the level of 25 GPLs was significantly altered, including reduction of several LysoPC acyls (LysoPC a C17:0, LysoPC a C18:2, LysoPC a C20:3, LysoPC a C20:4) and PC acyl-alkyls (PC ae C36:2, PC ae C36:4, PC ae C38:2, PC ae C38:3, PC ae C38:5, PC ae C40:3), as well as elevation of several PC diacyls (PC aa C32:3, PC aa C34:3, PC aa C36:1, PC aa C36:2, PC aa C38:1, PC aa C38:4, PC aa C38:6, PC aa C40:2, PC aa C40:3, PC aa C40:5, PC aa C40:6, PC aa C42:2, PC aa C42:4, PC aa C42:5). Similar to Bl6 mice, the most significant alteration was the elevation of sphingolipids. It is noteworthy that no changes were observed in the level of hexoses in 129Sv mice. The most significant results are highlighted in Figure 4.

The pattern of altered metabolite levels in 129Sv differed from that of Bl6. The 1.5-hour LPS exposure caused fewer changes in 129Sv than seen in Bl6. 1.5 hours after LPS administration, only 9 altered concentrations of metabolites and their ratios were detected, including a decrease in SCACs (C2, C3, C4-, C5-), citrulline, ratios of C3/C3, C5-/0, Tyr/Phe, and an increase in PC diacyl PC aa C42:0. Detailed results are shown in supplementary Table 2 of paper I.

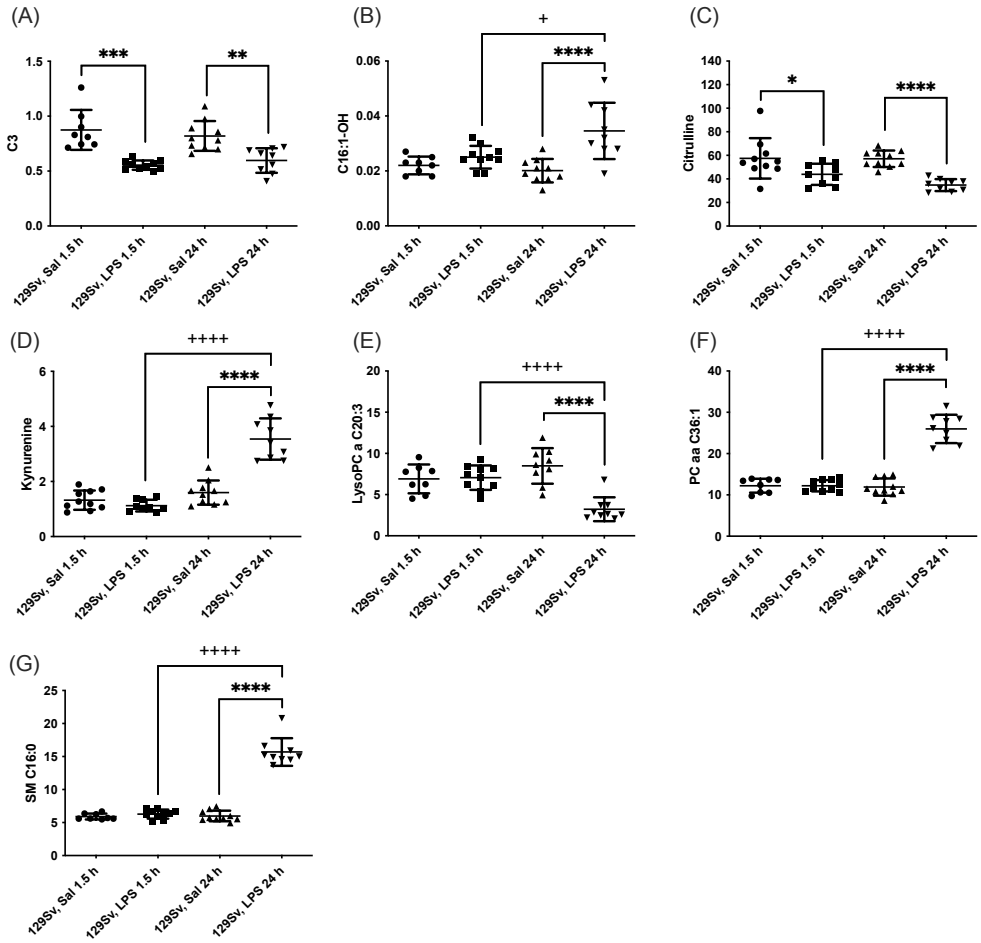

Figure 4. LPS treatment-induced changes in concentrations of (A) SCACs (C3), (B) hydroxylated LCACs (C16:1-OH), (C) citrulline, (D) kynurenine, (E) lysophosphatidylcholines (C20:3), (F) phosphatidylcholine diacyls (C36:1) and (G) sphingolipids (C16:0) in 129Sv mice 1.5 and 24 h after administration. Data was analyzed by two-way ANOVA followed by the Bonferroni post hoc test. *significant *p*-value between saline and LPS treatment; +significant *p*-value between 1.5 h and 24 h LPS treatments. *$p \leq 0.05$, **$p \leq 0.01$, ***$p \leq 0.001$, ****$p \leq 0.0001$, ++++$p \leq 0.0001$.

24 h after LPS administration large-scale alterations were observed in the metabolic profile, including 71 altered concentrations of metabolites and their ratios. Citrulline was the only amino acid significantly reduced in 129Sv. Accordingly, the Arg/citrulline ratio was increased. Similar to Bl6 mice, 129Sv showed a significant decrease in SCACs (C3) and an increase in LCACs (C12, C14:1, C14:1-OH, C14:2, C14:2-OH, C16, C16-OH, C16:1, C16:1-OH, C16:2, C16:2-OH, C18, C18:1, C18:1-OH, C18:2). However, the number of altered LCACs was greater than seen in Bl6 mice. In addition, the sum of hydroxylated LCACs was significantly increased. Similar to the Bl6 strain, the ratios of acylcarnitines

to free carnitine (CRT-1 and CPT-1) were significantly increased. In 129Sv mice, 24 h LPS treatment caused a significant change in the levels of biogenic amines serotonin and kynurenine. The level of serotonin was significantly decreased, whereas the level of kynurenine was increased. Furthermore, the ratio of kynurenine/Trp was increased, whereas the ratio of serotonin/Trp was decreased. In addition, the ratio kynurenine/alpha-AAA was significantly increased. Among 90 circulating glycerophospholipids (GPLs), the level of 25 GPLs was significantly changed, including the reduction of several LysoPC acyls (LysoPC a C17:0, LysoPC a C18:2, LysoPC a C20:3, LysoPC a C20:4) and PC acyl-alkyls (PC ae C36:2, PC ae C36:4, PC ae C38:2, PC ae C38:3, PC ae C38:5, PC ae C40:3), as well as the increase of several PC diacyls (PC aa C32:3, PC aa C34:3, PC aa C36:1, PC aa C36:2, PC aa C38:1, PC aa C38:4, PC aa C38:6, PC aa C40:2, PC aa C40:3, PC aa C40:5, PC aa C40:6, PC aa C42:2, PC aa C42:4, PC aa C42:5). Similar to Bl6 mice, the most significant change was the increase in sphingolipids. It is noteworthy that no changes in hexose content were observed in 129Sv mice. The main results are highlighted in Figure 4.

1.4.1. GLM analysis of LPS-induced alterations in 129Sv

Similar to the Bl6 strain, the GLM model of the 1.5 h LPS challenge in 129Sv displayed a strong main effect of treatment [$F_{(7,9)}$= 18.29, p = 0.0001]. Significantly altered shifts of metabolites included SCACs C2 ($p < 0.0001$), C3 ($p < 0.0001$), C4- ($p < 0.0001$) and C5- ($p = 0.0002$), citrulline ($p = 0.001$), PC aa C42:0 ($p = 0.006$), and SM (OH) C16:1 ($p = 0.002$; Table 7). All metabolites altered in the 1.5 h LPS challenge exhibited a decline, except for complex lipids [PC aa C42:0 and SM (OH) C16:1], which were elevated (Supplementary Table 4, paper I).

Table 7. Effect of LPS treatment after 1.5 h on metabolite levels among 129Sv mice. Statistically significant regression coefficients (*ß*), confidence intervals (CI) and *t*- and *p*-values (derived from GLM analysis) of $\log_{10}$-transformed metabolite levels.

129Sv 1.5 h LPS				
Metabolites	**Beta (ß)**	**ß (95 % CI)**	***t*-value**	***p*-value**
Acetylcarnitine (C2)	-0.84	-1.14, -0.54	-5.93	<0.0001
Propionylcarnitine (C3)	-0.87	-1.14, -0.60	-6.81	<0.0001
Butyryl- and isobutyrylcarnitine (C4-)	-0.85	-1.14, -0.56	-6.22	<0.0001
Isovaleryl- and 2-methybutyryl-carnitine (C5-)	-0.78	-1.12, -0.43	-4.78	0.0002
PC aa C42:0	0.64	0.22, 1.06	3.22	0.006
SM (OH) C16:1	0.56	0.11, 1.02	2.64	0.02

The 24 h LPS administration also showed strong main effect of treatment [$F_{(16,1)}$ = 437.3, p = 0.004]. The most significant effect (t-values > 10, p-values < 0.0001) was observed in BW change and blood levels of PC diacyls (PC aa C36:1, PC aa C40:6) and sphingolipids [SM (OH) C22:1, SM (OH) C22:2, SM C16:0, SM C16:1 and SM C24:1]. Moderate (t-values > 5 < 10, p-values ≤ 0.0001) LPS-induced alterations were observed in C18:1, citrulline, kynurenine, GPLs (LysoPC a C20:3, PC aa C38:6, PC aa C42:5) and sphingolipids [SM (OH) C14:1, SM (OH) C16:1, SM (OH) C24:1, SM C18:0, SM C18:1 and SM C24:0]. Minor alterations (t-values < 5, p-values < 0.001) included LCACs C14:1, C16 and C16-OH (Table 8).

Table 8. Effect of LPS treatment after 24 h on metabolite levels among 129Sv mice. Statistically significant regression coefficients (ß), confidence intervals (CI) and t- and p-values (derived from GLM analysis) of $\log_{10}$-transformed metabolite levels.

129Sv 24 h LPS				
Metabolites	**Beta (ß)**	**ß (95 % CI)**	***t*-value**	***p*-value**
Δ body weight	-0.93	-1.12, -0.74	-10.19	<0.0001
Tetradecenoylcarnitine (C14:1)	0.76	0.42, 1.11	4.73	0.0002
Hexadecanoylcarnitine (C16)	0.77	0.43, 1.11	4.83	0.0002
Hydroxyhexadecanoylcarnitine (C16-OH)	0.76	0.42, 1.10	4.70	0.0002
Octadecenoylcarnitine (C18:1)	0.78	0.45, 1.11	5.04	0.0001
Citrulline (Cit)	-0.89	-1.13, -0.65	-7.77	<0.0001
Kynurenine	0.87	0.61, 1.13	7.01	<0.0001
lysoPC a C20:3	-0.85	-1.13, -0.56	-6.34	<0.0001
PC aa C36:1	0.93	0.74, 1.12	10.19	<0.0001
PC aa C38:6	0.85	0.58, 1.13	6.52	<0.0001
PC aa C40:6	0.95	0.80, 1.11	12.82	<0.0001
PC aa C42:5	0.80	0.48, 1.12	5.36	<0.0001
SM (OH) C14:1	0.88	0.64, 1.13	7.55	<0.0001
SM (OH) C16:1	0.79	0.47, 1.12	5.23	<0.0001
SM (OH) C22:1	0.95	0.79, 1.11	12.55	<0.0001
SM (OH) C22:2	0.95	0.80, 1.11	12.40	<0.0001
SM (OH) C24:1	0.92	0.72, 1.13	9.73	<0.0001
SM C16:0	0.97	0.84, 1.10	15.98	<0.0001
SM C16:1	0.94	0.75, 1.12	10.60	<0.0001
SM C18:0	0.91	0.70, 1.13	8.91	<0.0001
SM C18:1	0.92	0.71, 1.13	9.39	<0.0001
SM C24:0	0.93	0.72, 1.13	9.74	<0.0001
SM C24:1	0.98	0.88, 1.08	20.55	<0.0001

2. LPS-induced differences in neuroinflammation (Paper II)

2.1. Body temperature and weight

Bl6 and 129Sv mice were administered a single intraperitoneal injection of LPS (0.5 mg/kg), and body weight and temperature were measured before and 24 hours after LPS and saline administration. Groups were compared using two-way ANOVA (strain × treatment) followed by Bonferroni post-hoc test.

Administration of LPS resulted in a significant decrease in body weight in both strains (treatment: $F_{(1,\ 125)} = 651.9$, $p < 0.0001$; strain: $F_{(1,\ 125)} = 52.7$, $p < 0.0001$; strain × treatment: $F_{(1,\ 125)} = 48.19$, $p < 0.0001$). However, the LPS-induced body weight loss was much more pronounced in Bl6 mice, as the mean percent body weight loss in Bl6 mice was 12.6 ± 0.4%, while the decrease in 129Sv mice was only 7.5 ± 0.3% of the initial body weight (Figure 5A).

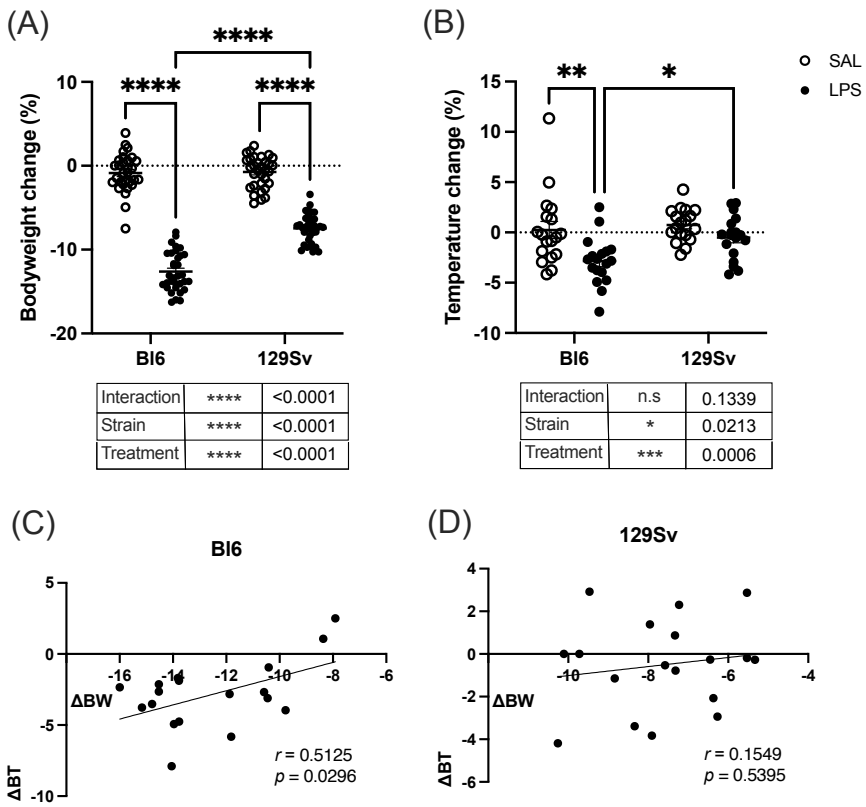

Interaction	****	<0.0001
Strain	****	<0.0001
Treatment	****	<0.0001

Interaction	n.s	0.1339
Strain	*	0.0213
Treatment	***	0.0006

Figure 5. LPS-induced body weight and temperature alterations. The bodyweight and temperature of Bl6 and 129Sv mice was measured before and after 24 h of LPS (0.5 mg/kg, i.p) and saline administration. (A) Bodyweight change (%). (B) Body temperature change (%). Pearson correlation between bodyweight (ΔBW) and body temperature change (ΔBT) in Bl6 (C) and 129Sv (D) mice. Data are expressed as mean values ± SEM: *$p \leq 0.05$, **$p \leq 0.01$, ***$p \leq 0.001$, ****$p \leq 0.0001$.

Strain-specific effects on body temperature were observed in LPS-treated animals (treatment: $F_{(1, 68)} = 12.98$, $p = 0.0006$; strain $F_{(1, 68)} = 5.56$, $p = 0.02$; strain × treatment: $F_{(1, 125)} = 2.3$, $p = 0.13$). After 24 h of LPS administration, the body temperature of Bl6 mice decreased significantly (-2.9 ± 0.6%), while LPS did not cause a statistically significant change in body temperature in 129Sv mice (-0.5 ± 0.5%). After LPS administration, the differences in body temperature between the two strains became statistically significant, indicating a more pronounced effect of LPS on the Bl6 strain (Figure 5B). A moderate positive correlation ($r = 0.51$, $p = 0.03$) was observed between body weight loss and temperature change 24 hours after LPS injection in Bl6 mice, while no significant correlation was observed in the 129Sv strain (Figure 5C, D).

2.2. LPS-induced depression of locomotor activity

Next, we examined LPS-induced changes in locomotor activity to determine whether the observed changes in body temperature and body weight were related to changes in motor activity. Bl6 and 129Sv mice were administered a single intraperitoneal injection of LPS (0.5 mg/kg), and motor activity was recorded for 24 hours in phenotyper cages (Figure 6A). Total distance traveled in the whole arena and in the central and peripheral zones of the arena, as well as time spent moving, were recorded. Locomotor data was $\log_{10}$-transformed before two-way ANOVA (strain × treatment) analysis to ensure that the data correspond to a normal distribution. Pearson correlation analysis was then performed to analyze the correlations between the 24-h locomotor parameters and body weight and temperature change.

During the 24-hour cycle, LPS caused significant suppression of locomotor activity in the whole arena (treatment: $F_{(1, 23)} = 38.41$, $p < 0.0001$; Figure 6B) and in the central zone of the arena (treatment: $F_{(1, 23)} = 28.58$, $p < 0.0001$; Figure 6E) in both strains of mice. When dividing the 24 h cycle into light/dark periods, LPS-induced suppression of locomotor activity in the central zone was only significant during the lights-off period (treatment: $F_{(1, 22)} = 29.05$, $p < 0.0001$; Figure 6F,G), whereas in the whole arena, locomotor activity remained suppressed in light (treatment: $F_{(1, 23)} = 24.51$, $p < 0.0001$; Figure 6C) and dark periods (treatment: $F_{(1, 23)} = 37.92$, $p < 0.0001$; Figure 6D).

As expected, LPS suppressed the time spent moving in both strains, compared to their control counterparts in the whole arena (treatment: $F_{(1, 23)} = 136.5$, $p < 0.0001$; Figure 6H) as well as in peripheral (treatment: $F_{(1, 23)} = 135.9$, $p < 0.0001$; Figure 6I) and central (treatment: $F_{(1, 23)} = 67.45$, $p < 0.0001$; Figure 6J) zones. However, Bl6 control group mice spent significantly more time moving compared to 129Sv control mice in the whole arena, which was even more prominent in the central zone. This probably reflects a higher anxiety level of 129Sv mice.

Pearson's correlation analysis showed no significant relationship between 24 h locomotor activity parameters and bodyweight and temperature change (Supplementary Table S1, paper II).

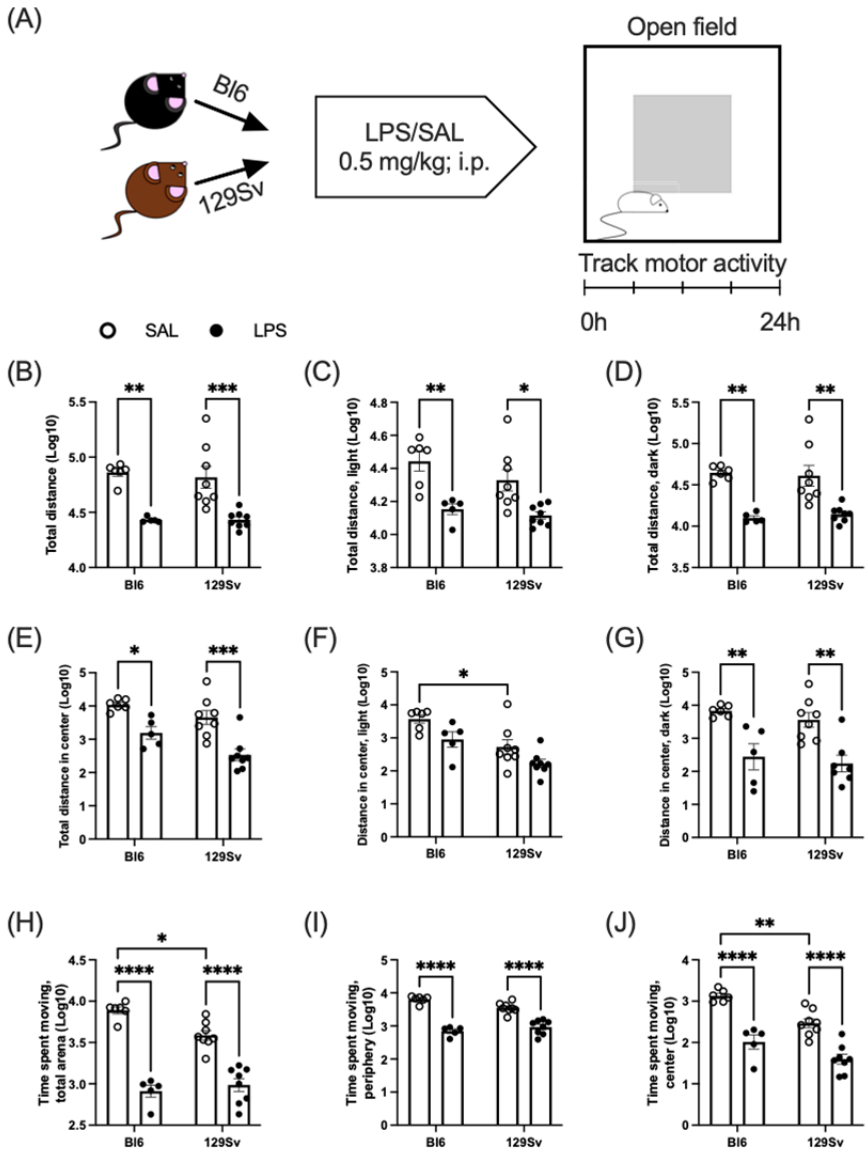

Figure 6. The effect of LPS administration on locomotor activity (Log_{10} values, data expressed as mean ± SEM). (A) Schematic overview of the experiment: Bl6 (n = 16) and 129Sv (n = 16) mice were injected with LPS (0.5 mg/kg; i.p), and locomotor activity was recorded for 24 h in phenotyper cages. Total distance traveled in 24 h (B), lights-on (C), and lights-off (D) period. Total distance traveled in the center of the arena in 24 h cycle (E), lights-on (F), and lights-off (G) periods. Time spent moving in the whole arena (H), peripheral (I), and central (J) zones. Data was analyzed by two-way ANOVA followed by the Bonferroni post hoc test: *$p \leq 0.05$, **$p \leq 0.01$, ***$p \leq 0.001$; ****$p \leq 0.0001$.

2.3. Microglial profile and subpopulations

We next questioned whether a systemic immune challenge with LPS may induce a different microglial response in Bl6 and 129Sv strains. A combination of cell-specific markers was used to identify $CD11b^{+}CD45^{intermediate}$ microglia, $CD11b^{+}CD45^{high}$ infiltrating myeloid cells (mainly macrophages and neutrophils), and $O4^{+}$ oligodendrocyte progenitor cells (OPCs). To characterize the activation profile of microglia after LPS stimulation, microglia cells were analyzed for MHC-II and CD206 surface markers. We also investigated CD11b and CX3CR1 expression on microglial cells. Although CD11b is constitutively expressed by microglia, the expression increases upon microglial activation (Hynes, 1992; Marshall et al., 2013).

When comparing the control and LPS groups, we found that microglia cell percentages were slightly increased among both strains after 24 h, although this elevation did not reach the statistical significance level in 129Sv mice (cerebellum − treatment: $F_{(1, 15)} = 16.5$, $p = 0.001$; strain: $F_{(1, 15)} = 8.16$, $p = 0.01$; strain × treatment: $F_{(1, 15)} = 0.6$, $p = 0.44$; hippocampus − treatment: $F_{(1, 15)} = 21.61$, $p = 0.0003$; strain: $F_{(1, 15)} = 0.4$, $p = 0.5$; strain × treatment: $F_{(1, 15)} = 2.49$, $p = 0.14$). As expected, the quantities of neutrophils and macrophages were elevated in the cerebellum (treatment: $F_{(1, 15)} = 51.53$, $p < 0.0001$; strain: $F_{(1, 15)} = 10.10$, $p = 0.006$; strain × treatment: $F_{(1, 15)} = 0.53$, $p = 0.48$) and hippocampus (treatment: $F_{(1, 15)} = 43.43$, $p < 0.0001$; strain: $F_{(1, 15)} = 10.04$, $p = 0.007$; strain × treatment: $F_{(1, 15)} = 1.49$, $p = 0.24$) after LPS administration in both strains.

As previous studies have demonstrated that LPS-activated microglia mediate oligodendrocyte progenitor cell (OPC) death (Pang et al., 2010), we next sought to investigate the effect of LPS administration on OPCs. The percentage of OPCs was substantially lower in LPS-treated mice 24 h after LPS administration compared to their control counterparts. For Bl6 mice, the decline of OPCs was statistically significant solely in the cerebellum. On the contrary, 129Sv mice exhibited significant decline in OPCs only in the hippocampus. It should be noted, however, that the same downtrend was seen in both brain regions in both strains (Figure 7).

Thereafter, we questioned whether there could be strain-specific differences in microglial activation in response to LPS. Thus, we chose to investigate LPS-induced changes in fractalkine receptor (CX3CR1), cluster of differentiation molecule 11b (CD11b), major histocompatibility complex II (MHC-II), and mannose receptor (CD206).

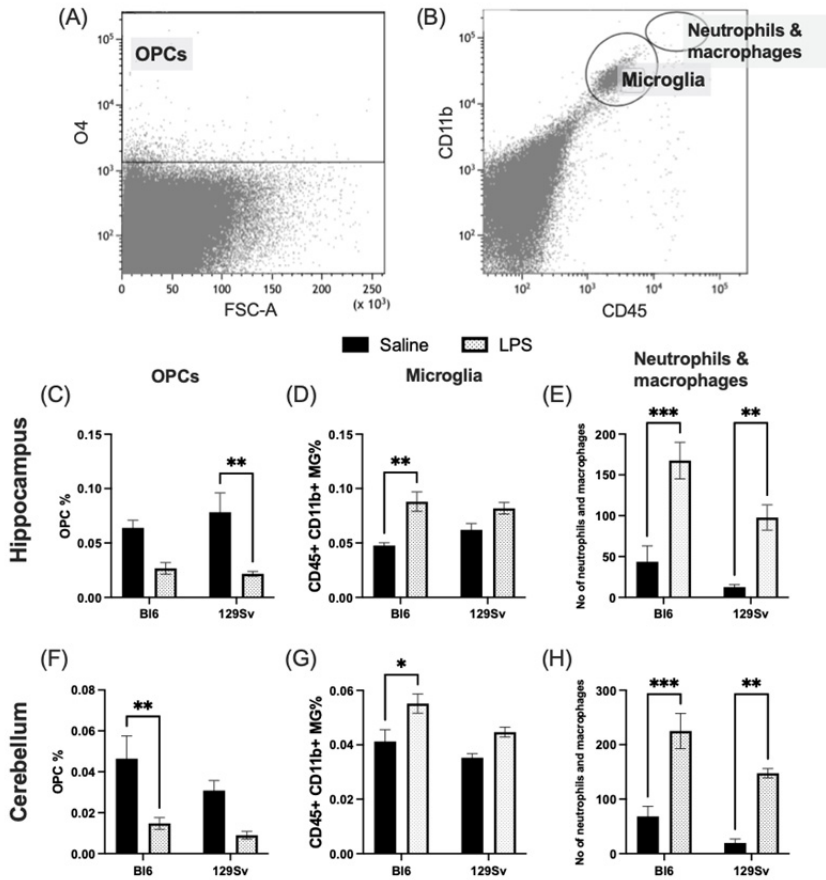

Figure 7. LPS-induced alterations in cell abundance of oligodendrocyte progenitor cells (OPCs), microglia, and neutrophils and macrophages within the brains of Bl6 and 129Sv mice. A representative gating strategy for (A) O4 positive OPC population, (B) CD11b+CD45intermediate microglia population, and CD11b+CD45high neutrophil and macrophage population. (C) Percentage of OPCs, (D) microglial cells, and (E) number of neutrophils and macrophages in hippocampus. (F) Percentage of OPCs, (G) microglial cells, and (H) number of neutrophils and macrophages in cerebellum. Data are expressed as mean values ± SEM. Data was analyzed by two-way ANOVA followed by the Bonferroni post hoc test: $*p \leq 0.05$, $**p \leq 0.01$, $***p \leq 0.001$.

It has been suggested previously that CX3CR1-CX3CL1 interaction serves as a communication tool between neurons and microglia and could play a role in the microglial activation process (Cardona et al., 2006; Hughes et al., 2002). To evaluate the LPS-induced alterations in CX3CR1 expression level, we quantified the mean fluorescence intensity (MFI) level of CX3CR1 on microglial cells (Figure 8A–C). LPS induced significant elevation of CX3CR1 expression in the cerebellum of 129Sv mice, whereas no alterations were observed in the hippocampus. In Bl6 mice, LPS did not alter CX3CR1 surface expression.

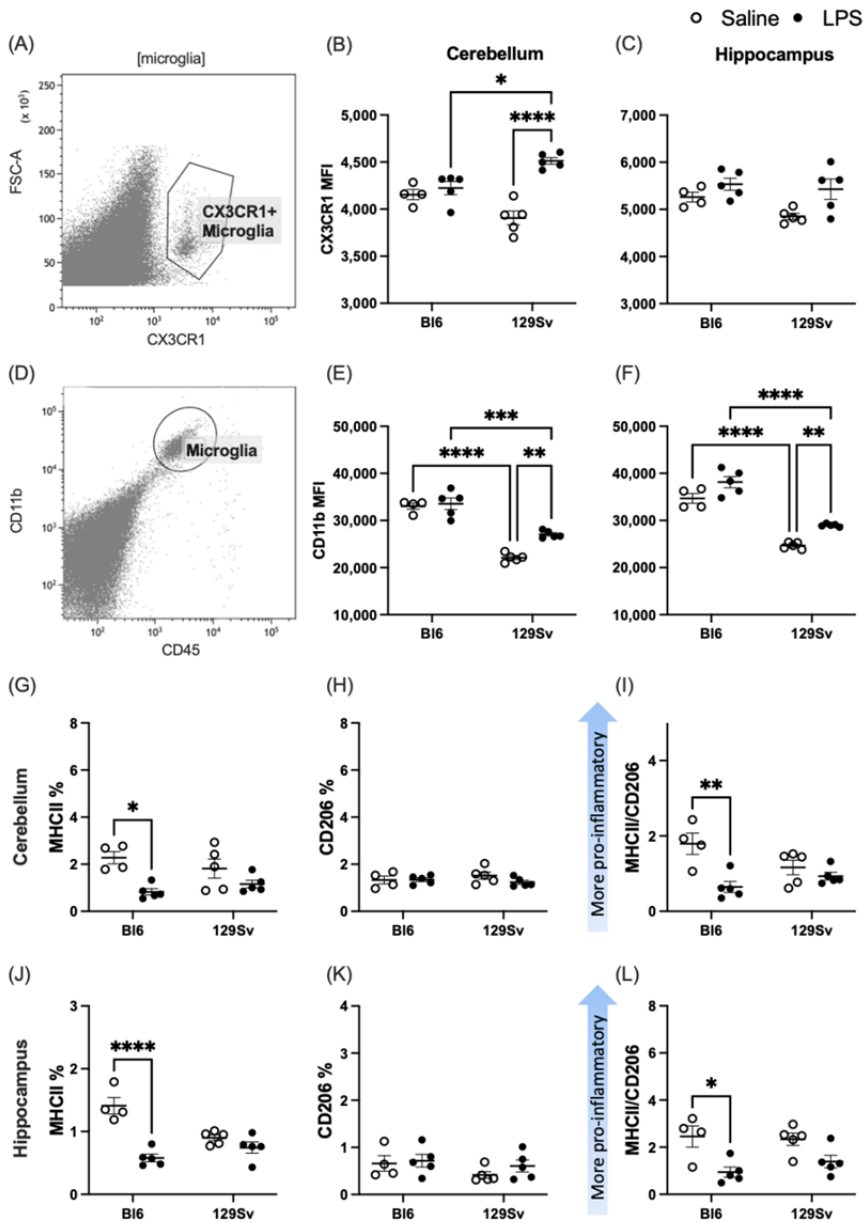

Figure 8. Microglial surface expression of CX3XR1, CD11b, MHC-II, and CD206 molecules. A representative gating strategy for CX3CR1- (A) and CD11b- (D) positive microglia population. MFI of CX3CR1 in cerebellum (B) and hippocampus (C). MFI of CD11b in cerebellum (E) and hippocampus (F). Percentages of (G) MHC-II and (H) CD206 and (I) ratios of MHC-II versus CD206 microglia in cerebellum. Percentages of (J) MHC-II and (K) CD206 and (L) ratios of MHC-II versus CD206 microglia in the hippocampus: *$p \leq 0.05$, **$p \leq 0.01$, ***$p \leq 0.001$, ****$p \leq 0.0001$.

Furthermore, we found a significant increase of CD11b-reactive microglia in response to LPS stimulation in the hippocampus and cerebellum of 129Sv mice, whereas LPS did not alter the surface expression of CD11b on microglial cells of Bl6 mice. However, compared to 129Sv, the level of CD11b was higher in Bl6 mice, regardless of the nature of treatment. Elevated expression of CD11b reflects a stable and fundamental activation status of microglia in the Bl6 strain.

To study the polarization of the proinflammatory microglial ratio after systemic LPS challenge, we evaluated MHC-II and CD206 expression on microglial cells. Surprisingly, the percentage of MHC-II on microglial cells was significantly decreased in response to LPS stimulation in the cerebellum and hippocampus of Bl6 mice. The percentages of CD206 remained unaffected in both Bl6 and 129Sv strains. Accordingly, the MHC-II/CD206 microglial ratio was significantly lower 24 h after LPS administration in Bl6 mice, whereas no alterations were observed in 129Sv mice (Figure 8G–L).

2.4. MHC-I pathway-related gene expression profile

Since we, surprisingly, observed LPS-induced downregulation of MHC-II in the brain of Bl6 mice, we next sought to investigate mRNA levels of genes related to the MHC-I pathway. We focused on the following genes: β-2-microglobulin (*β2m*), transporter associated with antigen processing (TAP) subunits 1 and 2 (*Tap1* and *Tap2*), the bridging factor tapasin (*Tapbp*), and immunoproteasome subunit *Lmp2*. Gene expression analysis was carried out in six different brain regions: hippocampus, hypothalamus, midbrain, frontal cortex, olfactory bulb, and cerebellum.

In the hippocampus, hypothalamus, and midbrain we observed a significantly higher baseline level of *β2m* mRNA in saline-treated Bl6 control mice compared to 129Sv control mice. Additionally, in the hypothalamus the baseline level of the *Tapbp* gene was also higher in Bl6 compared to 129Sv mice.

LPS treatment significantly increased the expression of all MHC-I-related genes (*Tapbp*, *β2m*, *Tap1*, *Tap2*), apart from immunoproteasome gene *Lmp2*, in both strains compared to their respective saline-controls (Figure 9; all $p < 0.05$). However, when comparing Bl6 and 129Sv mice, LPS-induced increase of these MHC-I components was significantly higher in Bl6 mice.

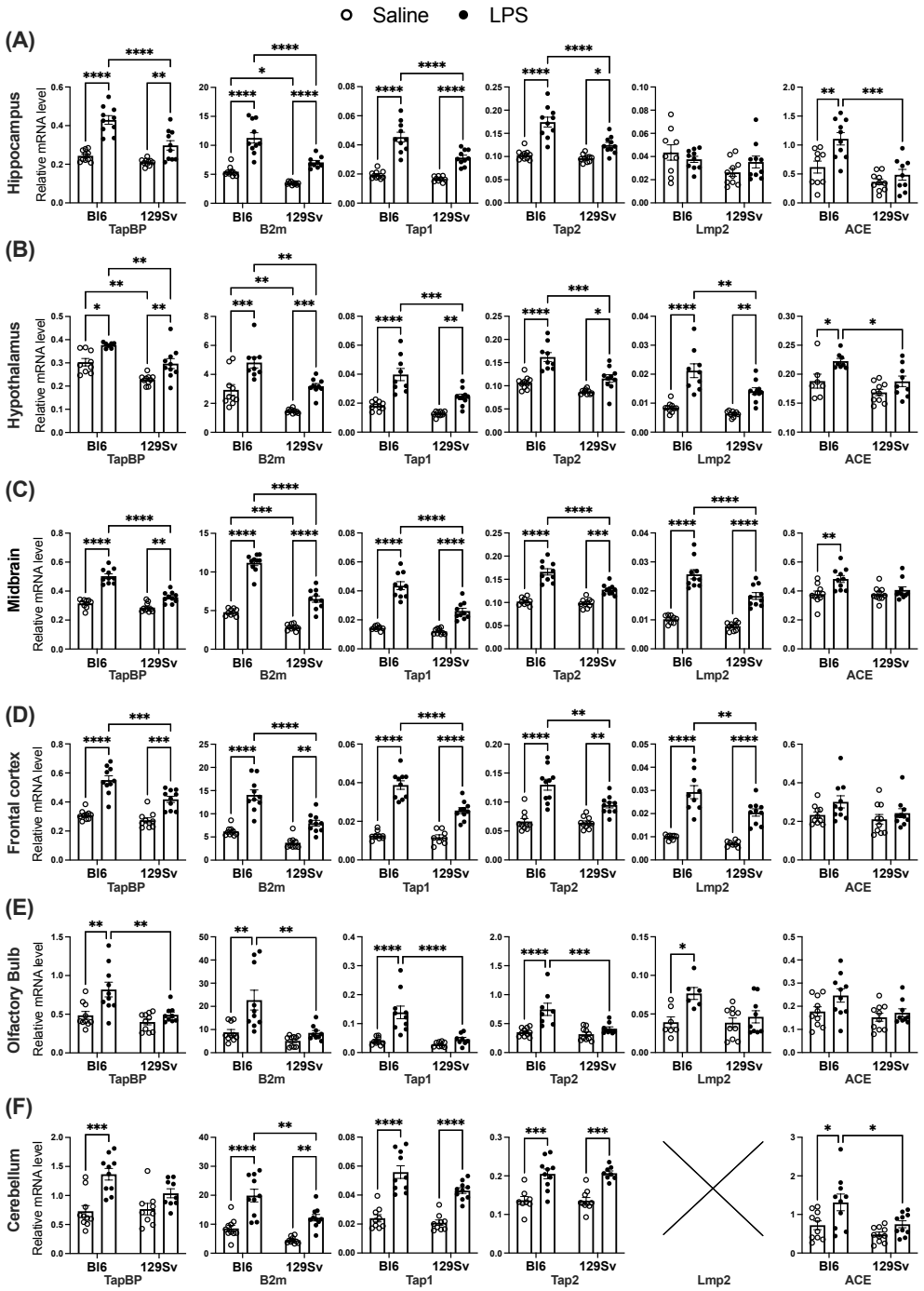

Figure 9. The mRNA expression of MHC-I-related genes in hippocampus (A), hypothalamus (B), midbrain (C), frontal cortex (D), olfactory bulb (E), and cerebellum (F): × – no expression of *Lmp2* was detected in the cerebellum. Data were analyzed by two-way ANOVA with Bonferroni post hoc test and presented as mean ± SEM: *$p \leq 0.05$, **$p \leq 0.01$, ***$p \leq 0.001$, ****$p \leq 0.0001$.

Similarly, LPS increased the expression of *Tapbp*, *β2m*, *Tap1*, *Tap2*, and *Lmp2* mRNA in the hypothalamus, midbrain, and frontal cortex of Bl6 and 129Sv mice (Figure 9; all $p < 0.05$ versus corresponding saline treatment group). However, for all genes, the LPS-induced increase of relative mRNA levels was greater in Bl6 mice than in 129Sv mice.

The most substantial strain-specific differences were observed in the olfactory bulbs. As seen in other brain regions, LPS also increased the expression of *Tapbp*, *β2m*, *Tap1*, *Tap2*, and *Lmp2* mRNA in the olfactory bulb of Bl6 mice (Figure 9; all $p < 0.05$ versus saline). However, in the olfactory bulb of 129Sv mice, the expression of MHC-I related genes was not influenced by LPS challenge.

In the cerebellum, we could not detect any expression of *Lmp2* in Bl6 or 129Sv mice. The mRNA level of *Tapbp* was solely upregulated in Bl6 mice after LPS administration (Figure 9; $p < 0.05$ versus saline), and no changes occurred in 129Sv mice. *β2m*, *Tap1*, and *Tap2* were all significantly upregulated in both strains. However, in the cerebellum only the expression of *β2m* was greater in Bl6 than in 129Sv mice after LPS challenge (Figure 9; $p < 0.05$ Bl6 LPS versus 129Sv LPS).

In addition, since the dipeptidase angiotensin converting enzyme (ACE) has been identified as having a physiological role in the processing of peptides for MHC-I, we thereafter questioned whether the mRNA level of *ACE* was also differently affected by LPS. When comparing control and LPS groups, we found that, while *ACE* gene expression in 129Sv mice was not affected by LPS challenge, in Bl6 mice LPS induced a significant increase in the *ACE* mRNA level in the hippocampus, hypothalamus, midbrain, and cerebellum (Figure 9; all brain regions $p < 0.05$ Bl6 saline versus Bl6 LPS). Although the level of *ACE* in the frontal cortex and olfactory bulbs was not statistically significantly increased by LPS treatment, it showed a tendency towards increase in Bl6 mice.

2.5. MHC-I-pathway protein levels

In order to provide further validation of strain-specific, LPS-induced alterations seen in mRNA levels, we next performed Western blot analysis. We selected β2m, Tapbp, and ACE genes to further explore the protein levels in the hippocampus and olfactory bulbs of Bl6 and 129Sv mice. Although the LPS-induced effects were less prominent at the protein level than that observed at mRNA level, the main effect was, for the most part, similar. We confirmed that the upregulation of ACE and β2m was greater in Bl6 mice compared to 129Sv in the hippocampus (Figure 10A,B,D). However, no significant upregulation was detected in the Tapbp protein level (Figure 10C) in the hippocampus, which was different from that of the transcript level. Western blot results from olfactory bulb tissue were consistent with qPCR results, confirming increase of Tapbp and β2m in Bl6 and no significant change in 129Sv mice after exposure to LPS (Figure 10G,H). No statistically significant change in the expression of ACE

protein was observed in the olfactory bulbs of Bl6 and 129Sv. Although similar to qPCR, it showed a tendency towards increase in Bl6 mice (Figure 10F).

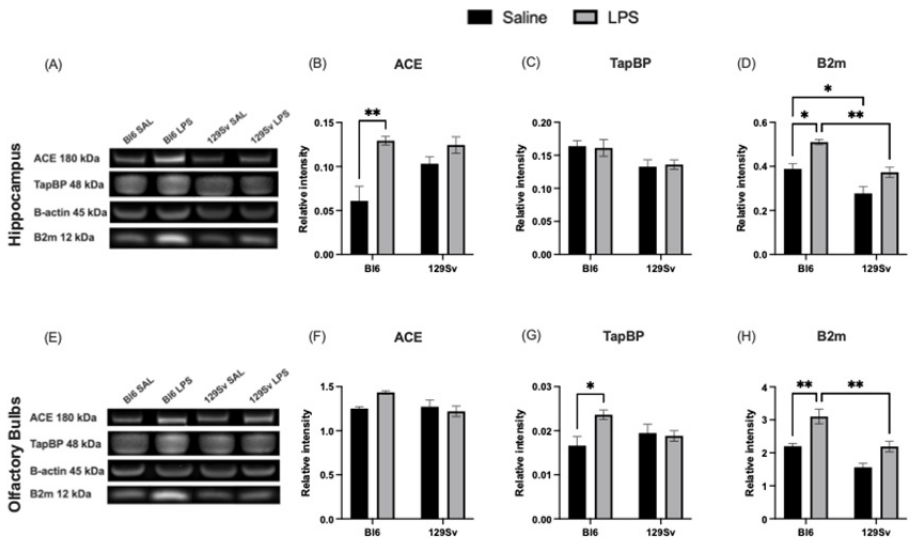

Figure 10. Representative immunoblots (A) and protein expression analysis of ACE (B), Tapbp (C), and β2m (D) in hippocampus. Representative immunoblots (E) and protein expression analysis of ACE (F), Tapbp (G), and β2m (H) in olfactory bulbs. Data were analyzed by two-way ANOVA with Bonferroni post hoc test and presented as mean ± SEM (n = 3–6): *$p \leq 0.05$, **$p \leq 0.01$.

2.6. Association analysis

To find out whether the upregulation of MHC-I genes had any correlation with bodyweight and temperature change, we then analyzed the LPS groups by Pearson's analysis.

We found that bodyweight change was positively significantly correlated with *β2m* ($r = 0.77$, $p = 0.009$; Figure 11A), *Tapbp* ($r = 0.74$, $p = 0.01$; Figure 11B), and *Tap1* ($r = 0.66$, $p = 0.04$; Figure 11C) in the olfactory bulbs of Bl6 mice and with *Tap1* ($r = 0.65$, $p = 0.04$; Supplementary Table S2, paper II) in the cerebellum of Bl6 mice. No significant correlations were established in the olfactory bulbs and cerebellum of 129Sv mice (Figure 11F–J). However, we found that bodyweight change was positively significantly correlated with *Tapbp* ($r = 0.73$, $p = 0.02$; Figure 12G), *Tap1* ($r = 0.71$, $p = 0.02$; Figure 12H), and *Lmp2* ($r = 0.63$, $p = 0.05$; Figure 12J) in the frontal cortex of 129Sv mice, while no significant correlations were established in the frontal cortex of Bl6 mice (Figure 12A–E).

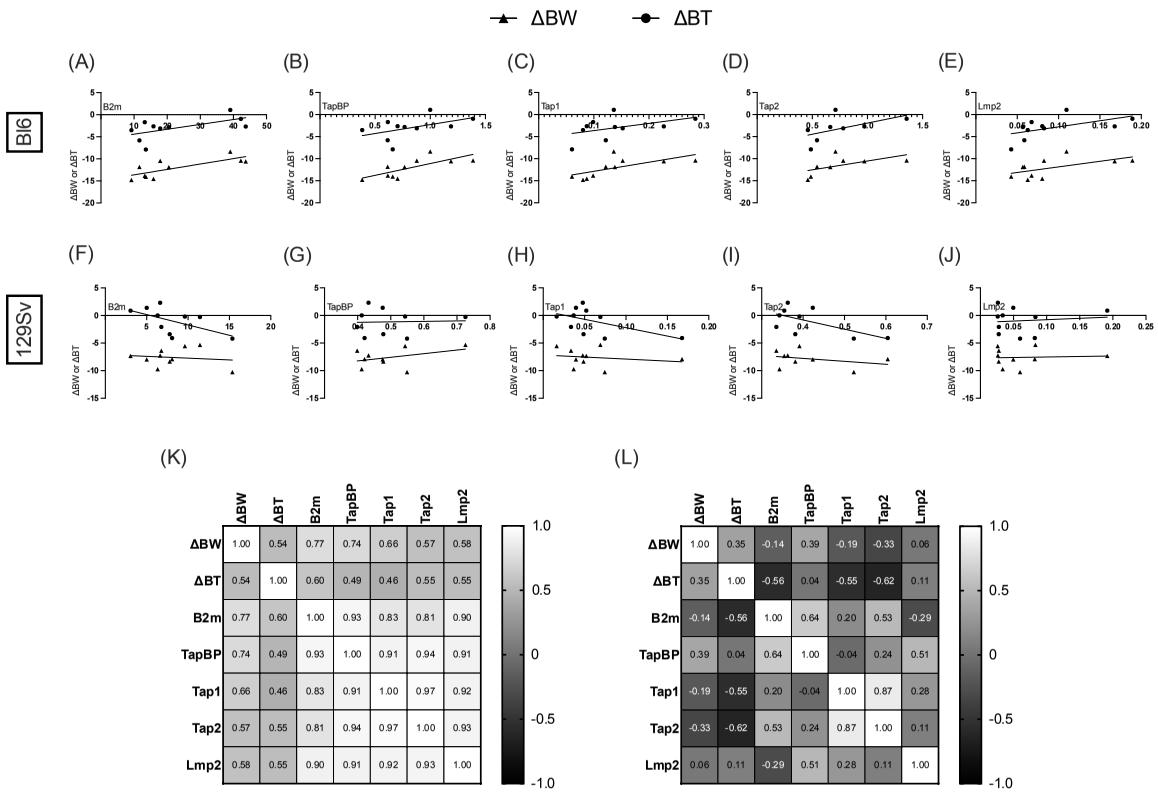

Figure 11. Correlation of MHC-I pathway gene expressions with bodyweight (ΔBW) and temperature (ΔBT) change in olfactory bulb. Pearson correlation of ΔBW and ΔBT with *β2m* (A), *Tapbp* (B), *Tap1* (C), *Tap2* (D), and *Lmp2* (E) in Bl6 mice. Pearson correlation of ΔBW and ΔBT with *β2m* (F), *Tapbp* (G), *Tap1* (H), *Tap2* (I), and *Lmp2* (J) in 129Sv mice. Heatmap of Pearson correlation coefficients between ΔBW, ΔBT, and MHC-I-pathway gene expressions in Bl6 (K) and 129Sv (L) mice.

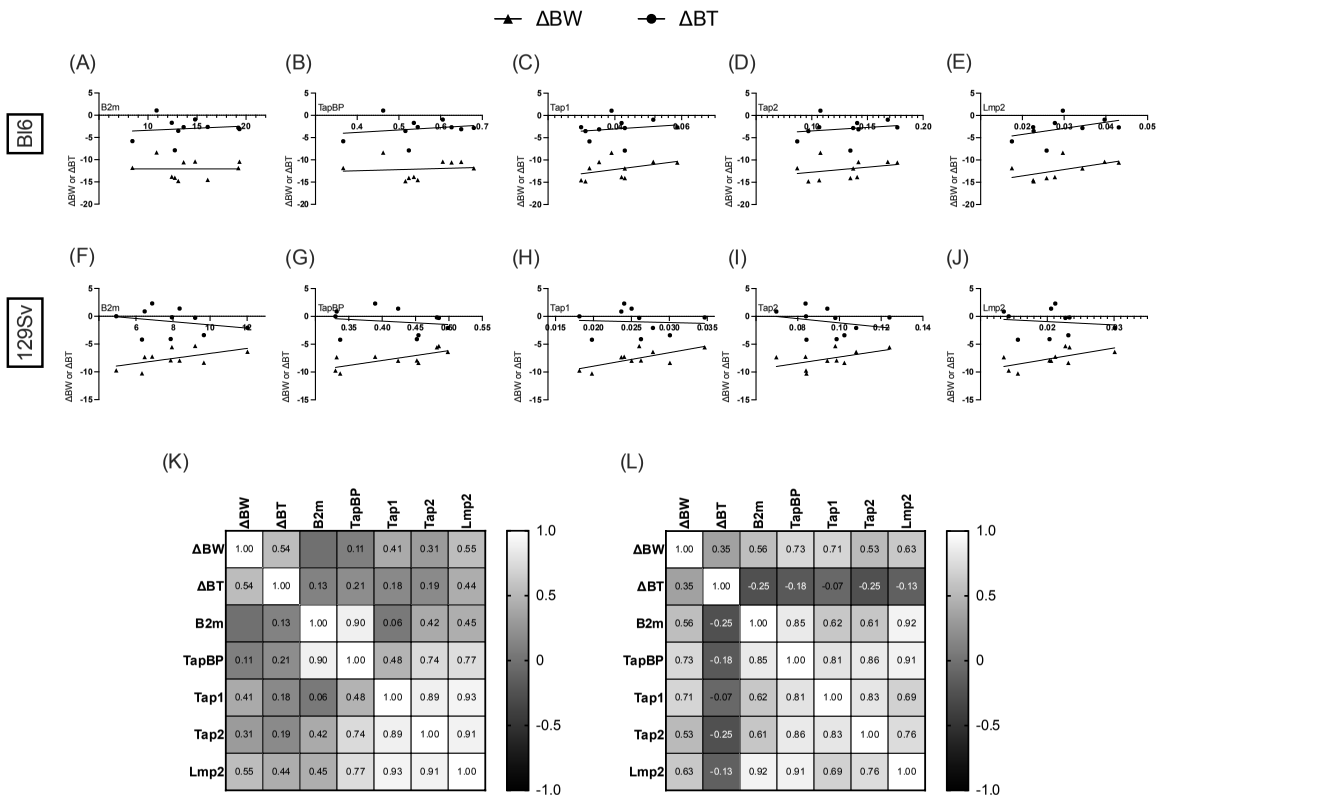

Figure 12. Correlation of MHC-I pathway gene expressions with bodyweight (ΔBW) and temperature (ΔBT) change in frontal cortex. Pearson correlation of ΔBW and ΔBT with *β2m* (A), *Tapbp* (B), *Tap1* (C), *Tap2* (D), and *Lmp2* (E) in Bl6 mice. Pearson correlation of ΔBW and ΔBT with *β2m* (F), *Tapbp* (G), *Tap1* (H), *Tap2* (I), and *Lmp2* (J) in 129Sv mice. Heatmap of Pearson correlation coefficients between ΔBW, ΔBT, and MHC-I-pathway gene expressions in Bl6 (K) and 129Sv (L) mice.

3. HFD-induced differences in metabolite profile (Paper III)

3.1. Body weight dynamics, food and water intake

Bl6 and 129Sv mice were fed HFD or control diet (Figure 13K) for 9 weeks. Food and water consumption and body mass of each animal was recorded weekly. The initial body weight of all mice was approximately the same in all four groups. During the 9-week study period, the body weight gain of Bl6 mice fed with HFD did not differ from that of control diet. It means that weekly body weight dynamics of HFD-fed mice followed the same pattern as in control animals (Figure 13A). HFD-fed 129Sv mice began to weigh significantly more than control diet mice starting from the second week of dietary exposure (Figure 13D).

Food and water consumption was measured by subtracting the mass (g) or volume (mL) of remaining food and water from the initial food and water mass or volume provided to each cage weekly and was corrected for the number of animals per cage. Food intake amount in HFD-fed 129Sv and Bl6 mice was significantly lower than in control chow-fed mice (Figure 13B,E). Water intake did not differ between HFD and control diet groups (Figure 13C,F).

Body weight and food and water intake was compared between strains by calculating the area under the curve (AUC). Differences among groups were assessed by two-way ANOVA (strain × diet) followed by Bonferroni post hoc test. For body weight, two-way ANOVA yielded a significant strain-by-diet interaction effect ($F_{(1, 54)} = 6.21$, $p = 0.02$). Comparison of groups demonstrated that AUC of body weight was significantly higher in HFD-fed 129Sv mice compared with 129Sv control mice (Figure 13G). The effect of food intake was also significant for strain ($F_{(1, 8)} = 17.56$, $p = 0.003$). Food intake of HFD-fed 129Sv mice was significantly lower compared with their control counterparts (Figure 13H). No significant difference was detected in water consumption between groups (Figure 13I).

Furthermore, two-way ANOVA demonstrated significant increase in 9-week body weight change (in %) between the HFD and control-diet-fed 129Sv mice (diet: $F_{(1, 54)} = 23.45$, $p < 0.0001$; strain: $F_{(1, 54)} = 2.09$, $p = 0.15$; strain × diet: $F_{(1, 54)} = 3.81$, $p = 0.056$). The 9-week weight gain of Bl6 mice fed with HFD was also slightly higher compared with their control counterparts; however, it did not reach statistical significance level (Figure 13J).

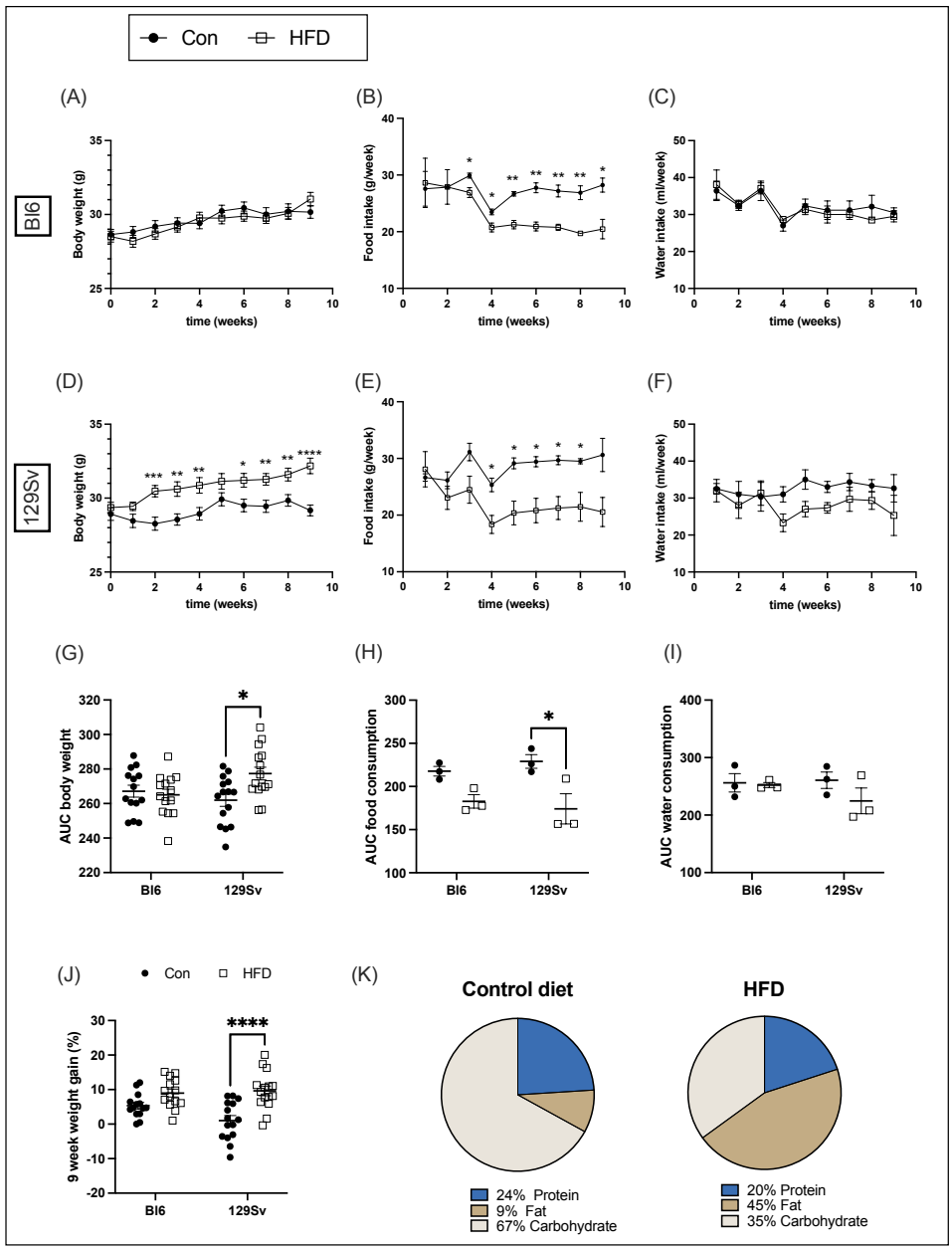

Figure 13. Effects of HFD on body weight and food and water intake in Bl6 and 129Sv mice. Weekly body weight measurements of Bl6 (A) and 129Sv (D) mice during 9 weeks of HFD experiment. Weekly measurements of food (B,E) and water (C,F) intake of Bl6 (B,C) and 129Sv (E,F) mice. AUC of body weight (G), food (H), and water (I) intake. (J) Nine-week weight gain. (K) Macronutrient content of control diet and HFD. Data are expressed as mean values ± SEM. *$p \leq 0.05$, **$p \leq 0.01$, ***$p \leq 0.001$, ****$p \leq 0.0001$ (diet effect).

3.2. Impact of HFD on locomotor activity

Open-field testing was conducted at the beginning of dietary intervention and 9 weeks later. Locomotor activity was recorded for 24 h in phenotyper cages. The open-field arena was virtually divided into central, peripheral, and food zones (Figure 14Y). Total distance traveled in the whole arena and the time spent in the center and food zone were recorded and divided into light and dark cycles. Locomotor data was $\log_2$-transformed prior to repeated-measures ANOVA (time × diet) or two-way ANOVA (stain × diet) analyzes to make the data correspond to normal distribution.

We first examined whether there are differences between day 1 and week 9 open-field testing. Control-diet-fed Bl6 mice tended to spend less time in the center and in the food zone on week 9 compared with day 1 (Figure 14B,C). HFD-fed Bl6 mice spent significantly less time in the food zone compared with their control counterparts on day 1 and on week 9 (time: $F_{(1, 20)} = 6.98$, $p = 0.02$; diet: $F_{(1, 22)} = 15.05$, $p = 0.0008$; Figure 14C). Open-field activity of 129Sv mice was significantly reduced on week 9 compared with total distance traveled on day 1 in both control and HFD groups. During the 24 h cycle, HFD-fed 129Sv mice displayed a significant suppression of locomotor activity in the whole arena on day 1 and at week 9 (time: $F_{(1, 21)} = 28.86$, $p < 0.0001$; diet: $F_{(1, 21)} = 19.81$, $p = 0.0002$; Figure 14D). Interestingly, these HFD-fed mice displayed higher anxiety-like behavior as they spent significantly less time in the center zone compared with control-diet-fed 129Sv mice (time: $F_{(1, 21)} = 11.05$, $p = 0.003$; diet: $F_{(1, 21)} = 13.19$, $p = 0.002$; Figure 14E) on week 9.

Comparison of Bl6 and 129Sv strains revealed significant differences in total distance traveled and time spent in the center zone between HFD-fed mice on day 1 (Figure 14G,H) and on week 9 (Figure 14J,K). More precisely, HFD-fed Bl6 mice traveled a greater distance in the whole arena (day 1 – strain: $F_{(1, 43)} = 27.29$, $p < 0.0001$, diet: $F_{(1, 43)} = 5.46$, $p = 0.02$; week 9 – strain: $F_{(1, 43)} = 58.73$, $p < 0.0001$, diet: $F_{(1, 43)} = 6.93$, $p = 0.01$) as well as spending more time in the center zone (day 1 – strain: $F_{(1, 43)} = 13.48$, $p = 0.0007$; week 9 – strain: $F_{(1, 44)} = 17.24$, $p = 0.0001$, diet: $F_{(1, 44)} = 6.95$, p = 0.01, interaction: $F_{(1, 44)} = 5.94$, $p = 0.02$) compared with HFD-fed 129Sv mice. Bl6 control mice spent significantly more time in the food zone compared with 129Sv control mice on day 1 (strain: $F_{(1, 42)} = 18.18$, $p = 0.0001$, diet: $F_{(1, 42)} = 15.93$, $p = 0.0003$; Figure 14I) and on week 9 (strain: $F_{(1, 44)} = 13.77$, $p = 0.0006$, diet: $F_{(1, 44)} = 8.19$, $p = 0.006$; Figure 14L).

When dividing the 24 h cycle into light/dark periods, differences in open-field activity between strains were more distinct in the light phase. Regardless of diet, Bl6 mice traveled greater distances and spent more time in the center zone on day 1 (Figure 14M,N) and at week 9 (Figure 14S,T) in the light phase. These differences were no longer evident in the dark phase on day 1 (Figure 14P,Q). However, on week 9, Bl6 mice traveled greater distances in the whole arena compared with 129Sv mice (strain: $F_{(1, 44)} = 39.33$, $p < 0.0001$) in the dark phase (Figure 14V), regardless of diet. Furthermore, on week 9, HFD-fed 129Sv

mice spent significantly less time in the center zone compared with HFD-fed Bl6 mice (strain: $F_{(1, 44)} = 9.13$, $p = 0.004$; diet: $F_{(1, 44)} = 5.65$, $p = 0.02$) in the dark phase (Figure 14W).

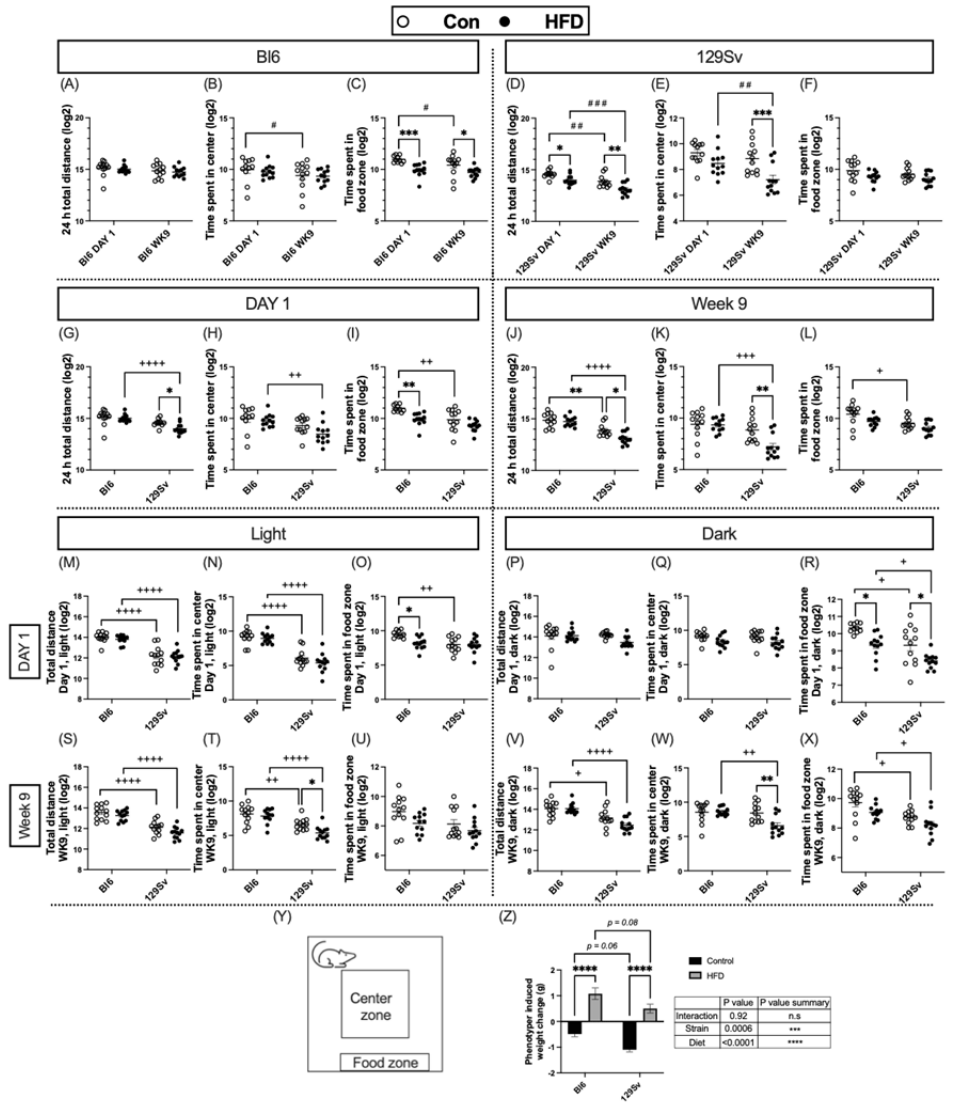

Figure 14. HFD impact on locomotor parameters (Log_2 values, data expressed as mean ± SEM). Bl6: Total distance traveled in 24 h (A), time spent in center (B) and food (C) zone day 1 vs. week 9. 129Sv: Total distance traveled in 24 h (D), time spent in center (E) and food (F) zone day 1 vs. week 9. At the beginning of dietary intervention: Total distance traveled in 24 h (G), time spent in center (H) and food (I) zone Bl6 vs. 129Sv. Week 9 of dietary intervention: Total distance traveled in 24 h (J), time spent in center (K) and food (L) zone Bl6 vs. 129Sv. Total distance traveled at day 1 (M) and week 9 (S) at lights on period. Total distance traveled on day 1 (P) and week 9 (V) at dark period. Time spent at the center zone on day 1 (N) and week 9 (T) at lights on period.

Time spent at the center zone on day 1 (Q) and week 9 (W) at dark period. Time spent at the food zone on day 1 (O) and week 9 (U) at lights on period. Time spent at the food zone on day 1 (R) and week 9 (X) at dark period. (Y) Representation of phenotyper test arena indicating the location of defined zones of interest including food and water zone and center zone. (Z) Weight change (g) of Bl6 and 129Sv mice induced by week 9 phenotyper testing. *$p \leq 0.05$, **$p \leq 0.01$, ***$p \leq 0.001$, ****$p \leq 0.0001$ (diet effect), + $p \leq 0.05$, ++ $p \leq 0.01$, +++ $p \leq 0.001$, ++++ $p \leq 0.0001$ (strain effect). # $p \leq 0.05$, ## $p \leq 0.01$, ### $p \leq 0.001$ (time effect).

When dividing the 24 h cycle into hourly data, clearly different motor responses between Bl6 and 129Sv emerged within the 2 h of behavioral testing (Supplementary Figure S1, paper III). On the first day of the diet, total distance traveled and time spent in the center zone were significantly lower in 129Sv mice compared with Bl6 mice regardless of diet. In addition, 129Sv mice fed HFD spent significantly less time in the center zone than their respective control counterparts during the first hour. At week 9, the total distance traveled remained lower in 129Sv mice compared with Bl6 mice during the first 3 h. However, during the first hour, we observed an interesting HFD-induced motor suppression in 129Sv mice, as HFD-fed mice traveled significantly shorter distances compared with 129Sv mice fed the control diet. At week 9, 129Sv mice also spent significantly less time in the center zone, but this difference was only evident in the first hour. Similar to day 1, 129Sv mice fed with HFD spent significantly less time in the center zone than their corresponding control mice in the first hour.

At week 9, the body weight of Bl6 and 129Sv mice was measured before and after the phenotyper trial. We observed an interesting strain and diet effect in the animals' weight (diet: $F_{(1, 43)} = 13.79$, $p = 0.0006$; strain: $F_{(1, 43)} = 98.78$, $p < 0.0001$). Bl6 and 129Sv mice fed with standard diet exhibited weight loss, whereas mice fed with HFD exhibited weight gain. Phenotyper testing induced greater weight loss in 129Sv (-1.10 ± 0.08 g) mice in the control group compared with Bl6 (-0.49 ± 0.10 g) control mice (Figure 14Z). Both strains in HFD groups gained significant weight compared with their control counterparts. However, the weight gain was greater in Bl6 mice in the HFD (1.08 ± 0.23 g) group compared with HFD-fed 129Sv mice (0.50 ± 0.17 g). This could mean that 129Sv mice placed in social isolation conditions could be in a greater state of stress.

Subsequently a Pearson correlation coefficient matrix was created to measure the relationships between the locomotor parameters and 9-week body weight change. In Bl6 mice, 9-week body weight change was positively correlated with total distance traveled in the light phase ($r = 0.61$, $p = 0.04$) and time spent in the center zone in the light phase ($r = 0.65$, $p = 0.02$) (Figure 15A). On the contrary, in 129Sv mice, 9-week body weight change was negatively correlated with total distance traveled in 24 h ($r = -0.60$, $p = 0.04$), in light phase ($r = -0.66$, $p = 0.02$), time spent in the center zone in light phase ($r = -0.65$, $p = 0.02$), and time spent in the food zone in light phase ($r = -0.59$, $p = 0.04$) (Figure 15B).

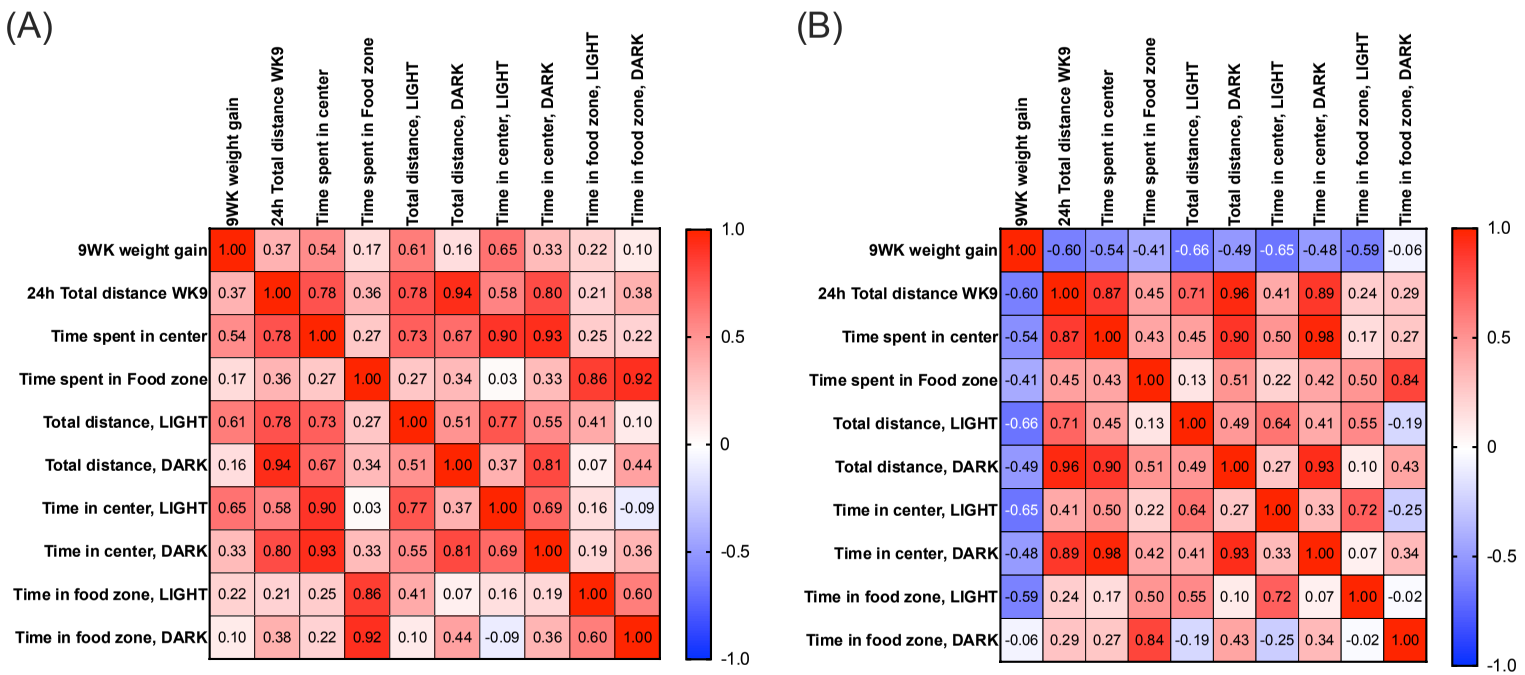

Figure 15. Heat-map of Pearson correlation coefficients between 9-week weight gain and locomotor parameters in (A) Bl6 and (B) 129Sv HFD-fed mice.

3.3. Metabolic Changes Induced by HFD

We next examined the metabolic response to a HFD in Bl6 and 129Sv mouse strains. Metabolites from plasma were measured using the AbsoluteIDQ p180 kit (Biocrates Life Sciences AG, Innsbruck, Austria), which detects 186 metabolites in 5 compound classes (acylcarnitines, amino acids, biogenic amines, hexoses, and phospho- and sphingolipids).

3.3.1. Acylcarnitine profile

Plasma levels of short-chain acylcarnitines (SCACs) in HFD-fed Bl6 and 129Sv mice compared with the corresponding controls were significantly lower (Figure 16F). More specifically HFD induced a significant decrease in the concentrations of C0, C2, and C4- in Bl6 mice and C0, C2, C3, C4-, and C4:1 in 129Sv mice (Figure 16A,E). Medium-chain acylcarnitines (MCACs) remained unaffected by HFD in both strains. However, plasma levels of long-chain acylcarnitines (LCACs) were specifically altered in HFD-fed 129Sv mice compared with control-diet-fed 129Sv mice (Figure 16L). More precisely, HFD induced a significant decrease in plasma levels of C12, C12:1, C14, C14:2, C16, C16:1, C16:2, C16:2-OH, C18:1-OH, and C18:2 in 129Sv mice. In HFD-fed Bl6 mice, only the concentration of C18:2 was significantly lower compared with control-diet-fed Bl6 mice. C18 was the only acylcarnitine that exhibited HFD-induced increase in both stains (Figure 16J).

Additionally, the ratio of LCACs to free carnitine [(C16 + C18)/C0] was significantly upregulated by HFD in both strains, which reflects a higher activity of carnitine palmitoyltransferase 1 (CPT1). This ratio was significantly higher in HFD-fed 129Sv mice compared with HFD-fed Bl6 mice. Additionally, the ratio of the CPT2 [(C16:0 + C18:1)/C2] was higher in HFD-fed Bl6 and 129Sv mice compared with their respective control animals. Moreover, the ratio of dicarboxy-acylcarnitines to total acylcarnitines (total AC-DC/total AC) was significantly elevated in HFD-fed mice of both strains, indicating higher ω-oxidation of fatty acids.

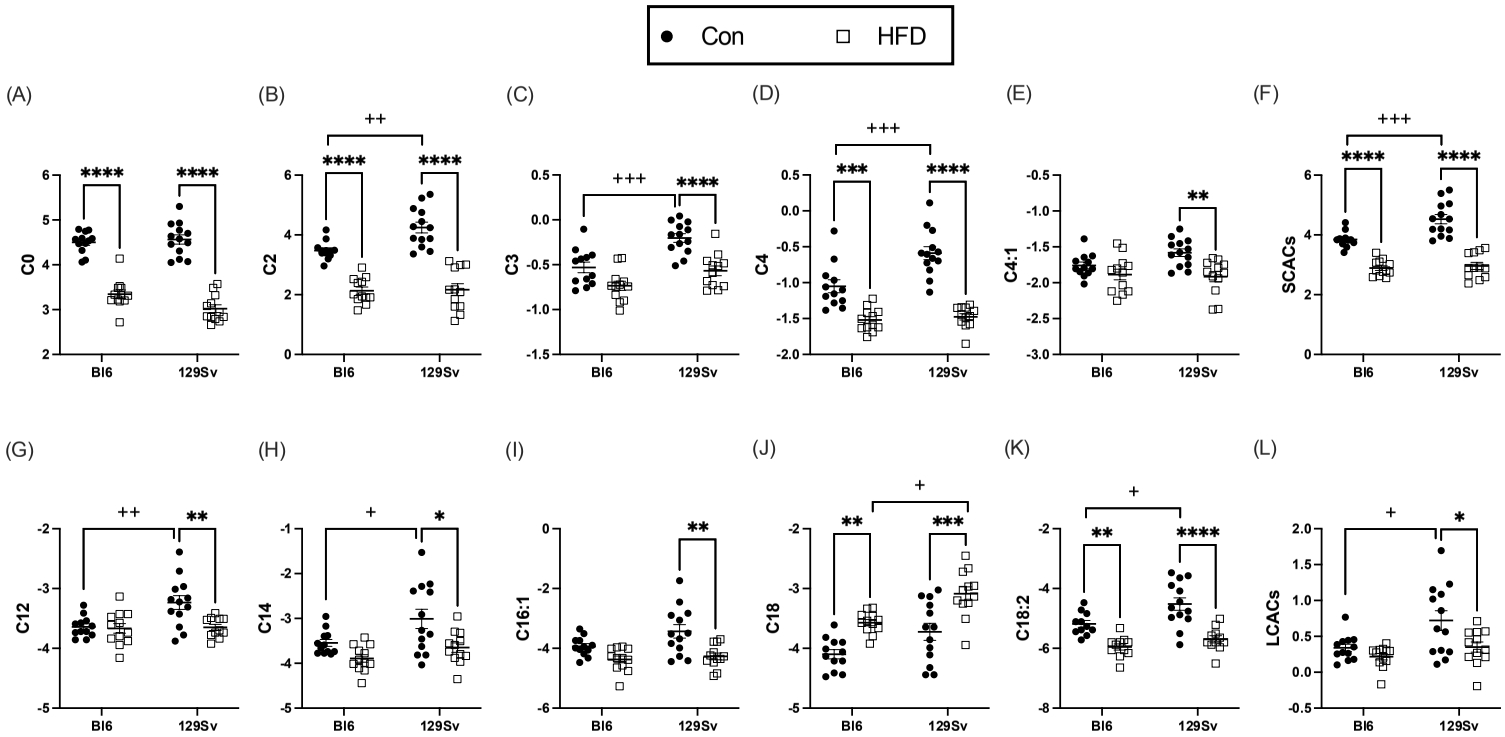

Figure 16. Effect of HFD on the level of selected acylcarnitines (Log_2 values, data expressed as mean ± SEM). The level of short-chain acylcarnitines (A) C0, (B) C2, (C) C3, (D) C4-, and (E) C4:1 and (F) the sum of SCACs. The level of long-chain acylcarnitines (G) C12, (H) C14, (I) C16:1, (J) C18, and (K) C18:2 and (L) the sum of LCACs. Two-way ANOVA (Bonferroni post hoc test): * $p \leq 0.05$, ** $p \leq 0.01$, *** $p \leq 0.001$, **** $p \leq 0.0001$ (diet effect), + $p \leq 0.05$, ++ $p \leq 0.01$, +++ $p \leq 0.001$ (strain effect).

3.3.2. Amino Acids and biogenic amines

HFD induced an increase in circulating branched-chain amino acids (BCAAs) in 129Sv mice (Figure 17A). While the BCAAs leucine (Leu) and isoleucine (Ile) showed only a trend toward being increased in HFD-fed 129Sv mice, plasma valine (Val) levels (Figure 17B) were significantly increased in HFD-fed 129Sv mice compared with 129Sv control-diet-fed mice. Additionally, HFD resulted in a significant decrease in plasma levels of the non-essential glucogenic amino acid glycine (Gly) in 129Sv mice (Figure 17C). Only the amino acid citrulline (Cit) was affected by HFD in Bl6 mice (Figure 17D). Cit was significantly elevated in HFD-fed Bl6 mice compared with their control counterparts. Furthermore, the ratio of citrulline to ornithine (Cit/Orn) was specifically increased in HFD-fed Bl6 mice (Figure 17E), possibly indicating increased ornithine transcarbamylase activity in Bl6 mice.

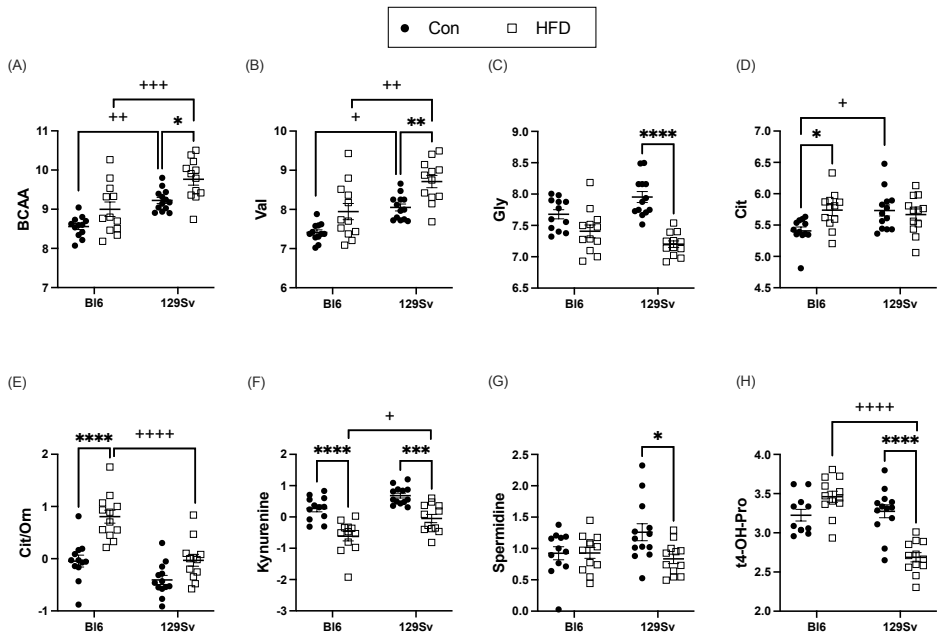

Figure 17. Effect of HFD on the level of selected amino acids and their derivatives biogenic amines (Log_2 values, data expressed as mean ± SEM). (A) sum of branched-chain amino acids (BCAAs), (B) valine (Val), (C) glycine (Gly), (D) citrulline (Cit), (E) ratio of citrulline to ornithine (Cit/Orn), (F) kynurenine, (G) spermidine, and (H) trans-4-hydroxyproline (t4-OH-Pro). Two-way ANOVA (Bonferroni post hoc test): *$p \leq 0.05$, **$p \leq 0.01$, ***$p \leq 0.001$, ****$p \leq 0.0001$ (diet effect), + $p \leq 0.05$, ++ $p \leq 0.01$, +++ $p \leq 0.001$, ++++ $p \leq 0.0001$ (strain effect).

HFD induced a significant decrease in kynurenine in both strains (Figure 17F). However, this decrease was significantly more pronounced in Bl6 mice compared with 129Sv. The ratio of kynurenine to tryptophan (Trp) was also significantly reduced after exposure to HFD in both strains, indicating decreased indole dioxygenase activity. Plasma levels of spermidine and trans-4-hydroxyproline (t4-OH-Pro) were significantly diminished in HFD-fed 129Sv compared with control mice, whereas no alterations were observed in Bl6 mice (Figure 17G,H).

3.3.3. Lipid profile

The total level of lysophosphatidylcholine acyls (LysoPCs; Figure 18A) and sphingomyelins (SMs; Figure 18D) was significantly elevated by HFD in both strains. More precisely, HFD induced an increase in LysoPCs C18:0, C18:1, C18:2, C20:3, C26:0, and C28:1 in both strains. However, LysoPC a C17:0 exhibited HFD-induced decrease in 129Sv mice (Figure 18B). SMs SM(OH) C14:1, SM(OH) C16:1, SM C16:0, SM C16:1, SM C18:0, and SM C18:1 were all significantly elevated in HFD-fed mice of both strains. However, SM (OH) C22:2 exhibited significant HFD-induced decrease in both strains (Figure 18E). Moreover, SM (OH) C22:1, SM C22:3, and SM C24:0 (Figure 18F) were specifically elevated in HFD-fed Bl6 mice compared with control-diet-fed Bl6 mice and no HFD-induced alterations were observed in 129Sv mice.

Out of 38 PC diacyls (PC aa-s), 15 were significantly elevated after HFD in both strains (Supplementary Table S1). HFD induced an increase in PC aa-s C30:0, C32:1, C34:2, and C36:4 specifically in Bl6 mice, whereas PC aa-s C42:2 and C42:5 were specifically decreased in 129Sv mice on HFD. Out of 37 PC acyl-alkyls (PC ae-s) 26 were significantly affected by HFD (Supplementary Table S1). HFD induced a significant elevation in unsaturated (UFA) PC aa-s and PC ae-s in both Bl6 and 129Sv mice (Figure 18G,H). When subdividing UFA lipids into polyunsaturated fatty acids (PUFAs) and monounsaturated fatty acids (MUFAs), the HDF-induced increase in 129Sv mice was only evident in MUFA PC ae-s and did not affect PUFA PC ae levels (Figure 18I,J). However, in Bl6 mice, both PC ae PUFAs and MUFAs were affected by HFD and were both significantly elevated. PUFAs and MUFAs of PC aa species were significantly elevated by HFD in both strains.

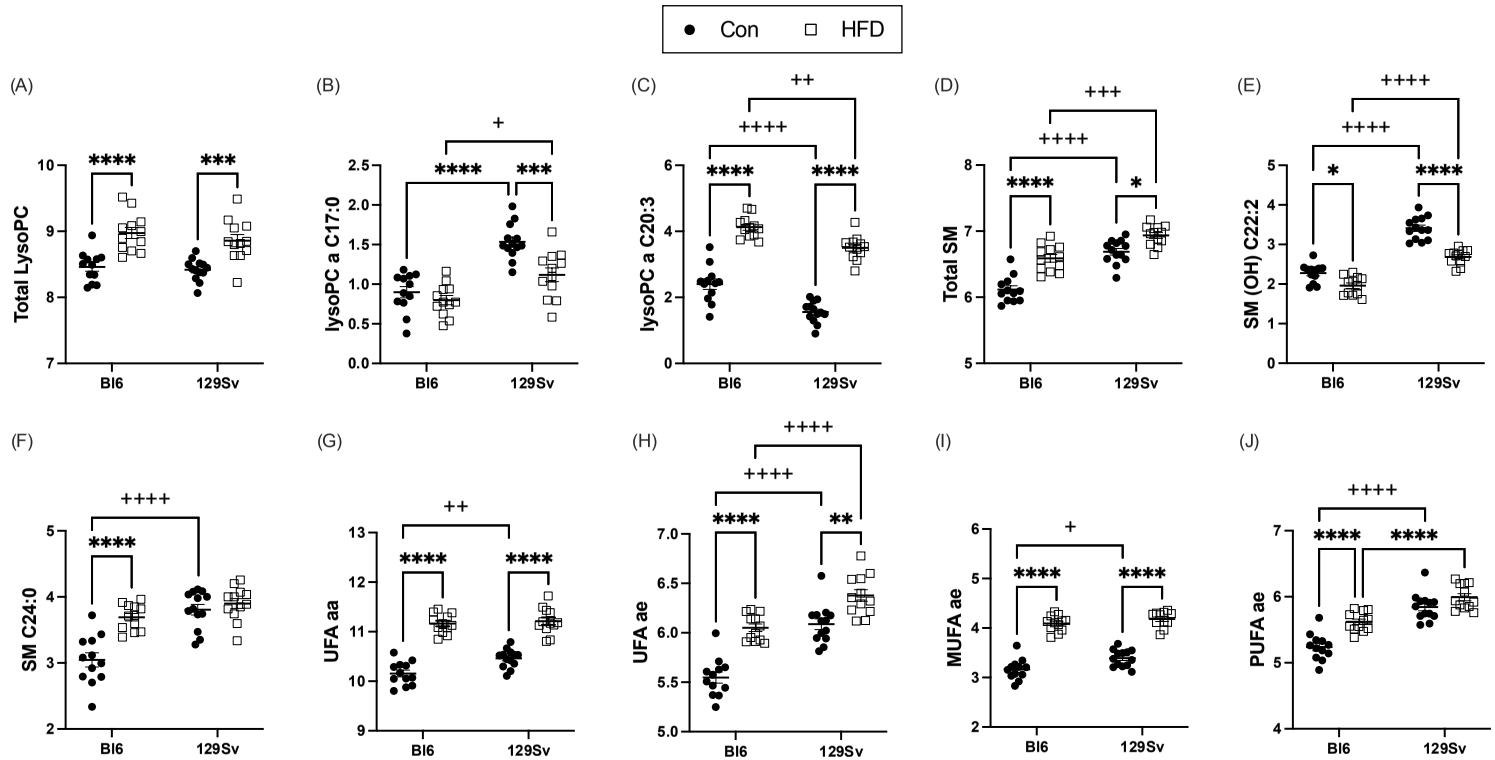

Figure 18. Effect of HFD on the level of selected lipids (Log_2 values, data expressed as mean ± SEM). (A) sum of lysoPCs, (B) lysoPC a C17:0, (C) lysoPC a C20:3, (D) sum of sphingomyelins, (E) SM (OH) C22:2, (F) SM C24:0, unsaturated (UFA) PC aa-s, (G) and PC ae-s (H), (I) monounsaturated fatty acids (MUFA) and (J) polyunsaturated fatty acids (PUFA) of PC ae species. Two-way ANOVA (Bonferroni post hoc test): *$p \leq 0.05$, **$p \leq 0.01$, ***$p \leq 0.001$, ****$p \leq 0.0001$ (diet effect), + $p \leq 0.05$, ++ $p \leq 0.01$, +++ $p \leq 0.001$, ++++ $p \leq 0.0001$ (strain effect).

3.4. Metabolite differences highlighted by GLM analysis

For the association analysis of metabolites, body weight change, and locomotor activity parameters, we used multivariate general linear model (GLM) analysis. To map out the most important differences, we used unpaired t-tests and Bonferroni correction to correct for multiple testing ($p \leq 0.00027$). Significant markers that exceeded the Bonferroni threshold were incorporated into the GLM analysis.

3.4.1. Metabolic profile differences between Bl6 and 129Sv

After applying Bonferroni correction ($p < 0.00027$), 45 metabolites remained statistically significant. The vast majority (42) were significantly higher in 129Sv mice, and only 3 were higher in Bl6 mice. These metabolites in Bl6 mice were carnosine, lysoPC a C16:1 and lysoPC a C20:3. Metabolites that were higher in 129Sv included acylcarnitine C3, BCAAs (Ile, Leu, Val), lysine (Lys), ornithine (Orn), serine (Ser), 6 PC aa-s, 19 PC ae-s, and 8 SMs (Supplementary Table S2, paper III). The following comparison of metabolites in the HFD group altered the list of significantly different markers (Supplementary Table S2, paper III). Only 26 metabolites remained significantly different after Bonferroni correction and there was a moderate shift toward the Bl6 strain. In Bl6 strain 9 and in 129Sv mice 17 metabolites were significantly higher. In Bl6 mice, carnosine, lysoPC a C16:1 and lysoPC a C20:3 remained higher, as in the case of standard diet. The metabolites included to the list of Bl6 with HFD were alpha-AAA, putrescine, t4-OH-proline, PC aa C32:1, PC aa C34:3, and SM C20:2. The list of 129Sv included 2 PC aa-s, 9 PC ae-s, and 6 SMs. The strongest markers favoring 129Sv were sphingolipids SM (OH) C14:1 and SM (OH) C22:2) (t-values in both cases > 8) (Table 9). This shows a stronger dominance of lipid metabolism in 129Sv mice compared with Bl6 mice. Although not statistically significant after the Bonferroni correction, comparison of hexoses in the HFD groups revealed significantly higher levels in Bl6 mice compared with 129Sv ($t = 3.03$, $p = 0.006$). This is possible showing the stronger impact of glucose metabolism in Bl6 mice.

Table 9. Effect of mouse strain on blood plasma levels of metabolites and locomotor parameters between standard diet groups and HFD groups.

Standard Diet				**HFD**			
	ß (95% CI)	*t*-value	*p*-value		ß (95% Cl)	*t*-value	*p*-value
total distance, light	0.76 (0.46, 1.05)	5.29	0.00003	total distance	0.81 (0.48, 1.13)	5.26	0.0001
Ile	-0.77 (-1.06, -0.49)	-5.60	0.00002	total distance, light	0.83 (0.52, 1.14)	5.67	0.00005
Leu	-0.76 (-1.06, -0.47)	-5.37	0.00003	center time	0.72 (0.34, 1.10)	4.06	0.001
Val	-0.75 (-1.05, -0.44)	-5.14	0.00004	center time, light	0.83 (0.52, 1.14)	5.78	0.00004
Carnosine	0.87 (0.64, 1.09)	7.92	< 0.00001	alpha-AAA	0.85 (0.56, 1.14)	6.24	0.00002
lysoPC a C16:1	0.81 (0.55, 1.08)	6.42	< 0.00001	Carnosine	0.81 (0.49, 1.13)	5.52	0.00007
lysoPC a C17:0	-0.83 (-1.08, -0.57)	-6.72	< 0.00001	Putrescine	0.71 (0.32, 1.10)	3.88	0.001
lysoPC a C24:0	-0.77 (-1.06, -0.48)	-5.58	0.00002	t4-OH-Pro	0.79 (0.46, 1.13)	5.07	0.0001
PC aa C30:2	-0.77 (-1.06, -0.48)	-5.54	0.00002	lysoPC a C16:1	0.71 (0.32, 1.10)	3.89	0.001
PC aa C36:0	-0.73 (-1.04, -0.42)	-4.94	0.00007	lysoPC a C20:3	0.71 (0.32, 1.10)	3.86	0.002
PC aa C36:2	-0.85 (-1.09, -0.60)	-7.26	< 0.00001	PC aa C32:1	0.70 (0.31, 1.10)	3.85	0.002
PC aa C40:2	-0.74 (-1.04, -0.43)	-4.98	0.00006	PC aa C34:3	0.81 (0.49, 1.13)	5.40	0.00007
PC aa C40:5	-0.77 (-1.06, -0.48)	-5.47	0.00002	PC ae C32:1	-0.77 (-1.12, -0.41)	-4.61	0.0003

Standard Diet				HFD			
	ß (95% CI)	*t*-value	*p*-value		ß (95% Cl)	*t*-value	*p*-value
PC aa C40:6	-0.74 (-1.05, -0.44)	-5.05	0.00005	PC ae C34:2	-0.84 (-1.14, -0.54)	-6.04	0.00002
PC ae C30:2	-0.85 (-1.09, -0.61)	-7.42	< 0.00001	PC ae C36:2	-0.85 (-1.14, -0.56)	-6.24	0.00002
PC ae C32:1	-0.80 (-1.07, -0.53)	-6.09	< 0.00001	PC ae C36:5	-0.75 (-1.11, -0.38)	-4.33	0.0006
PC ae C34:0	-0.81 (-1.08, -0.55)	-6.35	< 0.00001	PC ae C38:2	-0.80 (-1.13, -0.48)	-5.25	0.0001
PC ae C34:2	-0.74 (-1.04, -0.43)	-5.03	0.00006	PC ae C38:6	-0.85 (-1.14, -0.56)	-6.31	0.00001
PC ae C34:3	-0.88 (-1.10, -0.66)	-8.50	< 0.00001	PC ae C40:6	-0.82 (-1.13, -0.50)	-5.50	0.00006
PC ae C36:1	-0.80 (-1.07, -0.53)	-6.10	< 0.00001	SM (OH) C14:1	-0.87 (-1.14, -0.59)	-6.76	< 0.00001
PC ae C36:2	-0.92 (-1.10, -0.74)	-10.61	< 0.00001	SM (OH) C16:1	-0.85 (-1.14, -0.57)	-6.32	0.00001
PC ae C38:2	-0.92 (-1.10, -0.75)	-11.09	< 0.00001	SM (OH) C22:1	-0.81 (-1.13, -0.49)	-5.37	0.00008
PC ae C38:3	-0.83 (-1.08, -0.58)	-6.85	< 0.00001	SM (OH) C22:2	-0.85 (-1.14, -0.55)	-6.12	0.00002
PC ae C38:4	-0.87 (-1.09, -0.65)	-8.07	< 0.00001	SM C16:0	-0.74 (-1.11, -0.38)	-4.31	0.0006
PC ae C38:6	-0.87 (-1.09, -0.65)	-8.14	< 0.00001	SM C16:1	-0.83 (-1.14, -0.52)	-5.72	0.00004
PC ae C40:2	-0.84 (-1.09, -0.60)	-7.20	< 0.00001	SM C20:2	0.81 (0.49, 1.13)	5.42	0.00007
PC ae C40:4	-0.78 (-1.07, -0.50)	-5.77	0.00001				

Standard Diet				HFD			
	ß (95% CI)	*t*-value	*p*-value		ß (95% Cl)	*t*-value	*p*-value
PC ae C40:5	-0.82 (-1.08, -0.56)	-6.63	< 0.00001				
PC ae C40:6	-0.87 (-1.09, -0.65)	-8.16	< 0.00001				
PC ae C42:5	-0.82 (-1.08, -0.56)	-6.56	< 0.00001				
SM (OH) C14:1	-0.90 (-1.10, -0.70)	-9.26	< 0.00001				
SM (OH) C16:1	-0.85 (-1.09, -0.60)	-7.25	< 0.00001				
SM (OH) C22:1	-0.92 (-1.10, -0.74)	-10.55	< 0.00001				
SM (OH) C22:2	-0.92 (-1.10, -0.75)	-11.04	< 0.00001				
SM C16:0	-0.86 (-1.09, -0.63)	-7.80	< 0.00001				
SM C16:1	-0.90 (-1.10, -0.69)	-9.23	< 0.00001				
SM C24:0	-0.81 (-1.07, -0.55)	-6.40	< 0.00001				
SM C24:1	-0.85 (-1.09, -0.62)	-7.52	< 0.00001				

Statistically significant regression coefficients (ß), confidence intervals (CI) and t- and p-values (derived from GLM analysis) of log_2-transformed variables in standard diet and HFD groups.

GLM confirmed a significant main effect ($F_{(1, 16)}$ = 908.5; p = 0.03) of mouse strain on the levels of several variables in the standard diet group as well as in the HFD group ($F_{(1, 16)}$ = 5269.3; p = 0.01). Significant biomarkers in the GLM model are highlighted in Table 9. Significant GLM model under basal conditions included total distance traveled in light phase, BCAAs (Ile, Leu, and Val), carnosine, 3 lysoPCs, 6 PC aa-s, 16 PC ae-s, and 8 SMs. Significant GLM model under HFD included total distance traveled (light and dark), time spent in center (in light period), 4 biogenic amines (alpha-AAA, carnosine, putrescine, and t4-OH-Pro), 2 lysoPCs, 2 PC aa-s, 7 PC ae-s, and 7 SMs.

In both control- and HFD-fed conditions, the groups showed significantly different metabolite levels between Bl6 and 129Sv, including carnosine, lysoPC a C16:1, 6 PC ae-s (PC ae C32:1, PC ae C34:2, PC ae C36:2, PC ae C38:2, PC ae C38:6 and PC ae C40:6), 6 SMs (SM (OH) C14:1, SM (OH) C16:1, SM (OH) C22:1, SM (OH) C22:2, SM C16:0, and SM C16:1) and total distance traveled in light period.

3.4.2. HFD-induced metabolic profile changes in Bl6 Mice

GLM confirmed a significant main effect ($F_{(1, 20)}$ = 360.13, p = 0.04) of diet on metabolite levels in Bl6 mice. The final GLM model retained 47 metabolites: 5 acylcarnitines (C0, C2, C4-, C18 and C18:2), 1 biogenic amine (kynurenine), 4 lysoPCs, 13 PC aa-s, 16 PC ae-s, and 8 SMs (Table 10). The majority of metabolites were increased due to HFD. The exceptions were acylcarnitines C0, C2, C4-, C18:2, and kynurenine, being decreased with HFD. The strongest associations (ß > 0.90) in Bl6 were established for C0, 5 PC aa-s, 4 ae-s, and SM C16:0.

Table 10. Effect of HFD on metabolite levels among Bl6 and 129Sv mice.

Bl6				129Sv			
	ß (ß 95% CI)	*t*-value	*p*-value		ß (ß 95% CI)	*t*-value	*p*-value
C0	0.91 (0.72, 1.10)	9.90	< 0.00001	9-week weight gain (%)	-0.60 (-1.02, -0.18)	-3.01	0.008
C2	0.89 (0.69, 1.10)	8.94	< 0.00001	C0	0.94 (0.76, 1.12)	11.14	< 0.00001
C4	0.70 (0.36, 1.03)	4.36	0.0003	C2	0.85 (0.57, 1.13)	6.45	< 0.00001
C18	-0.77 (-1.07, -0.47)	-5.34	0.00003	C3	0.68 (0.30, 1.07)	3.74	0.002
C18:2	0.75 (0.43, 1.06)	5.00	0.00007	C4	0.89 (0.65, 1.13)	7.90	< 0.00001
Kynurenine	0.73 (0.41, 1.05)	4.73	0.0001	C14:2	0.77 (0.43, 1.11)	4.77	0.0002
lysoPC a C18:0	-0.78 (-1.07, -0.48)	-5.52	0.00002	C18:2	0.78 (0.45, 1.11)	5.04	0.0001
lysoPC a C18:1	-0.88 (-1.10, -0.66)	-8.40	< 0.00001	Gly	0.83 (0.53, 1.12)	5.85	0.00002
lysoPC a C20:3	-0.89 (-1.10, -0.67)	-8.58	< 0.00001	Kynurenine	0.64 (0.23, 1.05)	3.34	0.004
lysoPC a C26:0	-0.70 (-1.03, -0.36)	-4.34	0.0003	t4-OH-Pro	0.76 (0.41, 1.10)	4.63	0.0003
PC aa C28:1	-0.83 (-1.09, -0.57)	-6.71	< 0.00001	lysoPC a C18:0	-0.75 (-1.10, -0.40)	-4.58	0.0003
PC aa C30:2	-0.88 (-1.10, -0.66)	-8.43	< 0.00001	lysoPC a C18:1	-0.88 (-1.13, -0.63)	-7.49	< 0.00001

Bl6				129Sv			
	ß (ß 95% CI)	*t*-value	*p*-value		ß (ß 95% CI)	*t*-value	*p*-value
PC aa C32:1	-0.81 (-1.08, -0.53)	-6.14	< 0.00001	lysoPC a C20:3	-0.94 (-1.12, -0.75)	-10.60	< 0.00001
PC aa C34:1	-0.96 (-1.09, -0.82)	-14.97	< 0.00001	lysoPC a C26:0	-0.58 (-1.01, -0.15)	-2.88	0.01
PC aa C34:2	-0.76 (-1.07, -0.46)	-5.30	0.00003	lysoPC a C28:1	-0.82 (-1.12, -0.53)	-5.84	0.00003
PC aa C36:1	-0.97 (-1.08, -0.86)	-17.93	< 0.00001	PC aa C28:1	-0.89 (-1.13, -0.65)	-7.87	< 0.00001
PC aa C36:2	-0.95 (-1.09, -0.82)	-14.31	< 0.00001	PC aa C30:2	-0.93 (-1.13, -0.73)	-9.97	< 0.00001
PC aa C36:3	-0.94 (-1.10, -0.78)	-12.20	< 0.00001	PC aa C32:3	-0.80 (-1.12, -0.48)	-5.33	0.00007
PC aa C38:0	-0.71 (-1.04, -0.38)	-4.49	0.0002	PC aa C34:1	-0.86 (-1.13, -0.60)	-6.85	< 0.00001
PC aa C38:3	-0.92 (-1.10, -0.75)	-10.87	< 0.00001	PC aa C36:1	-0.96 (-1.11, -0.80)	-13.06	< 0.00001
PC aa C38:4	-0.68 (-1.02, -0.34)	-4.19	0.0005	PC aa C36:2	-0.94 (-1.12, -0.77)	-11.50	< 0.00001
PC aa C38:5	-0.67 (-1.01, -0.32)	-4.00	0.0007	PC aa C36:3	-0.92 (-1.13, -0.71)	-9.43	< 0.00001
PC aa C40:3	-0.69 (-1.03, -0.36)	-4.30	0.0004	PC aa C38:1	-0.77 (-1.11, -0.44)	-4.87	0.0002
PC ae C30:2	-0.79 (-1.08, -0.51)	-5.81	0.00001	PC aa C38:3	-0.92 (-1.13, -0.72)	-9.73	< 0.00001
PC ae C32:1	-0.76 (-1.06, -0.45)	-5.17	0.00005	PC aa C38:5	-0.77 (-1.11, -0.44)	-4.87	0.0002

Bl6				129Sv			
	ß (ß 95% CI)	*t*-value	*p*-value		ß (ß 95% CI)	*t*-value	*p*-value
PC ae C32:2	-0.91 (-1.10, -0.72)	-10.08	< 0.00001	PC aa C40:3	-0.62 (-1.03, -0.20)	-3.12	0.007
PC ae C34:1	-0.95 (-1.10, -0.80)	-13.15	< 0.00001	PC aa C40:5	-0.81 (-1.12, -0.50)	-5.55	0.00004
PC ae C34:3	-0.80 (-1.08, -0.52)	-5.98	< 0.00001	PC ae C30:2	0.84 (0.56, 1.13)	6.24	0.00001
PC ae C36:0	-0.84 (-1.09, -0.59)	-6.97	< 0.00001	PC ae C32:1	-0.72 (-1.09, -0.35)	-4.10	0.0008
PC ae C36:1	-0.96 (-1.09, -0.84)	-16.05	< 0.00001	PC ae C32:2	-0.87 (-1.13, -0.62)	-7.18	< 0.00001
PC ae C36:2	-0.73 (-1.05, -0.41)	-4.79	0.0001	PC ae C34:1	-0.87 (-1.13, -0.60)	-6.92	< 0.00001
PC ae C36:3	-0.89 (-1.10, -0.68)	-8.85	< 0.00001	PC ae C34:3	-0.73 (-1.09, -0.37)	-4.30	0.0006
PC ae C36:4	-0.71 (-1.04, -0.38)	-4.48	0.0002	PC ae C36:0	-0.74 (-1.10, -0.39)	-4.42	0.0004
PC ae C38:1	-0.83 (-1.09, -0.57)	-6.58	< 0.00001	PC ae C36:1	-0.86 (-1.13, -0.58)	-6.65	< 0.00001
PC ae C38:3	-0.85 (-1.10, -0.61)	-7.31	< 0.00001	PC ae C36:3	-0.75 (-1.10, -0.40)	-4.58	0.0003
PC ae C38:4	-0.67 (-1.01, -0.32)	-4.00	0.0007	PC ae C36:5	-0.74 (-1.10, -0.38)	-4.39	0.0005
PC ae C38:5	-0.91 (-1.10, -0.71)	-9.74	< 0.00001	PC ae C38:1	-0.79 (-1.11, -0.46)	-5.15	0.0001
PC ae C40:5	-0.71 (-1.04, -0.38)	-4.50	0.0002	PC ae C38:2	0.91 (0.69, 1.13)	8.81	< 0.00001

Bl6				129Sv			
	ß (ß 95% CI)	*t*-value	*p*-value		ß (ß 95% CI)	*t*-value	*p*-value
PC ae C42:2	-0.81 (-1.08, -0.54)	-6.16	< 0.00001	PC ae C38:3	-0.83 (-1.13, -0.53)	-5.95	0.00002
SM (OH) C14:1	-0.83 (-1.09, -0.57)	-6.72	< 0.00001	PC ae C38:5	-0.88 (-1.13, -0.63)	-7.40	< 0.00001
SM (OH) C16:1	-0.71 (-1.04, -0.39)	-4.54	0.0002	PC ae C40:4	0.88 (0.62, 1.13)	7.26	< 0.00001
SM C16:0	-0.92 (-1.10, -0.74)	-10.49	< 0.00001	PC ae C42:0	0.77 (0.43, 1.11)	4.84	0.0002
SM C16:1	-0.80 (-1.08, -0.52)	-6.00	< 0.00001	PC ae C42:2	-0.76 (-1.10, -0.42)	-4.68	0.0003
SM C18:0	-0.87 (-1.10, -0.64)	-7.81	< 0.00001	SM (OH) C14:1	-0.90 (-1.13, -0.67)	-8.24	< 0.00001
SM C18:1	-0.70 (-1.04, -0.37)	-4.44	0.0002	SM (OH) C16:1	-0.88 (-1.13, -0.63)	-7.52	< 0.00001
SM C22:3	-0.66 (-1.01, -0.31)	-3.95	0.0008	SM (OH) C22:2	0.89 (0.65, 1.13)	7.89	< 0.00001
SM C24:0	-0.75 (-1.06, -0.44)	-5.06	0.00006	SM C16:0	-0.94 (-1.12, -0.76)	-11.14	< 0.00001
				SM C16:1	-0.76 (-1.10, -0.41)	-4.65	0.0003
				SM C18:1	-0.78 (-1.11, -0.44)	-4.94	0.0001

Statistically significant regression coefficients (ß), confidence intervals (CI) and t- and p-values (derived from GLM analysis) of log_2-transformed metabolite levels.

3.4.3. HFD-induced metabolic profile changes in 129Sv Mice

GLM confirmed a significant main effect ($F_{(1, 16)}$ = 811.11, p = 0.03) of diet in 129Sv mice. Similar to Bl6 mice, most HFD-induced alterations were observed in the lipid profile. The final GLM model retained 9-week weight gain and 48 metabolites: 6 acylcarnitines (C0, C2, C3, C4-, C14.2, C18:2), 1 amino acid (Gly), 2 biogenic amines (kynurenine and t4-OH-Pro), 5 lysoPCs, 13 PC aa-s, 16 PC ae-s, and 6 SMs (Table 10). The majority of metabolites were increased due to HFD. The exceptions were acylcarnitines C0, C2, C3, C4-, C14:2, C18:2, amino acids and their derivatives Gly, t4-OH-Pro, kynurenine and SM (OH) C22:2, being decreased with HFD. The strongest associations (ß > 0.90) in 129Sv were established for C0, lysoPC a C20:3, 5 PC aa-s, PC ae C38:2, and sphingolipids (SM (OH) C14:1, SM C16:0). It is worthy to note that associations of C0, PC aa 36:1, PC aa C36:2, PC aa C36:3, PC aa C38:3, and SM C16:0 were overlapping in Bl6 and 129Sv.

DISCUSSION

Previous studies have shown that different strains of mice exhibit very different immune responses, and genetic background is known to influence the outcomes of mouse models of human disease. For this reason, inbred mice with well-characterized genetics are essential for obtaining reliable and reproducible experimental data. Therefore, the aim of present work was to capture this variability in more detail. To this end, we investigated the effects of two inflammatory triggers, LPS and HFD, on metabolic and genetic parameters.

1. Basal metabolic differences between Bl6 and 129Sv (Paper I, III)

To determine the basal differences in metabolic profile between Bl6 and 129Sv, saline treated control animals were compared in paper I and control diet-fed mice in paper III. The metabolites that clearly stood out in the LPS study were biogenic amines Ac-Orn, alpha-AAA and carnosine that were significantly higher in Bl6 mice and C4-, C5- and sphingolipid SM (OH) C22:2, which were higher in 129Sv. These results are also supported by previous research (Narvik et al., 2018), suggesting that these metabolites are part of the metabolomic signature of these strains. Similarly to LPS cohorts, we observed differences in C4-, carnosine, alpha-aminoadipic acid (alpha-AAA), sphingolipid SM(OH) C22:2, and lysophosphatidylcholine acyl (lysoPC a) C16:1 levels in the HFD study. However, we did not find equivalent differences in AC C5- levels when comparing Bl6 and 129Sv mouse lines and the nature of this difference requires further research. Also, unfortunately Ac-Orn could not be properly quantified in most samples. Additionally, we observed differences in BCAAs (Ile, Leu, Val), which were all higher in 129Sv mice.

It has been reported that the increased level of alpha-AAA in Bl6 mice is caused by a defect in the *Dhtkd1* gene. Defects in this gene lead to accumulation of alpha-AAA (Wu et al., 2014; Leandro et al., 2019). Recently, a study found that alpha-AAA has protective properties against obesity and T2D (Xu et al., 2019). Alpha-AAA improved energy metabolism and reduced fat accumulation, improved glucose metabolism and increased insulin sensitivity in mice. Alpha-AAA has been shown to reduce adipocyte size, and smaller adipocytes are more sensitive to insulin stimulation (Blüher et al. 2002). Thus, the accumulation of alpha-AAA in Bl6 mice could give them an advantage in coping with HFD and reduce features of obesity. Carnosine is a dipeptide widely distributed in skeletal muscle, heart and CNS (Boldyrev et al., 2013). Carnosine has antioxidant properties and has been shown to scavenge reactive oxygen species (ROS) (Dawson et al., 2002; Rajanikant et al., 2007). In addition, carnosine has been found to act as a scavenger of reactive aldehydes from the oxidative degradation pathway of endogenous molecules such as sugars, polyunsaturated fatty acids

(PUFAs), and proteins (Guiotto et al., 2005). Furthermore, carnosine supplementation has been demonstrated to decrease lipid accumulation in the circulation and attenuate HFD-induced hepatic steatosis (Mong et al., 2011). Therefore, similarly to alpha-AAA, higher levels of carnosine could also be advantageous and contribute to protection against HFD-induced disorders in Bl6 mice, but also contribute to their being more capable of coping with infection. Circulating BCAA levels are increased in both humans and rodents with obesity and elevated plasma levels of these amino acids are associated with an increased risk for future development of T2D (Newgard et al., 2009; Zhou et al., 2019; Wang et al., 2011). Given these differences, we could hypothesize that 129Sv mice might exhibit stronger responses against LPS and HFD.

In addition, in the HFD study, we identified 3 lysoPCs, 6 PC aa-s, 16 PC ae-s, and 8 SMs to be significantly different between Bl6 and 129Sv mice. After the exposure to HFD metabolite differences between strains included alpha-AAA, carnosine, putrescine, t4-OH-Pro, 2 lysoPCs, 2 PC aa-s, 7 PC ae-s, and 7 SMs. This shows that HFD somewhat affects the differences between strains; nevertheless, the most significant differences remain (e.g., carnosine and lysoPC a C16:1).

2. LPS-induced differences (Paper I, II)

2.1. LPS-induced changes in body weight and temperature (Paper I, II)

LPS resulted in significant body weight loss in both strains 24 hours after treatment. However, the loss of body weight was more pronounced in Bl6 mice than in 129Sv mice. It has been reported that LPS administration significantly reduces food intake in Bl6 mice (Kim et al., 2013). In addition, overnight fasting in Bl6 mice results in a loss of approximately 16% of body weight (Ayala et al., 2006). Decreased appetite and weight loss are considered common hallmark physiological responses that occur in many infectious and inflammatory diseases. Previous studies have shown that LPS increases leptin synthesis and secretion, a known appetite suppressant (Mastronardi et al., 2001; Sarraf et al., 1997).

Another important feature of endotoxin-mediated inflammation is the change in body temperature. LPS resulted in a slight decrease in body temperature in Bl6 mice, but this did not reach statistical significance in paper I. However, using a larger experimental group in paper II, we demonstrated a significant LPS-induced decrease in body temperature in Bl6 mice 24 hours after administration. This hypothermic response was not observed in 129Sv mice. It is well known that thermoregulation is critical for host defense against invading pathogens and can be detrimental if impaired. A recent study showed that inflammation-induced hypothermia and hypometabolism are beneficial for host tolerance and improve survival (Ganeshan et al., 2019). In addition, Chisholm and colleagues demonstrated that reducing metabolic demand through hypo-

thermia increased survival of mice during endotoxemia (Chisholm et al., 2016). This may be one of the reasons why 129Sv mice appear to be more susceptible to infection. In addition, we found a moderate positive significant correlation between body weight and temperature loss in Bl6 mice, whereas no correlation was observed in the 129Sv strain.

2.2. LPS-induced suppression of locomotor activity (Paper I, II)

In addition to weight loss and changes in body temperature, decreased locomotor activity is another characteristic response associated with disease behavior. In the event of infection, the energy demands of the immune system increase, and locomotor retardation helps animals conserve energy, which is then redirected to maintenance and survival programs (Wang et al., 2019). Both Bl6 and 129Sv strains showed an overall similar pattern of motor activity depression in the 24 hours following LPS-induced inflammation. LPS significantly suppressed the time spent and total distance traveled in the whole arena and in the center zone compared to mice in the control group. A similar LPS-induced suppressive effect was observed throughout the arena in the light and dark phases of the 24-h cycle. Whereas in the central area, LPS-induced motor suppression was evident only in the dark phase.

Significant differences in the motor response between Bl6 and 129Sv mice in the control group appeared within 2 hours of the onset of behavioral testing. This may reflect higher anxiety-like behavior of 129Sv mice at the beginning of the experiment and passive adaptation to a stressful environment. The higher anxiety-like trait of 129Sv mice has been thoroughly investigated and well characterized by several studies (Võikar et al., 2001; Abramov et al., 2008; Heinla et al., 2014). Furthermore, saline-treated Bl6 control mice spent significantly more time exploring the center area compared to 129Sv control mice, demonstrating anxiolytic-like baseline behavior of Bl6 mice.

2.3. LPS-induced metabolite differences (Paper I)

In addition to LPS-induced differences in body weight, temperature, and motor activity between strains, metabolites in Bl6 and 129Sv were also differentially affected by LPS exposure after 1.5 and 24 hours. After 1.5 hours, the number of affected metabolites was greater in Bl6 than in 129Sv. Nevertheless, the inflammatory response at 24 hours included a wide range of changes in several different metabolite groups. In this case, the number of altered metabolites was much greater in 129Sv compared with Bl6.

2.3.1. Acylcarnitines

1.5 hours after LPS administration SCACs C3, C4-, and C5- were decreased in both strains. Additionally, acetylcarnitine (C2) was decreased only in 129Sv, and several SCACs and MCACs were decreased only in the Bl6 strain. Previous findings suggest that medium- and long-chain acylcarnitines are involved in

proinflammatory signaling pathways (Rutkowsky et al., 2014; Ganeshan et al., 2019). In addition, several studies have reported alterations in the acylcarnitine profile in pathological conditions such as T2D (Adams et al., 2009), cardiovascular disease (Makrecka-Kuka et al., 2017), and first-episode psychosis (Kriisa et al., 2017). After applying GLM analysis, only four acylcarnitines remained statistically significant in the 1.5-h LPS exposure group. The decrease of C3 (a metabolite of Val and Ile catabolism) was significant in both strains, while the decrease of C2, C4- and C5- was significant only in 129Sv mice.

C3 was the only acylcarnitine that exhibited a decline during both 1.5- and 24-h LPS challenge in both strains. In addition, 24 hours after LPS administration, several LCACs exhibited significant increases in both strains. However, the altered profile of LCACs was wider in 129Sv mice and additionally included hydroxylated acylcarnitines. Long-chain fatty acids are transported to mitochondria in the form of acylcarnitines, where β-oxidation takes place to produce a major portion of the metabolic energy. Based on these findings, it appears that LPS induces incomplete β-oxidation of long-chain fatty acids in 129Sv, leading to accumulation of hydroxylated LCAC intermediates. In addition, some portion of the hydroxylated acylcarnitines could be produced due to a certain shift in oxidative catabolism of fatty acids, e.g., intensification of the omega and alpha oxidation pathways.

The 24-h LPS challenge caused a reduction of SCAC C4- in Bl6 as well as a reduction of free carnitine (C0) in 129Sv. The increase in plasma acylcarnitines and the decrease in plasma carnitine indicate an increased utilization of carnitine for the production of acylcarnitines in 129Sv. GLM analysis for 24-h LPS challenge revealed significant alterations in the acylcarnitine profile only in 129Sv, implying that the changes in acylcarnitine levels after LPS administration are specific to 129Sv.

2.3.2. Amino acids and biogenic amines

Citrulline was decreased in both strains compared with saline-treated controls 1.5 hours after LPS administration. Apart from citrulline, no other amino acids were altered in 129Sv. In contrast to this stability in 129Sv mice, Bl6 mice exhibited a decrease in several amino acids (Ala, Gly, His, Phe, Met, Pro, Ser, Thr, Val). The combination of several factors (intensification of the synthesis of protector proteins as well as inflammatory mediators, disease-associated malnutrition, intensification of the production of ketone bodies and gluconeogenesis) may cause the above-mentioned declines as Phe, Met, Thr, and Val are essential amino acids, Ala, Gly, His, Met, Pro, Ser, Thr, and Val are glucogenic amino acids, and Phe is a glucose-ketogenic amino acid. Therefore, one single factor such as short-term (1.5 h) fasting should not cause a depletion of plasma amino acid levels (Felig et al., 1969). In addition, the sum of glucogenic amino acids was significantly reduced in Bl6, whereas no significant changes were observed in 129Sv 1.5 hours after LPS administration. GLM analysis confirmed that amino acids were specifically reduced in Bl6 1.5 hours after LPS admi-

nistration. Although this profile was somewhat different, including Ala, Gly, His, Phe, Met, Pro, and Tyr.

At 24 hours after treatment, only the reduction of citrulline remained statistically significant. Citrulline is one of the key products of Arg catabolism. Nitric oxide synthase (NOS) catalyzes the hydrolysis of Arg to citrulline and NO. LPS and cytokines are known to induce the expression of NOS and thus the production of NO (Förstermann and Sessa, 2012). However, decreased concentration of citrulline indicates decreased NOS activity and NO production. This was further supported by a decrease in the plasma ratio of citrulline/Arg in both strains, reflecting decreased activity of NOS. In addition, plasma levels of the NOS inhibitors ADMA and SDMA were significantly elevated in the LPS-treated Bl6 mice after 24 h, but not in 129Sv. However, it is worth highlighting that plasma concentrations of ADMA and SDMA in 129Sv were already slightly elevated under control conditions and resembled Bl6 blood concentrations under inflammatory conditions, which has been also noted previously in these strains in home cage conditions (Narvik et al., 2018). This reflects increased NOS inhibition and thus decreased NO and citrulline production. Low plasma citrulline levels have previously been associated with acute respiratory distress syndrome in sepsis patients (Ware et al., 2013).

Alpha-AAA, Ac-Orn, and putrescine are examples of significantly reduced biogenic amines in Bl6 mice 1.5 h after LPS administration. In contrast, the ratio of spermidine/putrescine was elevated in Bl6 mice, indicating increased activity of spermidine synthase and conversion of putrescine to spermidine. No alterations in the profile of biogenic amines were detected in 129Sv.

LPS-response-specific biogenic amines that were altered 24 hours after LPS administration in both strains included kynurenine and serotonin. While serotonin concentration decreased, plasma kynurenine levels were significantly higher compared to saline-treated mice. Trp is metabolized via the kynurenine and serotonin pathway. Although no differences in plasma Trp levels were observed in the LPS-treated mice, there was a shift in favor of the kynurenine/Trp ratio over the serotonin/Trp ratio. This suggests that Trp metabolism via the kynurenine pathway is favored under inflammatory conditions. The conversion of Trp to kynurenine is catalyzed by the enzyme indoleamine 2,3-dioxygenase (IDO), which is activated by inflammatory cytokines, and it has been suggested that plasma levels of kynurenine directly reflect the activity of IDO (Moffett and Namboodiri, 2003). Kynurenine can be further converted into neuroprotective kynurenic acid or neurotoxic quinolinic acid, which is an intermediate of nicotinamide adenine dinucleotide (NAD+) biosynthesis. kynurenine in the blood is transported extensively to the brain. Under normal conditions, approximately 80% of kynurenine is transported from the blood to the brain, and under inflammatory conditions, this percentage is even further amplified reaching up to 98% (Kita et al., 2002). Because kynurenine competes with Leu for transport from blood to brain via large amino transporter LAT1, the fact that the Leu/kynurenine ratio was in favor of kynurenine under inflammatory conditions 24 hours after LPS administration may indicate that kynurenine is able to cross

the blood-brain barrier (BBB) more efficiently. This ratio was significantly altered only in Bl6 mice. Whether the kynurenine pathway favors the shift toward kynurenic acid or quinolinic acid in LPS-induced neuroinflammatory conditions in these strains requires further investigation. However, kynurenine and alpha-AAA are both substrates for the kynurenine aminotransferase II (KAT-II; also known as alpha-AAA aminotransferase II), which is responsible for transamination of kynurenine into kynurenic acid (Buchli et al., 1995; Hallen et al., 2013), and thus alpha-AAA levels indicate the availability of KAT-II for the transamination of kynurenine. The ratio of kynurenine/alpha-AAA was again in favor of kynurenine under inflammatory conditions 24 hours after LPS administration, providing further evidence that kynurenine may be transaminated to kynurenic acid. Individual differences between strains included a decrease in Ac-Orn and an increase in putrescine, ADMA, and SDMA in Bl6, whereas no strain-specific changes were observed in 129Sv. After applying GLM, only the decrease in Ac-Orn and increase in putrescine in Bl6 remained statistically significant, and the increase in kynurenine remained significant in both strains. Together with Arg, Ac-Orn is one of the precursors for ornithine synthesis, and from there on, putrescine is synthesized from ornithine. The decrease in Ac-Orn was also accompanied by a slight reduction of plasma ornithine in Bl6 mice. Increased levels of putrescine and decreased levels of ornithine and Ac-Orn suggest increased putrescine biosynthesis in the later stages of the inflammatory response in Bl6 mice. In addition, the ratio of spermidine to putrescine was decreased in Bl6 mice, indicating deteriorated activity of spermidine synthase and conversion of putrescine to spermidine. There were no changes observed in the putrescine synthesis pathway in 129Sv mice. Putrescine has been shown to possess neuroprotective activity in the CNS (Jänne et al., 2005).

2.3.3. Glycerophospholipids and sphingolipids

It is well established that inflammation leads to changes in lipid metabolism. These changes help to repair tissues and reduce the toxicity of a number of harmful agents by redistributing nutrients to cells involved in host defense.

Glycerophospholipids (GPLs) and sphingolipids (sphingomyelins, SMs) are considered inflammatory mediators, and altered levels of lipids reflect interplay between inflammation and lipid metabolism. Prominent members of the GPL family are phoshatidylcholines (PCs), which are main precursors of lysoPCs. In the 1.5-h LPS exposure, the only observed change was the increase of PC aa C42:0 in 129Sv. After applying GLM analysis, SM (OH) C16:1 was added to the list of significantly elevated lipids in 129Sv. No significant alterations in lipid metabolism were observed in Bl6.

24 hours after LPS administration, the most striking change in both strains was a decrease in lysoPCs and an increase in SMs. In addition, several PC diacyls were increased and PC acyl-alkyls were decreased in both strains. The inflammatory response caused the production of different patterning of these

metabolites through the influence of action of several enzymes in the metabolic network; while lysoPCs decrease, SM and PCs increase. However, the number of increased SMs and PCs was significantly higher in 129Sv mice. In particular, lysoPC a C16:1 and lysoPC a C18:1 were decreased in Bl6, which was accompanied by an increase in plasma PC aa C34:2. This may indicate a disturbance in the hydrolysis of PC aa C34:2 to lysoPC a C16:1 and lysoPC a C18:1 in Bl6. Moreover, the ratios between lysoPCs C16:1/C16:0 and C18:2/C18:1 were significantly lower after LPS administration, whereas no significant changes in these lysoPC ratios were observed in 129Sv.

GPLs and SMs are components of membrane bilayers that form a physical barrier against pathogens as a first line of defense and contain cell surface receptors such as Toll-like receptor 4 (TLR 4), which plays a key role in LPS-mediated signal transduction. Although often referred to as membrane lipids, studies have shown that PCs play a role in energy metabolism, lipoprotein transport, and cell signaling (van der Veen et al. 2017). Increased PC concentrations and decreased lysoPC concentrations may indicate diminished formation of lysoPCs from PCs due to decreased phospholipase enzyme activity.

2.3.4. Monosaccharides

Hexoses were significantly reduced in Bl6, whereas no changes were observed in 129Sv 24 h after administration of LPS. Metabolic energy is derived from the breakdown of monosaccharides, making them an essential source of energy, especially for the brain. Decreased levels of hexoses, including glucose, suggest that inflammation contributes to glucose metabolism disorder in Bl6 mice. This suggests that metabolism is slowed down in Bl6 mice under LPS-induced inflammatory conditions. LPS-induced lower blood glucose levels have been previously described in Bl6 mice (Ganeshan et al., 2019). A hypometabolic state is important for conserving metabolic energy under inflammatory conditions. An inflammatory response is energetically costly and requires redistribution of nutrients to support immune activation (Ganeshan and Chawla, 2014). Recent evidence suggests that a hypometabolic response to endotoxemia is essential for utilization of tissue tolerance as a defense against bacterial pathogens (Ganeshan et al., 2019). It appears that an energy conserving hypometabolic state is one possible mechanism that Bl6 mice use to cope with inflammation.

2.4. Microglial profile and subpopulations (Paper II)

We selected hippocampus and cerebellum brain regions to investigate cell populations and microglial profile. Cerebellum plays an important role in many pathological processes (Feys et al., 2005, Jensen and St Louis, 2005) and is thought to have increased sensitivity to circulating inflammatory agents due to its microvascular structure (Silwedel and Förster, 2006). It has been shown that microglia in the hippocampus and cerebellum exist in a more immune-vigilant

state and have a higher turnover rate than those in other brain regions (Grabert et al., 2016; Tay et al., 2017).

The CNS is considered immune privileged because the BBB limits the migration of peripheral immune cells into the CNS. However, in the presence of an inflammatory stimulus, the BBB may be compromised, and peripheral immune cells can infiltrate the CNS. As expected, 24 hours after LPS challenge, we observed an increase in infiltrating neutrophils and macrophages and an increase in microglial cells in the brains of both strains, however the increase in microglial cells was statistically significant only in Bl6 mice. We also investigated the effect of LPS on oligodendrocyte progenitor cells (OPCs), as previous studies have shown that upon activation, microglia mediate OPC death (Pang et al., 2010). The percentage of OPCs was substantially lower in LPS-treated mice compared with control mice. In Bl6 mice, the decrease in OPCs was statistically significant in the cerebellum and in 129Sv mice in the hippocampus, although the same downtrend was seen in both brain regions of both strains. Pang and colleagues demonstrated that LPS-activated microglia are detrimental to OPCs. They showed that cell damage occurred within 24 hours of LPS treatment and was mediated by nitric-oxide-dependent oxidative damage. They also showed that this damage can be prevented by inhibition of nitric oxide synthase (NOS) (Pang et al., 2010). As described above, we found that LPS-treated Bl6 mice had increased plasma levels of the endogenous NOS inhibitors ADMA and SDMA.

We next examined the profile of microglial activation in Bl6 and 129Sv mice after exposure to LPS. We observed that Bl6 mice had significantly higher expression of CD11b on microglial cells than 129Sv mice under control conditions. However, after LPS stimulation, the surface expression of CD11b on microglial cells was increased only in 129Sv mice. Although CD11b is constitutively expressed by microglia, its expression is upregulated under inflammatory conditions. Thus, the increased expression of CD11b reflects the activation status of microglia. This may imply that microglia in Bl6 mice are in a higher immune-alert state under physiological conditions than in 129Sv mice. Moreover, we detected a significant increase in microglial surface expression of CX3CR1 in the cerebellum of 129Sv mice in response to LPS stimulation, whereas no changes were observed in Bl6 mice. CX3CR1 is a chemokine receptor that binds to its ligand fractalkine. Their interaction is associated with crosstalk between neurons and microglia and may play a role in the microglial activation process (Cardona et al., 2006; Hughes et al., 2002). Recent evidence suggests that CX3CR1 is associated with an inflammatory response in the brain of hypertensive animal models and that inhibition of CX3CR1-microglia signaling attenuates hypertension and chronic brain inflammation (Ho et al., 2020). This may suggest that LPS can induce hypertension and a higher inflammatory state in 129Sv mice.

Phenotypic markers such as MHC-II and CD206 are commonly used to identify classically activated M1 and alternatively activated M2 (respectively) polarized microglial cells (Kigerl et al., 2009; David and Kroner, 2011). How-

ever, it is important to note that the M1/M2 classification is highly simplified and does not fully reflect the diversity of microglial phenotypes. The percentage of CD206+ microglial cells remained unaffected in both Bl6 and 129Sv strains after LPS stimulation. Interestingly, we observed an immune-suppressive response in the hippocampus and cerebellum of Bl6 mice characterized by downregulation of the MHC-II$^+$ microglial cell percentage. Moreover, when comparing the MHC-II/CD206$^+$ microglial ratio, we found that the ratio was decreased in response to LPS in Bl6 mice, whereas no alterations were observed in 129Sv mice. There are somewhat conflicting data regarding microglial MHC-II regulation after LPS administration. Although most studies report upregulation of MHC-II$^+$ microglia after LPS exposure, a recent study described a specific immune-suppressive response in midbrain microglia under inflammatory conditions characterized by downregulation of MHC-II microglial expression and upregulation of anti-inflammatory cytokines (Abellanas et al., 2019).

These data suggest that microglia of 129Sv mice exhibit an elevated inflammatory status in response to activation by LPS, whereas microglia of Bl6 mice appear to be in a higher baseline immune-alert state. Furthermore, the downregulation of MHC-II could reflect a protective reaction to the inflammatory response aimed at preventing cell damage in Bl6 mice. The more severe inflammatory status observed in 129Sv mice may be connected in some way to the mutation in the *Disc1* gene. Disruption of the Disc1 protein in mice has been shown to modulate the expression of inflammatory gene networks (Trossbach et al., 2019). Previous work has used immune activation along with *Disc1* mutation to produce schizophrenia-related pathology in mice. LPS-activated microglia become phagocytic and may over activate synaptic pruning processes during critical periods. Moreover, the combination of immune activation and *Disc1* mutations could synergistically induce schizophrenia-like behavior in mice (Lipina et al. 2013; Uzuneser et al. 2019; Xu et al. 2021).

2.5. LPS-induced changes in the MHC-I pathway (paper II)

The major histocompatibility (MHC) class I molecules are loaded with peptides derived from exogenous sources (mainly of viral origin) and presented on the plasma membrane of the cell to communicate with cytotoxic T-cells and thereby regulate their effector or regulatory functions. In addition to their classically known function of antigen presentation for T-cell activation, MHC-I molecules have been shown to have a negative effect on inflammatory responses triggered by Toll-like receptors (TLR). According to recent research, MHC-I reverse signaling is involved in regulating the defense against bacterial and viral infections (Muntjewerff et al., 2020). MHC-I molecules have been found to attenuate innate inflammatory responses, protecting mice from sepsis (Xu et al., 2012). The interaction between MHC-I-expressing cells and cytotoxic T cells has been shown to suppress TLR-triggered cytokine production (Xu et al., 2012).

Because we observed LPS-induced downregulation of MHC-II+ microglial cells in Bl6 mice, we wondered whether the MHC-I pathway would be altered

differently after LPS exposure. We performed RT-qPCR analyses and examined the relative mRNA levels of the following genes associated with the MHC-I pathway: β-2-microglobulin (*β2m*), transporter associated with antigen processing subunits 1 and 2 (*Tap1* and *Tap2*), the bridging factor tapasin (*Tapbp*), and the immunoproteasome subunit *Lmp2* in the hippocampus, hypothalamus, midbrain, frontal cortex, olfactory bulb, and cerebellum.

Gene expression analysis revealed that LPS administration resulted in an increase in all components of the MHC-I pathway in the hippocampus, hypothalamus, midbrain, frontal cortex, and cerebellum in both strains. However, Bl6 mice exhibited greater LPS-induced upregulation of these genes compared to 129Sv mice. The most substantial difference was observed in the olfactory bulb, which exhibited LPS-induced upregulation of MHC-I-pathway related genes only in Bl6 mice but remained unaffected by LPS exposure in 129Sv mice. This may imply that the olfactory bulb of Bl6 mice is in a more immunocompetent state than that of 129Sv mice.

We also investigated the expression of angiotensin converting enzyme (ACE). ACE controls blood pressure by catalyzing the conversion of angiotensin I to the active vasoconstrictor angiotensin II, which increases blood pressure by causing blood vessels to constrict. ACE is a major component of the renin-angiotensin system (RAS) in the brain. We found that gene expression of ACE was unaffected by LPS in 129Sv mice, whereas LPS triggered a significant increase in ACE mRNA levels in the hippocampus, hypothalamus, midbrain, and cerebellum in Bl6 mice. ACE plays an important role in the immune response of myeloid cells and is important for the neutrophil immune response to bacterial infections. Previous studies have shown that ACE is required for normal neutrophil antibacterial activity and that upregulation of ACE in neutrophils increases antibacterial immunity in mice (Khan et al., 2017). Therefore, it appears that greater upregulation of ACE and MHC-I pathway genes is beneficial for host defense and may be advantageous in defense against bacteria in Bl6 mice.

Next, we performed Western blot analysis to characterize the expression of β2m, Tapbp, and ACE at the protein level in the hippocampus and olfactory bulb of Bl6 and 129Sv mice. β2m is an essential component of the MHC-I complex, being part of the functional MHC-I heterodimer on the cell surface. Tapbp is another critical factor in the MHC-I pathway required for the assembly of MHC-I heterodimers with peptides in the endoplasmic reticulum (ER). Apart from their importance in the MHC-I pathway, β2m and Tapbp were selected for protein analysis because we observed differences in their basal gene expression between Bl6 and 129Sv mice. In addition, we selected ACE for further analysis since LPS triggered upregulation of ACE specifically in Bl6 mice, whereas it was unaffected by LPS challenge in 129Sv mice. LPS stimulation led to upregulation of protein expression of ACE and β2m in the hippocampus and Tapbp and β2m in the olfactory bulbs of Bl6 mice. No statistically significant changes were observed in either brain region of the 129Sv mice. These results

give further support to the idea that LPS causes greater upregulation of components of the MHC-I pathway in Bl6 mice compared to 129Sv mice.

Since we observed significant upregulation of MHC-I pathway genes, we next sought to investigate the associations between body weight and temperature change with MHC-I gene expressions. Interestingly, when aligning the body weight and temperature change in the LPS-treated mice with their MHC-I gene expressions, we observed significant positive correlations between body weight decrease and β2m, Tapbp, and Tap1 expressions in the olfactory bulbs of Bl6 mice, whereas in 129Sv mice, body weight decrease was positively correlated with Tapbp, Tap1, and Lmp2 expressions in the frontal cortex

This result is particularly interesting because the rodent frontal cortex is known to play an important role in stress-related behaviors and is involved in determining coping outcomes. It has been repeatedly shown that Bl6 and 129Sv mice exhibit markedly different coping strategies in response to different stressors. Bl6 mice have an active coping strategy in stressful situations, whereas the coping strategy of the 129Sv strain is considered passive (Varul et al., 2021). Moreover, as described above, we saw that Bl6 mice seem to actively cope with inflammation by inducing a stronger hypometabolic state, whereas the metabolism of 129Sv mice appears to enhance the proinflammatory status.

On the other hand, the olfactory bulb is considered an exceptional brain structure in terms of adult neurogenesis. Neurons in the olfactory bulb are constantly replaced by new neurons formed in the subventricular zone of the lateral ventricles. Mice rely on their sense of smell to locate and identify food sources, engage in social interactions, and avoid predators. In addition, behaviors such as learning and memory, social interaction, fear, and anxiety are closely related to their olfactory function. Previous work has shown that exposure of mice to cat odor elicits an anxiety response in Bl6 mice but not in the 129Sv strain (Raud et al., 2007). This indicates that these two strains of mice exhibit different olfactory and anxiety responses. Furthermore, previous findings have suggested that olfactory bulb microglia may function as tolerogenic antigen-presenting cells (APCs) (Dando et al., 2019). The fact that LPS induces significant upregulation of MHC-I genes in the olfactory bulbs of Bl6 mice and no changes in the olfactory bulbs of 129Sv mice suggests that the olfactory bulb of Bl6 mice is in a more immunocompetent state than 129Sv mice.

It should be noted that there may also be differences in the gut microbiota of these strains that we are not aware of. The gut microbiota may influence the development and function of the immune system and contribute to various immunological responses (Zheng et al., 2020). However, we believe that the specific microbiota acquired by these mice is due to their own genetic and immunological characteristics, as they have lived under the same conditions and consumed the same diet for several generations. A recent study has shown that the microbiota regulates the function of microglia via TLR4, priming these cells to respond to infection (Brown et al., 2019). Future research should be

considered to investigate the differences in microbiota and their potential impact on the immunological response of these strains.

3. HFD-induced differences (Paper III)

Previous studies have demonstrated that different inbred mouse strains differ significantly in their metabolic phenotype under physiological and pathological conditions. As described above, we demonstrated that there is significant metabolic heterogeneity between Bl6 and 129Sv and that systemic administration of LPS leads to hypometabolism (which is beneficial for host tolerance) in the Bl6 strain but increases the production of proinflammatory metabolites in the 129Sv strain. Several studies have also indicated that consumption of high-fat foods can induce systemic inflammation (Jeon et al., 2012; Miller and Spencer, 2014; Boitard et al., 2014). Therefore, we next aimed to investigate similarities and differences in a number of metabolic variables and their ratios in Bl6 and 129Sv mouse strains in response to a 9-week HFD.

3.1. HFD-induced changes in body weight

Bl6 and 129Sv mice were fed HFD or regular chow for 9 weeks. Body weight, food, and water intake were recorded weekly. HFD-fed 129Sv mice began to weigh significantly more than mice fed with standard chow starting from the second week of dietary exposure and continuing to week 9. In contrast, body weight gain of Bl6 mice was not affected by HFD during the 9-week study period. Previous studies have reported significant weight gain in C57BL/6NTac mice after HFD exposure, which contradicts the results of our study (Podrini et al. 2013; Gupta et al. 2017). There are at least two possibilities to explain this discrepancy. First, it has been suggested that the microbiota influences susceptibility to DIO. Bl6 mice bred by different vendors and housed in different animal facilities may have different microbiota that may affect DIO (Ussar et al. 2015; Fujisaka et al. 2018). Second, the environment of animal facilities. Differences between animal facilities have been shown to modulate morphological, physiological, and behavioral traits in a genetically homogeneous cohort, leading to facility-specific phenotypes, from the molecular to the behavioral level (Jaric et al. 2022). GLM analysis confirmed significant 9-week body weight gain in 129Sv mice. Interestingly, the weight gain of 129Sv mice was not related to higher amounts of food consumed as the food intake was significantly lower in both 129Sv and Bl6 HFD groups compared with their respective control diet groups. The difference in food consumption between HFD and control groups became evident from the second week of dietary exposure and remained lower until the end of dietary exposure. A similar effect has previously been observed in our laboratory (Kaare et al., 2021). Thus, while 129Sv mice responded strongly to HFD, the Bl6 strain was protected against diet-induced weight gain.

3.2. HFD-induced alterations in locomotor activity

The locomotor activity of Bl6 mice in the open field test remained the same regardless of diet, whereas HFD-exposed 129Sv mice traveled significantly shorter distances than their control diet counterparts, as well as HFD-fed Bl6 mice already at the beginning of the dietary exposure (day 1) and at the end of the dietary exposure (week 9). HFD also induced higher anxiety-like behavior in 129Sv mice, as they spent significantly less time in the center zone of the open field than control diet-fed 129Sv mice at week 9. When the 24-hour cycle was divided into light and dark phases, the difference between strains became even more prominent in the light phase. However, at week 9, HFD-fed 129Sv mice tended to spend less time in the center zone, regardless of the light or dark phase of the 24-hour cycle. On the other hand, HFD-exposed Bl6 mice visited the food zone significantly less at both the beginning and end of the dietary exposure. Additionally, when splitting the 24 h cycle into hourly data, clearly different motor response between Bl6 and 129Sv emerged within 2 h from the beginning of behavioral testing on the first day. 129Sv mice traveled significantly shorter distances in the total arena and spent significantly less time in the center zone than Bl6 mice during the first two hours. This difference was no longer evident from the third hour onward. This observation most likely reflects a higher anxiety-like trait of 129Sv at the beginning of behavioral testing, indicating passive adaptation. At week 9, the total distance traveled remained significantly different between strains even at the third hour. On the other hand, 129Sv spent significantly less time in the center zone only at the first hour and, starting from the second hour, it was already equivalent to that of Bl6 mice. In addition, we observed that at the end of the dietary intervention, the HFD-fed 129Sv mice traveled significantly shorter distances and spent significantly less time in the center zone than the control-diet-fed 129Sv mice in the first hour. This suggests that HFD exacerbates the anxiety-like state in 129Sv mice. Psychiatric disorders and type II diabetes (T2D) have been shown to be highly comorbid, and this may suggest that the 129Sv strain is well-suited for modeling the metabolic syndrome associated with psychiatric disorders.

In addition, we found that body weight gain of 129Sv mice was negatively correlated with total distance traveled and duration in the center and food zones during the light phase. In contrast, body weight gain of Bl6 mice was positively correlated with total distance traveled in the light phase and time spent in the center zone in the light phase. Thus, the increased body mass of the 129Sv mice caused a decrease in activity or *vice versa*. After the second open field test in phenotyper cages, we observed an interesting effect on weight in both strains. Control mice of both strains lost significant weight during the exposure, however this weight loss was greater in 129Sv mice. In animals exposed to HFD an opposite effect emerged, as mice from both strains exhibited weight gain during the exposure. However, it was more pronounced in Bl6 mice than in 129Sv mice, which differed from the general dynamics of body weight in the home

cage. This effect cannot be explained by increased locomotor activity of 129Sv mice, since it was significantly lower compared to Bl6 mice. Thus, it appears that 129Sv mice exhibit greater weight loss under stressful conditions, such as social isolation, which can be prevented by HFD. It has been shown that 129Sv mice gain more weight compared to Bl6 mice in a non-stressful home-cage environment. However, after repeated stressful interventions, 129Sv mice tend to lose body weight not seen in Bl6 mice (Narvik et al., 2018). It is well known that Bl6 mice are better able to tolerate stress and adapt to new environments than 129Sv mice (Võikar et al., 2001; Abramov et al., 2008; Heinla et al., 2014), and decreased movement and greater weight loss of 129Sv mice reflect the inability to cope in a novel environment.

3.3. HFD-induced metabolite differences

3.3.1. Acylcarnitines

Nine weeks of HFD induced a wide range of alterations in several different metabolite groups. Many of the metabolic shifts induced by HFD were similar in Bl6 and 129Sv mouse strains. HFD caused a decrease in carnitine (C0) and short-chain acylcarnitines (SCACs) (C2, C4-) in both strains of mice. However, the altered profile of SCACs was broader in 129Sv mice and additionally included C3 and C4:1. Acylcarnitine C3 is a by-product of Ile and Val catabolism which were also elevated specifically in 129Sv mice (Newgard et al., 2009). C0 is critical for the breakdown of long-chain fatty acids in mitochondria and is particularly important for energy production from high-fat diets. Plasma levels of long-chain acylcarnitines (LCAC) were specifically altered by HFD in 129Sv mice. More precisely, HFD significantly decreased plasma levels of C12, C12:1, C14, C14:2, C16, C16:1, C16:2, C16:2-OH, C18:1-OH, and C18:2 in 129Sv mice. Only the concentration of C18:2 was decreased in HFD-fed Bl6 mice. C18 was the only acylcarnitine that exhibited HFD-induced increase in both strains. Considering that C18 produces a substantial amount of ATP, the increase is likely a result of compensating for the energetic demand. LCACs are intermediates of intracellular fatty acid metabolism that are generated by transesterification of long-chain acyl-CoA with carnitine via carnitine palmitoyltransferase l (CPT1). Increasing C18 content, in turn, led to upregulation of the ratio of long-chain species to free carnitine and acylcarnitines in both HFD-fed strains, reflecting increased activity of CPT1 and CPT2. Long-chain fatty acids are transported into mitochondria via CPT1 and CPT2, located in the outer and inner mitochondrial membranes, respectively, and oxidized via β-oxidation pathway for energy production (Bonen et al., 2007). The fact that both strains exhibited increased CPT1 and CPT2 activity suggests a higher uptake of fatty acids into the mitochondria and possibly an increased rate of oxidation of long-chain fatty acids. Up-regulation of β-oxidation is expected because the HFD is responsible for the overload of fatty acid metabolism. Decreased C0 levels may indicate insufficient β-oxidation to compensate for the potential HFD-induced

increase in free fatty acids. In addition, we observed an increase in the ratio of dicarboxy-acylcarnitines to total acylcarnitines in HFD-fed mice of both strains, indicating an intensification of the ω-oxidation pathway. Activation of ω-oxidation has been described as a rescue mechanism for fatty acid disorders, as it could potentially alleviate the overload of lipid catabolism pathways (Wanders et al., 2011). GLM model confirmed a significant HFD-induced decrease in acylcarnitines C0, C2, C4-, and C18:2 in both strains. acylcarnitines C3 and C14:2 were specifically decreased in 129Sv mice and C18 was specifically increased in Bl6 mice. The classical understanding is that acylcarnitines are transported to mitochondria for energy production. However, under HFD conditions, they are also used for triglyceride synthesis. Our results may therefore suggest that 129Sv mice cannot adapt as effectively as Bl6 mice and that acylcarnitines may also be used for lipid droplet production in muscle cells. This could also explain why 129Sv mice gain more weight and become less active compared to Bl6 mice.

3.3.2. Amino acids and biogenic amines

HFD resulted in an increase in circulating ketogenic and branched-chain amino acids (BCAAs) in 129Sv mice, whereas no changes in BCAA levels were observed in Bl6 mice. Although the ketogenic BCAAs Leu and Ile were slightly increased in HFD-fed 129Sv mice, the level of Val, another BCAA, was significantly increased by HFD, suggesting disturbances in Val metabolism. BCAAs can be used for the rapid production of ketone bodies. In addition, since Leu is a direct trigger for protein synthesis, this could be another indication of the production and accumulation of lipid droplets in muscle cells, since these amino acids are used for protein synthesis and the formation of ketone bodies. An increase in BCAAs has also been associated with obesity, and in HFD-fed animals, BCAAs contribute to the development of insulin resistance associated with obesity (Newgard et al., 2009). The same study also reported that obese individuals have significantly lower Gly levels. A recent study showed that BCAA restriction can prevent excessive weight gain, adipose tissue accumulation, and HFD-induced adipocyte hypertrophy. In addition, BCAA restriction in HFD contributed to the maintenance of normal glucose and insulin levels and prevented insulin resistance (Liu et al., 2022). In addition, low plasma Gly concentrations have been reported to be associated with T2D (Guasch-Ferre et al., 2016). Accordingly, we observed that HFD caused a significant decrease in Gly in 129Sv mice. In Bl6 mice, the only amino acid affected by HFD was Cit, which was significantly increased. Orn levels were slightly lower in HFD-fed Bl6 mice, although this result was not statistically significant. Consequently, we observed an increased ratio of Cit to Orn in HFD-fed Bl6 mice, possibly indicating increased ornithine transcarbamylase activity, suggesting disturbances in urea cycle in Bl6 mice.

HFD affected the kynurenine metabolic pathway in both strains of mice. Mice exhibited HFD-induced decrease in kynurenine and in the ratio of kynu-

renine to Trp, indicating decreased indole dioxygenase activity and decreased Trp degradation. Kynurenine and Trp have been reported to be positively associated with obesity (Takashina et al., 2016). Trp is metabolized via the kynurenine pathway, producing kynurenine, which is further metabolized in three distinct routes to quinolinate, kynurenate, and xanthurenate, producing glutamate from α-ketoglutarate, which in turn is a key molecule in the TCA cycle. A small percentage of Trp is also hydroxylated to synthesize serotonin and melatonin. In our study, the fact that kynurenine levels were elevated in the HFD groups suggests an upregulation of the kynurenine pathway that could lead to an overproduction of xanthurenic acid, which is considered to be one of the factors promoting insulin resistance (Favennec et al., 2015). In addition, 129Sv mice exhibited decreased plasma levels of spermidine and t4-OH-Pro when consuming HFD. Decreased t4-OH-Pro has previously been associated with insulin dysregulation in horses (Kenéz et.al., 2018). Since proline hydroxylation requires ascorbic acid, it has been suggested that hydroxyproline could be an indirect marker of oxidative stress. T4-OH-Pro is also a major component of the protein collagen. It is produced by hydroxylation of the amino acid proline (Pro) and is therefore a post-translationally modified, non-essential amino acid. T4-OH-Pro and Pro play a key role in collagen stability, and the decreased concentrations observed here may reflect increased turnover of collagen. GLM analysis confirmed significant HFD-induced changes in kynurenine in both strains and revealed that t4-OH-Pro specifically belongs to the metabolic signature of HFD in 129Sv.

3.3.3. Glycerophospholipids and sphingolipids

Glycerophospholipids and sphingolipids were found to be the metabolites with the greatest differences between the dietary groups. Lipids are an important source and store of energy for metabolism. Both strains exhibited HFD-induced increases in the total level of lysoPCs, SMs, PC aa-s, and PC ae-s.

Out of 13 lysoPCs, HFD induced the elevation of 6 in both strains. We identified two additional lysoPCs that were specifically altered in HFD-fed 129Sv mice – lysoPC a C20:4 and lysoPC a C17:0. LysoPC a C20:4 exhibited HFD-induced increase in 129Sv mice. However, in contrast to the general upregulation of lysoPCs, lysoPC a C17:0 was significantly decreased in 129Sv mice. LysoPCs are bioactive proinflammatory lipids that are hydrolyzed derivatives of PCs. They play a role in modulating the immune response through immune cell activation and transport and these functions have been linked to various inflammatory diseases (Cas et al. 2020). Thus, elevated lysoPC levels may indicate HFD-induced inflammatory response in both Bl6 and 129Sv mice.

HFD-induced alterations of SMs in both strains. These alterations included increased levels of six SMs and significantly decreased levels of SM (OH) C22:2. We identified three additional SMs that were specifically increased in Bl6 mice – SM (OH) C22:1, SM C22:3, and SM C24:0. The changes in the SM profile were expected, since it is known that SM metabolism is significantly

affected by dietary nutrient oversupply that comes along with HFD. Due to the complexity of the sphingolipid metabolic network, it is difficult to determine the regulation and function of a single SM species in HFD-related physiology and pathology. SMs are precursors of several active sphingolipids, such as ceramides, sphingosine, and sphingosine-1-phosphate (S1P). In particular, HFD has been shown to cause an accumulation of ceramides that can promote insulin resistance, inflammation, and cell death (Norris et al. 2017).

We found that the concentrations of PCs were also significantly altered. A total of 15 PC aa-s and 26 PC ae-s were significantly increased in both strains. The saturated fatty acid (SFA) content of PC aa and ae species was not affected by HFD. However, we observed a significant HFD-induced increase in unsaturated fatty acid (UFA) PC aa and ae species in both Bl6 and 129Sv mice. When UFA lipids were further subdivided into monounsaturated fatty acids (MUFAs) and polyunsaturated fatty acids (PUFAs), the HFD-induced increase in both strains remained significant only for PC aa species. In 129Sv mice, HFD did not affect PUFA PC ae levels but increased MUFA PC ae species. On the other hand, both PUFAs and MUFAs of PC ae species were significantly increased in Bl6 mice. The HFD-induced changes in individual PC aa-s and PC ae-s were significantly greater in Bl6 mice than in 129Sv.

Considering that lysoPCs are metabolites of PC aa-s, it is important to highlight the following relationships under the influence of HFD in Bl6 mice. Indeed, in Bl6 mice, there is a clear relation between lysoPC a C16:1 and PC aa C32:1 as well as between lysoPC a C20:3 and PC aa C34:3. Therefore, it can be suggested that the processing of certain lipids is intensified under the influence of HFD in Bl6 mice.

4. Concluding remarks and future directions

There is increasing evidence of the pathophysiological features of disrupted homeostasis systems, particularly the hypothalamic-pituitary-adrenal axis and the inflammatory response, in individuals with various psychiatric disorders. These pathophysiological features are also associated with the development of metabolic syndrome. Considering that 129Sv mice have abolished production of Disc1 protein, which is a potential schizophrenia susceptibility gene, we wondered how this genetic background is affected by endotoxemia and dietary influences. To better understand the underlying genetic differences in Bl6 and 129Sv mouse strains, we applied a number of approaches to examine metabolomics profile, microglial activation, and overall severity of neuroinflammatory status after LPS or HFD interventions.

1.5 h after LPS administration, Bl6 exhibited hypometabolism of glucogenic amino acids as well as Ac-Orn. This hypometabolic reaction was further intensified after 24 h, as several metabolites were significantly lower in the LPS treated animals than the saline controls. Furthermore, we demonstrated increased production of putrescine in Bl6 mice, which is known to retain neuro-

protective properties. The change in metabolites was accompanied by strong body weight loss and hypothermic response not seen in 129Sv. In 129Sv, we observed elevation of PC aa C42:0 and SM (OH) C16:1 after 1.5 h LPS administration, which points to disturbances in lipid signaling pathways. Along with elevation of lipids, 129Sv displayed a significant decrease in SCACs and citrulline. 24 h later, LPS administration led to incomplete long-chain fatty acid β-oxidation in 129Sv, described by accumulation of hydroxylated LCAC intermediates, which was accompanied by moderate loss of body weight. Multiple studies have reported that LCACs can activate proinflammatory signaling pathways (Kouttab and De Simone, 1993; Rutkowsky et al., 2014; McCoin et al., 2015). Thus, the elevation of LCACs in 129Sv could indicate increased inflammatory status. On the other hand, inflammation-induced hypothermia and hypometabolism, seen in Bl6 mice, are essential for host tolerance and survival (Ganeshan et al., 2019). Microglia of 129Sv mice displayed also increased inflammatory status in response to activation by LPS. However, we did see that under baseline conditions, microglia of Bl6 mice seem to be in a higher immune-alert state. Furthermore, we observed downregulation of MHC-II in Bl6 mice, which could reflect a protective reaction to the inflammatory response aimed at preventing cell damage in Bl6 mice. Moreover, gene and protein expression analysis revealed that LPS administration induced a significantly stronger upregulation of MHC-I-pathway related components in the brain of Bl6 compared to 129Sv mice. Additionally, correlation analysis highlighted the olfactory bulb region of Bl6 mice and the frontal cortex of 129Sv mice as brain regions most affected by LPS in these strains. Based on these results, we hypothesize that the brain of Bl6 mice, particularly the olfactory bulb region, exists in a more immunocompetent state compared to that of 129Sv mice. Thus, our data suggests that Bl6 is actively coping with inflammation by suppressing normal production of metabolites and enhancing the production of neuroprotective metabolites and upregulating MHC-I pathway, which is accompanied by stronger body weight loss and hypothermia. On the contrary, the body weight loss of 129Sv was less severe, and metabolism appears to enhance the proinflammatory status by upregulating the levels of hydroxylated LCACs and increasing inflammatory status of microglia.

These mouse strains also displayed a striking difference in response to HFD. 129Sv mice exhibited significant weight gain on HFD with similar metabolite shifts to those seen in humans with metabolic syndrome, which were not seen in Bl6 mice. HFD feeding resulted in an inhibition of general locomotor activity in 129Sv mice, accompanied by signs of anxiety-like behavior. Metabolite profiling revealed that 129Sv mice had higher levels of circulating branched-chain amino acids, which were even more amplified by HFD. HFD also induced a decrease in glycine, spermidine and t4-OH-proline levels in 129Sv mice. Although acylcarnitines dominated in baseline conditions in 129Sv strain, this strain experienced significantly stronger acylcarnitine-reducing effects of HFD. Moreover, 129Sv mice had higher levels of lipids in baseline conditions, but HFD caused more pronounced alterations in lipids profile of Bl6 mice.

Our study highlighted the metabolites alpha-AAA and carnosine to belong to the specific metabolic profile of Bl6 mice. Alpha-AAA has protective properties against obesity and T2D (Xu et al., 2019). Carnosine has antioxidant properties and scavenges ROS (Dawson et al., 2002; Rajanikant et al., 2007). This may provide Bl6 mice a possible advantage in coping with HFD and LPS.

The results of the present study suggest that 129Sv mice exhibit greater immunologic dysregulation and stronger susceptibility to obesity and metabolic disease which are both important features of psychiatric disorders. Taken together, we conclude that the 129Sv mice can be considered potentially useful for modeling endophenotypes associated with psychiatric disorders.

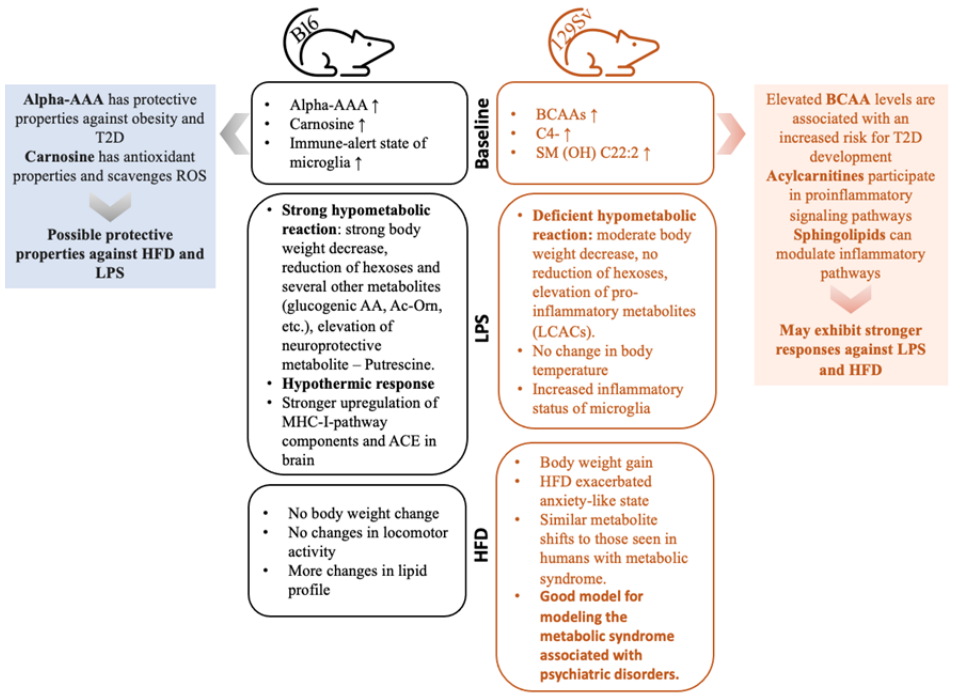

Figure 19. Concluding remarks for Bl6 and 129Sv strains.

SUMMARY AND CONCLUSIONS

The general aim of this dissertation was to provide a deeper insight into the coping strategies of two common inbred mouse strains: Bl6 and 129Sv, focusing on two inflammatory triggers – LPS and HFD. The main results are summarized as follows:

1. LPS induced strong hypometabolism in Bl6 mice, characterized by reduction of glucogenic amino acids, Ac-Orn, hexoses and several other metabolites. This was accompanied by strong body weight decrease and upregulation of metabolite putrescine, which is believed to have neuroprotective properties. Hypometabolism is known to be essential for host tolerance and survival. On the other hand, LPS caused deficient hypometabolic reactions in 129Sv mice, accompanied by moderate body weight loss. Instead LPS caused elevation of hydroxylated LCACs, reflecting incomplete β-oxidation of long-chain fatty acids and increased inflammatory status.
2. In paper 2 we demonstrated that Bl6 mice exhibit significant hypothermia, which is not seen in 129Sv mice. Inflammation-induced hypothermia is known as a strategy for inducing hypometabolism, which coincides with the results of the first paper. Neuroinflammation studies demonstrated that microglia of 129Sv mice displayed increased inflammatory status in response to LPS. However, under baseline conditions, microglia of Bl6 mice seem to be in a higher immune-alert state. Furthermore, we observed downregulation of MHC-II in Bl6 mice, which could reflect a protective reaction to the inflammatory response aimed at preventing cell damage. Moreover, gene and protein expression analysis revealed that LPS administration induced a significantly stronger upregulation of MHC-I-pathway related components in the brain of Bl6 compared to 129Sv mice.
3. 129Sv mice exhibited significant weight gain on HFD with similar metabolite shifts to those seen in humans with metabolic syndrome. HFD feeding resulted in an inhibition of general locomotor activity in 129Sv mice, accompanied by signs of anxiety-like behavior. Metabolite profiling revealed that 129Sv mice had higher levels of circulating branched-chain amino acids, which were even more amplified by HFD. HFD also induced a decrease in glycine, spermidine and t4-OH-proline levels in 129Sv mice. Although acylcarnitines dominated in baseline conditions in 129Sv strain, this strain experienced significantly stronger acylcarnitine-reducing effects of HFD. Moreover, 129Sv mice had higher levels of lipids in baseline conditions, but HFD caused more pronounced alterations in lipids profile of Bl6 mice.

It is critical for translational research that animal models be accurately characterized and validated as models of human disease. In the case of mice, and especially genetically modified models, special considerations must be made because these modifications are influenced by the genetics of the background strain, husbandry, and experimental conditions. Therefore, it is important to understand the translational value of these different mouse lines and to determine for which human pathology studies one or the other strain might be appropriate. Our studies show that active adaptation responses predominate in Bl6 mice, whereas passive adaptation predominates in 129Sv mice. Our studies have demonstrated that 129Sv mice are better suited to study anxiety-, depression-, and psychosis-like states. For example, in the present work, we can conclude that 129Sv mice can be considered a good model for modeling the metabolic syndrome associated with psychiatric disorders. At the same time, the Bl6 line is preferred in the study of social dominance, aggressiveness, addictive behavior, and conditions requiring rapid adaptation.

REFERENCES

Abramov U., Puussaar T., Raud S., Kurrikoff K., and Vasar E. (2008). Behavioural differences between C57BL/6 and 129S6/SvEv strains are reinforced by environmental enrichment. *Neurosci. Lett.* 443, 223–227. doi:10.1016/j.neulet.2008.07.075

Adams S. H., Hoppel C. L., Lok K. H., Zhao L., Wong S. W., Minkler P. E., Hwang D. H., Newman J. W., and Garvey W. T. (2009). Plasma Acylcarnitine Profiles Suggest Incomplete Long-Chain Fatty Acid β-Oxidation and Altered Tricarboxylic Acid Cycle Activity in Type 2 Diabetic African-American Women. *J Nutr* 139, 1073–1081. doi:10.3945/jn.108.103754

Attané C., Peyot M.-L., Lussier R., Zhang D., Joly E., Madiraju S. R. M., and Prentki M. (2016). Differential Insulin Secretion of High-Fat Diet-Fed C57BL/6NN and C57BL/6NJ Mice: Implications of Mixed Genetic Background in Metabolic Studies. *PLoS One* 11, e0159165. doi:10.1371/journal.pone.0159165

Ayala J. E., Bracy D. P., McGuinness O. P., and Wasserman D. H. (2006). Considerations in the design of hyperinsulinemic-euglycemic clamps in the conscious mouse. *Diabetes* 55, 390–397. doi:10.2337/diabetes.55.02.06.db05-0686

Bae O.-N., and Majid A. (2013). Role of histidine/histamine in carnosine-induced neuroprotection during ischemic brain damage. *Brain Res.* 1527, 246–254. doi:10.1016/j.brainres.2013.07.004

Banks W. A., Gray A. M., Erickson M. A., Salameh T. S., Damodarasamy M., Sheibani N., Meabon J. S., Wing E. E., Morofuji Y., Cook D. G., and Reed M. J. (2015). Lipopolysaccharide-induced blood-brain barrier disruption: roles of cyclooxygenase, oxidative stress, neuroinflammation, and elements of the neurovascular unit. *Journal of Neuroinflammation* 12, 223. doi:10.1186/s12974-015-0434-1

Batista C. R. A., Gomes G. F., Candelario-Jalil E., Fiebich B. L., and de Oliveira A. C. P. (2019). Lipopolysaccharide-Induced Neuroinflammation as a Bridge to Understand Neurodegeneration. *Int J Mol Sci* 20, 2293. doi:10.3390/ijms20092293

Belknap J. K., Crabbe J. C., and Young E. R. (1993). Voluntary consumption of ethanol in 15 inbred mouse strains. *Psychopharmacology (Berl.)* 112, 503–510. doi:10.1007/bf02244901

Blüher M., Michael M. D., Peroni O. D., Ueki K., Carter N., Kahn B. B., and Kahn C. R. (2002). Adipose tissue selective insulin receptor knockout protects against obesity and obesity-related glucose intolerance. *Dev Cell* 3, 25–38. doi:10.1016/s1534-5807(02)00199-5

Boitard C., Cavaroc A., Sauvant J., Aubert A., Castanon N., Layé S., and Ferreira G. (2014). Impairment of hippocampal-dependent memory induced by juvenile high-fat diet intake is associated with enhanced hippocampal inflammation in rats. *Brain Behav Immun* 40, 9–17. doi:10.1016/j.bbi.2014.03.005

Boldyrev A. A., Aldini G., and Derave W. (2013). Physiology and pathophysiology of carnosine. *Physiol Rev* 93, 1803–1845. doi:10.1152/physrev.00039.2012

Bonen A., Chabowski A., Luiken J. J. F. P., and Glatz J. F. C. (2007). Is membrane transport of FFA mediated by lipid, protein, or both? Mechanisms and regulation of protein-mediated cellular fatty acid uptake: molecular, biochemical, and physiological evidence. *Physiology (Bethesda)* 22, 15–29. doi:10.1152/physiologyonline.2007.22.1.15

Brown D. G., Soto R., Yandamuri S., Stone C., Dickey L., Gomes-Neto J. C., Pastuzyn E. D., Bell R., Petersen C., Buhrke K., Fujinami R. S., O'Connell R. M., Stephens W. Z., Shepherd J. D., Lane T. E., and Round J. L. The microbiota protects from

viral-induced neurologic damage through microglia-intrinsic TLR signaling. *eLife* 8, e47117. doi:10.7554/eLife.47117

Buchli R., Alberati-Giani D., Malherbe P., Köhler C., Broger C., and Cesura A. M. (1995). Cloning and functional expression of a soluble form of kynurenine/alpha-aminoadipate aminotransferase from rat kidney. *J. Biol. Chem.* 270, 29330–29335. doi:10.1074/jbc.270.49.29330

Cantin E., Tanamachi B., and Openshaw H. (1999). Role for Gamma Interferon in Control of Herpes Simplex Virus Type 1 Reactivation. *J Virol* 73, 3418–3423.

Cardona A. E., Pioro E. P., Sasse M. E., Kostenko V., Cardona S. M., Dijkstra I. M., Huang D., Kidd G., Dombrowski S., Dutta R., Lee J.-C., Cook D. N., Jung S., Lira S. A., Littman D. R., and Ransohoff R. M. (2006). Control of microglial neurotoxicity by the fractalkine receptor. *Nat Neurosci* 9, 917–924. doi:10.1038/nn1715

Cas M. D., Roda G., Li F., and Secundo F. (2020). Functional Lipids in Autoimmune Inflammatory Diseases. *Int J Mol Sci* 21, 3074. doi:10.3390/ijms21093074

Catorce M. N., and Gevorkian G. (2016). LPS-induced Murine Neuroinflammation Model: Main Features and Suitability for Pre-clinical Assessment of Nutraceuticals. *Curr Neuropharmacol* 14, 155–164. doi:10.2174/1570159x14666151204122017

Chen R., Zhang M., Park S., and Gnegy M. E. (2007). C57BL/6J mice show greater amphetamine-induced locomotor activation and dopamine efflux in the striatum than 129S2/SvHsd mice. *Pharmacol Biochem Behav* 87, 158–163. doi:10.1016/j.pbb.2007. 04.012

Chisholm K. I., Ida K. K., Davies A. L., Tachtsidis I., Papkovsky D. B., Dyson A., Singer M., Duchen M. R., and Smith K. J. (2016). Hypothermia protects brain mitochondrial function from hypoxemia in a murine model of sepsis. *J Cereb Blood Flow Metab* 36, 1955–1964. doi:10.1177/0271678X15606457

Chow J. C., Young D. W., Golenbock D. T., Christ W. J., and Gusovsky F. (1999). Toll-like receptor-4 mediates lipopolysaccharide-induced signal transduction. *J Biol Chem* 274, 10689–10692. doi:10.1074/jbc.274.16.10689

Crawley J. N., Belknap J. K., Collins A., Crabbe J. C., Frankel W., Henderson N., Hitzemann R. J., Maxson S. C., Miner L. L., Silva A. J., Wehner J. M., Wynshaw-Boris A., and Paylor R. (1997). Behavioral phenotypes of inbred mouse strains: implications and recommendations for molecular studies. *Psychopharmacology (Berl)* 132, 107–124. doi:10.1007/s002130050327

Dando S. J., Kazanis R., Chinnery H. R., and McMenamin P. G. (2019). Regional and functional heterogeneity of antigen presenting cells in the mouse brain and meninges. *Glia* 67, 935–949. doi:10.1002/glia.23581

David S., and Kroner A. (2011). Repertoire of microglial and macrophage responses after spinal cord injury. *Nat Rev Neurosci* 12, 388–399. doi:10.1038/nrn3053

Davidson S., Crotta S., McCabe T. M., and Wack A. (2014). Pathogenic potential of interferon αβ in acute influenza infection. *Nat Commun* 5, 3864. doi:10.1038/ncomms4864

Dawson R., Biasetti M., Messina S., and Dominy J. (2002). The cytoprotective role of taurine in exercise-induced muscle injury. *Amino Acids* 22, 309–324. doi:10.1007/s007260200017

Favennec M., Hennart B., Caiazzo R., Leloire A., Yengo L., Verbanck M., Arredouani A., Marre M., Pigeyre M., Bessede A., Guillemin G. J., Chinetti G., Staels B., Pattou F., Balkau B., Allorge D., Froguel P., and Poulain-Godefroy O. (2015). The kynurenine pathway is activated in human obesity and shifted toward kynurenine mono-

oxygenase activation. *Obesity (Silver Spring)* 23, 2066–2074. doi:10.1002/oby.21199

Felig P., Owen O. E., Wahren J., and Cahill G. F. (1969). Amino acid metabolism during prolonged starvation. *J. Clin. Invest.* 48, 584–594. doi:10.1172/JCI106017

Feng T., Tripathi A., and Pillai A. (2020). Inflammatory Pathways in Psychiatric Disorders: The case of Schizophrenia and Depression. *Curr Behav Neurosci Rep* 7, 128–138. doi:10.1007/s40473-020-00207-4

Fengler V. H. I., Macheiner T., Kessler S. M., Czepukojc B., Gemperlein K., Müller R., Kiemer A. K., Magnes C., Haybaeck J., Lackner C., and Sargsyan K. (2016). Susceptibility of Different Mouse Wild Type Strains to Develop Diet-Induced NAFLD/AFLD-Associated Liver Disease. *PLOS ONE* 11, e0155163. doi:10.1371/journal.pone.0155163

Feys P., Maes F., Nuttin B., Helsen W., Malfait V., Nagels G., Lavrysen A., and Liu X. (2005). Relationship between multiple sclerosis intention tremor severity and lesion load in the brainstem. *NeuroReport* 16, 1379–1382. doi:10.1097/01.wnr.0000176521.26971.58

Fujisaka S., Avila-Pacheco J., Soto M., Kostic A., Dreyfuss J. M., Pan H., Ussar S., Altindis E., Li N., Bry L., Clish C. B., and Kahn C. R. (2018). Diet, Genetics, and the Gut Microbiome Drive Dynamic Changes in Plasma Metabolites. *Cell Rep* 22, 3072–3086. doi:10.1016/j.celrep.2018.02.060

Förstermann U., and Sessa W. C. (2012). Nitric oxide synthases: regulation and function. *Eur Heart J* 33, 829–837. doi:10.1093/eurheartj/ehr304

Ganeshan K., and Chawla A. (2014). Metabolic Regulation of Immune Responses. *Annu. Rev. Immunol.* 32, 609–634. doi:10.1146/annurev-immunol-032713-120236

Ganeshan K., Nikkanen J., Man K., Leong Y. A., Sogawa Y., Maschek J. A., Van Ry T., Chagwedera D. N., Cox J. E., and Chawla A. (2019). Energetic Trade-Offs and Hypometabolic States Promote Disease Tolerance. *Cell* 177, 399-413.e12. doi:10.1016/j.cell.2019.01.050

Grabert K., Michoel T., Karavolos M. H., Clohisey S., Baillie J. K., Stevens M. P., Freeman T. C., Summers K. M., and McColl B. W. (2016). Microglial brain region-dependent diversity and selective regional sensitivities to ageing. *Nat Neurosci* 19, 504–516. doi:10.1038/nn.4222

Guasch-Ferré M., Hruby A., Toledo E., Clish C. B., Martínez-González M. A., Salas-Salvadó J., and Hu F. B. (2016). Metabolomics in Prediabetes and Diabetes: A Systematic Review and Meta-analysis. *Diabetes Care* 39, 833–846. doi:10.2337/dc15-2251

Guiotto A., Calderan A., Ruzza P., and Borin G. (2005). Carnosine and carnosine-related antioxidants: a review. *Curr Med Chem* 12, 2293–2315. doi:10.2174/0929867054864796

Gupta D., Jetton T. L., LaRock K., Monga N., Satish B., Lausier J., Peshavaria M., and Leahy J. L. (2017). Temporal characterization of β cell-adaptive and -maladaptive mechanisms during chronic high-fat feeding in C57BL/6NTac mice. *J Biol Chem* 292, 12449–12459. doi:10.1074/jbc.M117.781047

Hallen A., Jamie J. F., and Cooper A. J. L. (2013). Lysine metabolism in mammalian brain: an update on the importance of recent discoveries. *Amino Acids* 45, 1249–1272. doi:10.1007/s00726-013-1590-1

Heinla I., Leidmaa E., Visnapuu T., Philips M.-A., and Vasar E. (2014). Enrichment and individual housing reinforce the differences in aggressiveness and amphetamine

response in 129S6/SvEv and C57BL/6 strains. *Behav. Brain Res.* 267, 66–73. doi:10.1016/j.bbr.2014.03.024

Ho C.-Y., Lin Y.-T., Chen H.-H., Ho W.-Y., Sun G.-C., Hsiao M., Lu P.-J., Cheng P.-W., and Tseng C.-J. (2020). CX3CR1-microglia mediates neuroinflammation and blood pressure regulation in the nucleus tractus solitarii of fructose-induced hypertensive rats. *J Neuroinflammation* 17, 185. doi:10.1186/s12974-020-01857-7

Hotamisligil G. S. (2006). Inflammation and metabolic disorders. *Nature* 444, 860–867. doi:10.1038/nature05485

Hughes P. M., Botham M. S., Frentzel S., Mir A., and Perry V. H. (2002). Expression of fractalkine (CX3CL1) and its receptor, CX3CR1, during acute and chronic inflammation in the rodent CNS. *Glia* 37, 314–327. doi:10.1002/glia.10037

Hynes R. O. (1992). Integrins: versatility, modulation, and signaling in cell adhesion. *Cell* 69, 11–25. doi:10.1016/0092-8674(92)90115-s

Jaric I., Voelkl B., Clerc M., Schmid M. W., Novak J., Rosso M., Rufener R., von Kortzfleisch V. T., Richter S. H., Buettner M., Bleich A., Amrein I., Wolfer D. P., Touma C., Sunagawa S., and Würbel H. (2022). The rearing environment persistently modulates mouse phenotypes from the molecular to the behavioural level. *PLoS Biol* 20, e3001837. doi:10.1371/journal.pbio.3001837

Jänne J., Alhonen L., Keinänen T. A., Pietilä M., Uimari A., Pirinen E., Hyvönen M. T., and Järvinen A. (2005). Animal disease models generated by genetic engineering of polyamine metabolism. *J. Cell. Mol. Med.* 9, 865–882. doi:10.1111/j.1582-4934.2005.tb00385.x

Jensen M. B., and St. Louis E. K. (2005). Management of Acute Cerebellar Stroke. *Archives of Neurology* 62, 537–544. doi:10.1001/archneur.62.4.537

Jeon B. T., Jeong E. A., Shin H. J., Lee Y., Lee D. H., Kim H. J., Kang S. S., Cho G. J., Choi W. S., and Roh G. S. (2012). Resveratrol Attenuates Obesity-Associated Peripheral and Central Inflammation and Improves Memory Deficit in Mice Fed a High-Fat Diet. *Diabetes* 61, 1444–1454. doi:10.2337/db11-1498

Kaare M., Mikheim K., Lilleväli K., Kilk K., Jagomäe T., Leidmaa E., Piirsalu M., Porosk R., Singh K., Reimets R., Taalberg E., Schäfer M. K. E., Plaas M., Vasar E., and Philips M.-A. (2021). High-Fat Diet Induces Pre-Diabetes and Distinct Sex-Specific Metabolic Alterations in Negr1-Deficient Mice. *Biomedicines* 9, 1148. doi:10.3390/biomedicines9091148

Kanda H., Tateya S., Tamori Y., Kotani K., Hiasa K., Kitazawa R., Kitazawa S., Miyachi H., Maeda S., Egashira K., and Kasuga M. (2006). MCP-1 contributes to macrophage infiltration into adipose tissue, insulin resistance, and hepatic steatosis in obesity. *J Clin Invest* 116, 1494–1505. doi:10.1172/JCI26498

Kenéz Á., Warnken T., Feige K., and Huber K. (2018). Lower plasma trans-4-hydroxyproline and methionine sulfoxide levels are associated with insulin dysregulation in horses. *BMC Veterinary Research* 14, 146. doi:10.1186/s12917-018-1479-z

Khan Z., Shen X. Z., Bernstein E. A., Giani J. F., Eriguchi M., Zhao T. V., Gonzalez-Villalobos R. A., Fuchs S., Liu G. Y., and Bernstein K. E. (2017). Angiotensin-converting enzyme enhances the oxidative response and bactericidal activity of neutrophils. *Blood* 130, 328–339. doi:10.1182/blood-2016-11-752006

Kigerl K. A., Gensel J. C., Ankeny D. P., Alexander J. K., Donnelly D. J., and Popovich P. G. (2009). Identification of two distinct macrophage subsets with divergent effects causing either neurotoxicity or regeneration in the injured mouse spinal cord. *J Neurosci* 29, 13435–13444. doi:10.1523/JNEUROSCI.3257-09.2009

Kim K. K., Jin S. H., and Lee B. J. (2013). Herpes Virus Entry Mediator Signaling in the Brain Is Imperative in Acute Inflammation-Induced Anorexia and Body Weight Loss. *Endocrinol Metab (Seoul)* 28, 214–220. doi:10.3803/EnM.2013.28.3.214

Kita T., Morrison P. F., Heyes M. P., and Markey S. P. (2002). Effects of systemic and central nervous system localized inflammation on the contributions of metabolic precursors to the l-kynurenine and quinolinic acid pools in brain. *Journal of Neurochemistry* 82, 258–268. doi:10.1046/j.1471-4159.2002.00955.x

Klebanov G. I., Teselkin YuO null, Babenkova I. V., Lyubitsky O. B., Rebrova OYu null, Boldyrev A. A., and Vladimirov YuA null (1998). Effect of carnosine and its components on free-radical reactions. *Membr Cell Biol* 12, 89–99.

Koido K., Innos J., Haring L., Zilmer M., Ottas A., and Vasar E. (2016). Taurine and Epidermal Growth Factor Belong to the Signature of First-Episode Psychosis. *Front Neurosci* 10, 331. doi:10.3389/fnins.2016.00331

Koike H., Arguello P. A., Kvajo M., Karayiorgou M., and Gogos J. A. (2006). Disc1 is mutated in the 129S6/SvEv strain and modulates working memory in mice. *Proc. Natl. Acad. Sci. U.S.A.* 103, 3693–3697. doi:10.1073/pnas.0511189103

Kouttab N. M., and De Simone C. (1993). Modulation of cytokine production by carnitine. *Mediators Inflamm.* 2, S25-28. doi:10.1155/S0962935193000717

Kriisa K., Leppik L., Balõtšev R., Ottas A., Soomets U., Koido K., Volke V., Innos J., Haring L., Vasar E., and Zilmer M. (2017). Profiling of Acylcarnitines in First Episode Psychosis before and after Antipsychotic Treatment. *J. Proteome Res.* 16, 3558–3566. doi:10.1021/acs.jproteome.7b00279

Lalić I. M., Bichele R., Repar A., Despotović S. Z., Petričević S., Laan M., Peterson P., Westermann J., Milićević Ž., Mirkov I., and Milićević N. M. (2018). Lipopolysaccharide induces tumor necrosis factor receptor-1 independent relocation of lymphocytes from the red pulp of the mouse spleen. *Ann A*nat 216, 125–134. doi:10.1016/j.aanat.2017.12.002

Leandro J., Violante S., Argmann C. A., Hagen J., Dodatko T., Bender A., Zhang W., Williams E. G., Bachmann A. M., Auwerx J., Yu C., and Houten S. M. (2019). Mild inborn errors of metabolism in commonly used inbred mouse strains. *Mol. Genet. Metab.* 126, 388–396. doi:10.1016/j.ymgme.2019.01.021

Leppik L., Parksepp M., Janno S., Koido K., Haring L., Vasar E., and Zilmer M. (2019). Profiling of lipidomics before and after antipsychotic treatment in first-episode psychosis. *Eur Arch Psychiatry Clin Neurosci*. doi:10.1007/s00406-018-0971-6

Lipina T. V., Zai C., Hlousek D., Roder J. C., and Wong A. H. C. (2013). Maternal Immune Activation during Gestation Interacts with Disc1 Point Mutation to Exacerbate Schizophrenia-Related Behaviors in Mice. *J Neurosci* 33, 7654–7666. doi:10.1523/JNEUROSCI.0091-13.2013

Liu M., Huang Y., Zhang H., Aitken D., Nevitt M. C., Rockel J. S., Pelletier J.-P., Lewis C. E., Torner J., Rampersaud Y. R., Perruccio A. V., Mahomed N. N., Furey A., Randell E. W., Rahman P., Sun G., Martel-Pelletier J., Kapoor M., Jones G., Felson D., Qi D., and Zhai G. (2022). Restricting Branched-Chain Amino Acids within a High-Fat Diet Prevents Obesity. *Metabolites* 12, 334. doi:10.3390/metabo12040334

Lundberg P., Welander P., Openshaw H., Nalbandian C., Edwards C., Moldawer L., and Cantin E. (2003). A Locus on Mouse Chromosome 6 That Determines Resistance to Herpes Simplex Virus Also Influences Reactivation, While an Unlinked Locus Augments Resistance of Female Mice. *J Virol* 77, 11661–11673. doi:10.1128/JVI.77.21.11661-11673.2003

Makrecka-Kuka M., Sevostjanovs E., Vilks K., Volska K., Antone U., Kuka J., Makarova E., Pugovics O., Dambrova M., and Liepinsh E. (2017). Plasma acylcarnitine concentrations reflect the acylcarnitine profile in cardiac tissues. *Scientific Reports* 7, 17528. doi:10.1038/s41598-017-17797-x

Marshall S. A., McClain J. A., Kelso M. L., Hopkins D. M., Pauly J. R., and Nixon K. (2013). Microglial activation is not equivalent to neuroinflammation in alcohol-induced neurodegeneration: the importance of microglia phenotype. *Neurobiol Dis* 54, 239–251. doi:10.1016/j.nbd.2012.12.016

Mastronardi C. A., Yu W. H., Srivastava V. K., Dees W. L., and McCann S. M. (2001). Lipopolysaccharide-induced leptin release is neurally controlled. *Proc Natl Acad Sci U S A* 98, 14720–14725. doi:10.1073/pnas.251543598

McCoin C. S., Knotts T. A., and Adams S. H. (2015). Acylcarnitines--old actors auditioning for new roles in metabolic physiology. *Nat Rev Endocrinol* 11, 617–625. doi:10.1038/nrendo.2015.129

McCormack S. E., Shaham O., McCarthy M. A., Deik A. A., Wang T. J., Gerszten R. E., Clish C. B., Mootha V. K., Grinspoon S. K., and Fleischman A. (2013). Circulating branched-chain amino acid concentrations are associated with obesity and future insulin resistance in children and adolescents. *Pediatr Obes* 8, 52–61. doi:10.1111/j.2047-6310.2012.00087.x

Merino J., Leong A., Liu C.-T., Porneala B., Walford G. A., von Grotthuss M., Wang T. J., Flannick J., Dupuis J., Levy D., Gerszten R. E., Florez J. C., and Meigs J. B. (2018). Metabolomics insights into early type 2 diabetes pathogenesis and detection in individuals with normal fasting glucose. *Diabetologia* 61, 1315–1324. doi:10.1007/s00125-018-4599-x

Middaugh L. D., Kelley B. M., Bandy A. L., and McGroarty K. K. (1999). Ethanol consumption by C57BL/6 mice: influence of gender and procedural variables. *Alcohol* 17, 175–183. doi:10.1016/s0741-8329(98)00055-x

Miller A. A., and Spencer S. J. (2014). Obesity and neuroinflammation: a pathway to cognitive impairment. *Brain Behav Immun* 42, 10–21. doi:10.1016/j.bbi.2014.04.001

Moffett J. R., and Namboodiri M. A. (2003). Tryptophan and the immune response. *Immunology & Cell Biology* 81, 247–265. doi:10.1046/j.1440-1711.2003.t01-1-01177.x

Mong M., Chao C., and Yin M. (2011). Histidine and carnosine alleviated hepatic steatosis in mice consumed high saturated fat diet. *European Journal of Pharmacology* 653, 82–88. doi:10.1016/j.ejphar.2010.12.001

Montgomery M. K., Hallahan N. L., Brown S. H., Liu M., Mitchell T. W., Cooney G. J., and Turner N. (2013). Mouse strain-dependent variation in obesity and glucose homeostasis in response to high-fat feeding. *Diabetologia* 56, 1129–1139. doi:10.1007/s00125-013-2846-8

Mukaida N., Ishikawa Y., Ikeda N., Fujioka N., Watanabe S., Kuno K., and Matsushima K. (1996). Novel insight into molecular mechanism of endotoxin shock: biochemical analysis of LPS receptor signaling in a cell-free system targeting NF-kappaB and regulation of cytokine production/action through beta2 integrin in vivo. *J. Leukoc. Biol.* 59, 145–151. doi:10.1002/jlb.59.2.145

Muntjewerff E. M., Meesters L. D., van den Bogaart G., and Revelo N. H. (2020). Reverse Signaling by MHC-I Molecules in Immune and Non-Immune Cell Types. *Front Immunol* 11, 605958. doi:10.3389/fimmu.2020.605958

Narvik J., Vanaveski T., Innos J., Philips M.-A., Ottas A., Haring L., Zilmer M., and Vasar E. (2018). Metabolic profile associated with distinct behavioral coping

strategies of 129Sv and Bl6 mice in repeated motility test. *Sci Rep* 8, 3405. doi:10.1038/s41598-018-21752-9

Newgard C. B., An J., Bain J. R., Muehlbauer M. J., Stevens R. D., Lien L. F., Haqq A. M., Shah S. H., Arlotto M., Slentz C. A., Rochon J., Gallup D., Ilkayeva O., Wenner B. R., Yancy W. S., Eisenson H., Musante G., Surwit R. S., Millington D. S., Butler M. D., and Svetkey L. P. (2009). A Branched-Chain Amino Acid-Related Metabolic Signature that Differentiates Obese and Lean Humans and Contributes to Insulin Resistance. *Cell Metabolism* 9, 311–326. doi:10.1016/j.cmet.2009.02.002

Norris G. H., and Blesso C. N. (2017). Dietary and Endogenous Sphingolipid Metabolism in Chronic Inflammation. *Nutrients* 9, 1180. doi:10.3390/nu9111180

Paapstel K., Kals J., Eha J., Tootsi K., Ottas A., Piir A., Jakobson M., Lieberg J., and Zilmer M. (2018). Inverse relations of serum phosphatidylcholines and lysophosphatidylcholines with vascular damage and heart rate in patients with atherosclerosis. *Nutr Metab Cardiovasc Dis* 28, 44–52. doi:10.1016/j.numecd.2017.07.011

Pang Y., Campbell L., Zheng B., Fan L., Cai Z., and Rhodes P. (2010). Lipopolysaccharide-activated microglia induce death of oligodendrocyte progenitor cells and impede their development. *Neuroscience* 166, 464–475. doi:10.1016/j.neuroscience.2009.12.040

Park B. S., and Lee J.-O. (2013). Recognition of lipopolysaccharide pattern by TLR4 complexes. *Exp Mol Med* 45, e66. doi:10.1038/emm.2013.97

Qin L., Wu X., Block M. L., Liu Y., Breese G. R., Hong J.-S., Knapp D. J., and Crews F. T. (2007). Systemic LPS causes chronic neuroinflammation and progressive neurodegeneration. *Glia* 55, 453–462. doi:10.1002/glia.20467

Raetz C. R. H., and Whitfield C. (2002). Lipopolysaccharide endotoxins. *Annu Rev Biochem* 71, 635–700. doi:10.1146/annurev.biochem.71.110601.135414

Rajanikant G. k., Zemke D., Senut M.-C., Frenkel M. B., Chen A. F., Gupta R., and Majid A. (2007). Carnosine Is Neuroprotective Against Permanent Focal Cerebral Ischemia in Mice. *Stroke* 38, 3023–3031. doi:10.1161/STROKEAHA.107.488502

Raud S., Sütt S., Plaas M., Luuk H., Innos J., Philips M.-A., Kõks S., and Vasar E. (2007). Cat odor exposure induces distinct changes in the exploratory behavior and Wfs1 gene expression in C57Bl/6 and 129Sv mice. *Neurosci. Lett.* 426, 87–90. doi:10.1016/j.neulet.2007.08.052

Rivest S. (2003). Molecular insights on the cerebral innate immune system. *Brain Behav Immun* 17, 13–19. doi:10.1016/s0889-1591(02)00055-7

Rutkowsky J. M., Knotts T. A., Ono-Moore K. D., McCoin C. S., Huang S., Schneider D., Singh S., Adams S. H., and Hwang D. H. (2014). Acylcarnitines activate proinflammatory signaling pathways. *Am J Physiol Endocrinol Metab* 306, E1378–E1387. doi:10.1152/ajpendo.00656.2013

Sarna J. R., Dyck R. H., and Whishaw I. Q. (2000). The Dalila effect: C57BL6 mice barber whiskers by plucking. *Behav. Brain Res.* 108, 39–45. doi:10.1016/s0166-4328(99)00137-0

Sarraf P., Frederich R. C., Turner E. M., Ma G., Jaskowiak N. T., Rivet D. J., Flier J. S., Lowell B. B., Fraker D. L., and Alexander H. R. (1997). Multiple cytokines and acute inflammation raise mouse leptin levels: potential role in inflammatory anorexia. *J Exp Med* 185, 171–175. doi:10.1084/jem.185.1.171

Silva A. J., Simpson E. M., Takahashi J. S., Lipp H.-P., Nakanishi S., Wehner J. M., Giese K. P., Tully T., Abel T., Chapman P. F., Fox K., Grant S., Itohara S., Lathe R., Mayford M., McNamara J. O., Morris R. J., Picciotto M., Roder J., Shin H.-S., Slesinger P. A., Storm D. R., Stryker M. P., Tonegawa S., Wang Y., and Wolfer D.

P. (1997). Mutant Mice and Neuroscience: Recommendations Concerning Genetic Background. *Neuron* 19, 755–759. doi:10.1016/S0896-6273(00)80958-7

Silwedel C., and Förster C. (2006). Differential susceptibility of cerebral and cerebellar murine brain microvascular endothelial cells to loss of barrier properties in response to inflammatory stimuli. *Journal of Neuroimmunology* 179, 37–45. doi:10.1016/j.jneuroim.2006.06.019

Stempel H., Jung M., Pérez-Gómez A., Leinders-Zufall T., Zufall F., and Bufe B. (2016). Strain-specific Loss of Formyl Peptide Receptor 3 in the Murine Vomeronasal and Immune Systems. *J Biol Chem* 291, 9762–9775. doi:10.1074/jbc.M116.714493

Takashina C., Tsujino I., Watanabe T., Sakaue S., Ikeda D., Yamada A., Sato T., Ohira H., Otsuka Y., Oyama-Manabe N., Ito Y. M., and Nishimura M. (2016). Associations among the plasma amino acid profile, obesity, and glucose metabolism in Japanese adults with normal glucose tolerance. *Nutr Metab (Lond)* 13, 5. doi:10.1186/s12986-015-0059-5

Tay T. L., Mai D., Dautzenberg J., Fernández-Klett F., Lin G., Sagar, Datta M., Drougard A., Stempfl T., Ardura-Fabregat A., Staszewski O., Margineanu A., Sporbert A., Steinmetz L. M., Pospisilik J. A., Jung S., Priller J., Grün D., Ronneberger O., and Prinz M. (2017). A new fate mapping system reveals context-dependent random or clonal expansion of microglia. *Nat Neurosci* 20, 793–803. doi:10.1038/nn.4547

Thomson P. A., Malavasi E. L. V., Grünewald E., Soares D. C., Borkowska M., and Millar J. K. (2013). DISC1 genetics, biology and psychiatric illness. *Front Biol (Beijing)* 8, 1–31. doi:10.1007/s11515-012-1254-7

Trossbach S. V., Bader V., Hecher L., Pum M. E., Masoud S. T., Prikulis I., Schäble S., de Souza Silva M. A., Su P., Boulat B., Chwiesko C., Poschmann G., Stühler K., Lohr K. M., Stout K. A., Oskamp A., Godsave S. F., Müller-Schiffmann A., Bilzer T., Steiner H., Peters P. J., Bauer A., Sauvage M., Ramsey A. J., Miller G. W., Liu F., Seeman P., Brandon N. J., Huston J. P., and Korth C. (2016). Misassembly of full-length Disrupted-in-Schizophrenia 1 protein is linked to altered dopamine homeostasis and behavioral deficits. *Mol. Psychiatry* 21, 1561–1572. doi:10.1038/mp.2015.194

Trossbach S. V., Hecher L., Schafflick D., Deenen R., Popa O., Lautwein T., Tschirner S., Köhrer K., Fehsel K., Papazova I., Malchow B., Hasan A., Winterer G., Schmitt A., Meyer zu Hörste G., Falkai P., and Korth C. (2019). Dysregulation of a specific immune-related network of genes biologically defines a subset of schizophrenia. *Transl Psychiatry* 9, 156. doi:10.1038/s41398-019-0486-6

Tuboly G., Tar L., Bohar Z., Safrany-Fark A., Petrovszki Z., Kekesi G., Vecsei L., Pardutz A., and Horvath G. (2015). The inimitable kynurenic acid: the roles of different ionotropic receptors in the action of kynurenic acid at a spinal level. *Brain Res. Bull.* 112, 52–60. doi:10.1016/j.brainresbull.2015.02.001

Ulland T. K., Jain N., Hornick E. E., Elliott E. I., Clay G. M., Sadler J. J., Mills K. A. M., Janowski A. M., Volk A. P. D., Wang K., Legge K. L., Gakhar L., Bourdi M., Ferguson P. J., Wilson M. E., Cassel S. L., and Sutterwala F. S. (2016). Nlrp12 mutation causes C57BL/6J strain-specific defect in neutrophil recruitment. *Nat Commun* 7, 13180. doi:10.1038/ncomms13180

Ussar S., Griffin N. W., Bezy O., Fujisaka S., Vienberg S., Softic S., Deng L., Bry L., Gordon J. I., and Kahn C. R. (2015). Interactions between Gut Microbiota, Host Genetics and Diet Modulate the Predisposition to Obesity and Metabolic Syndrome. *Cell Metab* 22, 516–530. doi:10.1016/j.cmet.2015.07.007

Uzuneser T. C., Speidel J., Kogias G., Wang A.-L., de Souza Silva M. A., Huston J. P., Zoicas I., von Hörsten S., Kornhuber J., Korth C., and Müller C. P. (2019). Disrupted-in-Schizophrenia 1 (DISC1) Overexpression and Juvenile Immune Activation Cause Sex-Specific Schizophrenia-Related Psychopathology in Rats. *Front. Psychiatry* 10,. doi:10.3389/fpsyt.2019.00222

Varul J., Eskla K.-L., Piirsalu M., Innos J., Philips M.-A., Visnapuu T., Plaas M., and Vasar E. (2021). Dopamine System, NMDA Receptor and EGF Family Expressions in Brain Structures of Bl6 and 129Sv Strains Displaying Different Behavioral Adaptation. *Brain Sci* 11, 725. doi:10.3390/brainsci11060725

van der Veen J. N., Kennelly J. P., Wan S., Vance J. E., Vance D. E., and Jacobs R. L. (2017). The critical role of phosphatidylcholine and phosphatidylethanolamine metabolism in health and disease. *Biochimica et Biophysica Acta (BBA) - Biomembranes* 1859, 1558–1572. doi:10.1016/j.bbamem.2017.04.006

Võikar V., Kõks S., Vasar E., and Rauvala H. (2001). Strain and gender differences in the behavior of mouse lines commonly used in transgenic studies. *Physiol. Behav.* 72, 271–281.

Võikar V., Vasar E., and Rauvala H. (2004). Behavioral alterations induced by repeated testing in C57BL/6J and 129S2/Sv mice: implications for phenotyping screens. *Genes Brain Behav.* 3, 27–38. doi:10.1046/j.1601-183x.2003.0044.x

Wanders R. J. A., Komen J., and Kemp S. (2011). Fatty acid omega-oxidation as a rescue pathway for fatty acid oxidation disorders in humans. *FEBS J* 278, 182–194. doi:10.1111/j.1742-4658.2010.07947.x

Wang T. J., Larson M. G., Vasan R. S., Cheng S., Rhee E. P., McCabe E., Lewis G. D., Fox C. S., Jacques P. F., Fernandez C., O'Donnell C. J., Carr S. A., Mootha V. K., Florez J. C., Souza A., Melander O., Clish C. B., and Gerszten R. E. (2011). Metabolite profiles and the risk of developing diabetes. *Nat Med* 17, 448–453. doi:10.1038/nm.2307

Wang A., Luan H. H., and Medzhitov R. (2019). An evolutionary perspective on immunometabolism. *Science* 363, eaar3932. doi:10.1126/science.aar3932

Wang T. J., Ngo D., Psychogios N., Dejam A., Larson M. G., Vasan R. S., Ghorbani A., O'Sullivan J., Cheng S., Rhee E. P., Sinha S., McCabe E., Fox C. S., O'Donnell C. J., Ho J. E., Florez J. C., Magnusson M., Pierce K. A., Souza A. L., Yu Y., Carter C., Light P. E., Melander O., Clish C. B., and Gerszten R. E. (2013). 2-Aminoadipic acid is a biomarker for diabetes risk. *J. Clin. Invest.* 123, 4309–4317. doi:10.1172/JCI64801

Ware L. B., Magarik J. A., Wickersham N., Cunningham G., Rice T. W., Christman B. W., Wheeler A. P., Bernard G. R., and Summar M. L. (2013). Low plasma citrulline levels are associated with acute respiratory distress syndrome in patients with severe sepsis. *Crit Care* 17, R10. doi:10.1186/cc11934

Wu H. Q., Ungerstedt U., and Schwarcz R. (1995). L-alpha-aminoadipic acid as a regulator of kynurenic acid production in the hippocampus: a microdialysis study in freely moving rats. *Eur. J. Pharmacol.* 281, 55–61. doi:10.1016/0014-2999(95)00224-9

Wu Y., Williams E. G., Dubuis S., Mottis A., Jovaisaite V., Houten S. M., Argmann C. A., Faridi P., Wolski W., Kutalik Z., Zamboni N., Auwerx J., and Aebersold R. (2014). Multilayered genetic and omics dissection of mitochondrial activity in a mouse reference population. *Cell* 158, 1415–1430. doi:10.1016/j.cell.2014.07.039

Xu S., Liu X., Bao Y., Zhu X., Han C., Zhang P., Zhang X., Li W., and Cao X. (2012). Constitutive MHC class I molecules negatively regulate TLR-triggered inflamma-

tory responses via the Fps-SHP-2 pathway. *Nat Immunol* 13, 551–559. doi:10.1038/ni.2283

Xu W.-Y., Shen Y., Zhu H., Gao J., Zhang C., Tang L., Lu S.-Y., Shen C.-L., Zhang H.-X., Li Z., Meng P., Wan Y.-H., Fei J., and Wang Z.-G. (2019). 2-Aminoadipic acid protects against obesity and diabetes. *J Endocrinol* 243, 111–123. doi:10.1530/JOE-19-0157

Xu X., Song L., and Hanganu-Opatz I. L. (2021). Knock-Down of Hippocampal DISC1 in Immune-Challenged Mice Impairs the Prefrontal-Hippocampal Coupling and the Cognitive Performance Throughout Development. *Cereb Cortex* 31, 1240–1258. doi:10.1093/cercor/bhaa291

Yoshiki A., and Moriwaki K. (2006). Mouse phenome research: implications of genetic background. *ILAR J* 47, 94–102. doi:10.1093/ilar.47.2.94

Yuan W., Zhang J., Li S., and Edwards J. L. (2011). Amine metabolomics of hyperglycemic endothelial cells using capillary LC-MS with isobaric tagging. *J. Proteome Res.* 10, 5242–5250. doi:10.1021/pr200815c

Zeitoun-Ghandour S., Leszczyszyn O. I., Blindauer C. A., Geier F. M., Bundy J. G., and Stürzenbaum S. R. (2011). C. elegans metallothioneins: response to and defence against ROS toxicity. *Mol Biosyst* 7, 2397–2406. doi:10.1039/c1mb05114h

Zheng D., Liwinski T., and Elinav E. (2020). Interaction between microbiota and immunity in health and disease. *Cell Res* 30, 492–506. doi:10.1038/s41422-020-0332-7

Zhou M., Shao J., Wu C.-Y., Shu L., Dong W., Liu Y., Chen M., Wynn R. M., Wang J., Wang J., Gui W.-J., Qi X., Lusis A. J., Li Z., Wang W., Ning G., Yang X., Chuang D. T., Wang Y., and Sun H. (2019). Targeting BCAA Catabolism to Treat Obesity-Associated Insulin Resistance. *Diabetes* 68, 1730–1746. doi:10.2337/db18-0927

SUMMARY IN ESTONIAN

Põletiku ja dieedi mõju Bl6 and 129Sv hiireliinide metaboolsele profiilile ja valitud geneetilistele parameetritele

Hiirtel on inimestega palju füsioloogilisi ja geneetilisi sarnasusi, mistõttu on neist saanud ravimiarenduse valdkonnas ohutuse testimisel ja inimeste haiguste modelleerimisel vältimatult oluline mudelorganism. Ravimikandidaat peab läbima ulatuslikud prekliinilised efektiivsus- ja ohutustestid, enne kui selle saab heaks kiita kliinilisteks inimkatseteks. Sel põhjusel on inbriiditud hiireliinid meditsiinis ja bioloogilistes uuringutes hädavajalikud. Kuna nad on geneetiliselt identsed soo ja liini piires, puudub neil inimpopulatsioonidele omane geneetiline heterogeensus. Hiirte ja eriti geneetiliselt muundatud mudelite puhul tuleb erilist tähelepanu pöörata taustaliinile, kuna geneetiliste manipulatsioonide tagajärjel tekkinud fenotüüp on tugevalt mõjutatud taustaliinide geneetikast, kasvatus- ja katsetingimustest. Seetõttu võivad erinevad hiireliinid anda erinevaid ning isegi vastukäivaid tulemusi. Siirdemeditsiiniliste uuringute läbiviimisel on oluline, et loommudelid oleks täpselt iseloomustatud ja kinnitatud inimeste haiguste mudelitena ning seetõttu on oluline põhjalikult kaardistada hiireliinide erinevusi.

Käesolevas doktoritöös võrdlen kahte inbriiditud hiireliini: C57BL/6NTac (Bl6) ja 129S6/SvEvTac (129Sv), kes erinevad üksteisest käitumuslike iseärasuste tõttu. Need hiired on teadusuuringutes ühed kõige laialdasemalt kasutatavad hiireliinid ning kuldstandardiks transgeensete mudelite loomisel. Bl6 hiired on aktiivsemad, uudishimulikud ja uues keskkonnas paremad kohanejad, seevastu 129Sv hiired on passiivsemad ja oluliselt haavatavamad stressirohketes olukordades. Oluline on ka teada, et Bl6 ja 129Sv hiirete vahel esineb märkimisväärne heterogeensus metaboolses profiilis. Bl6 hiireliinile iseloomulike metaboliitide hulka kuuluvad biogeensed amiinid atsetüül-ornitiin, karnosiin, alfa-aminoadipaat ja lüsofosfatidüülkoliin C16:1. Seevastu 129Sv hiirtel domineerivad lühikese ahelalised atsüülkarnitiinid C4-, C5- ja sfingomüeliin SM (OH) C22:2 (Narvik et al., 2018). Kaks metaboliiti, mis selgelt silma paistavad on karnosiin ja alfa-aminoadipaat. Karnosiinil on antioksüdantsed omadused, mis pidurdavad ja reguleerivad vabade radikaalide teket (Guiotto et al., 2005; Dawson et al., 2002; Rajanikant et al., 2007). Alfa-aminoadipaadi puhul on aga näidatud kaitsvat efekti rasvumise ja diabeedi tekkes (Xu et al., 2019). Lisaks on 129Sv liinil *Disc1* geen mittefunktsionaalne, mida on seostatud mitmete psühhiaatriliste häirete väljakujunemisega (Thomson et al., 2013). Sellest lähtuvalt sobivad 129Sv hiired paremini psühhiaatriliste häiretega seotud käitumisomaduste uurimiseks. Erinevate psühhiaatriliste häirete tekkega on seostatud immuunsüsteemi talitluse häireid ning varasemad uuringud on näidanud nende häirete komorbiidsust metaboolse sündroomiga. Seda silmas pidades oli antud doktoritöö eesmärgiks avardada teadmisi Bl6 ja 129Sv hiirte toimetulekustrateegiate kohta, pöörates erilist tähelepanu põletikule ja metaboolse sündroomi tekkele.

Süsteemse põletiku indutseerimiseks manustasime hiirtele intraperitoneaalse süstiga lipopolüsahhariidi (LPS; *E.coli* O111:B4), mis on Gram-negatiivsete bakterite välismembraani peamine koostisosa ning seondudes TLR4 retseptoriga aktiveerib NF-κB signaaliraja ning indutseerib põletikutsütokiinide ekspressiooni ja immuunvastuse tekke. Esimeses artiklis analüüsisime erinevusi atsüülkarnitiinide, aminohapete, glütserofosfolipiidide, sfingolipiidide ja biogeensete amiinide profiilis varases (1.5 h) ning hilises (24 h) akuutses põletikumudelis. Näitasime, et LPS kutsub Bl6 hiirtel esile hüpometaboolse reaktsiooni, millel on oluline roll energia säästmisel põletikulistes tingimustes (Ganeshan et al., 2019). Seda hüpometaboolset seisundit iseloomustas 1.5 h peale LPS-i manustamist glükogeensete aminohapete ja atsetüül-ornitiini taseme langus. Hüpometaboolne reaktsioon võimendus veelgi enam 24 h peale LPS-i manustamist, mida iseloomustas heksooside ja mitmete teiste metaboliitide taseme langus. Lisaks oli Bl6 hiirtel suurenenud neuroprotektiivse toimega putrestsiini tootmine. Nende muutustega kaasnes ka tugev kehakaalu langus. Seevastu 129Sv hiireliinis Bl6 hiireliinile omast hüpometaboolset reaktsiooni ei esinenud, vaid metabolismi iseloomustas suurenenud lipiidide tootmine 1.5 h peale LPS-i manustamist. 24 h hiljem olid tõusnud lisaks lipiidide tasemele ka hüdroksüleeritud atsüülkarnitiinid, mille kuhjumine peegeldab pika ahelaga rasvhapete mittetäielikku β-oksüdatsiooni ja suurenenud põletikulist seisundit. Nende muutustega kaasnes mõõdukas kehakaalu langus. Kokkuvõtvalt leidsime, et Bl6 hiired võitlevad aktiivselt põletikuga, pärssides metaboliitide normaalset tootmist ja suurendades neuroprotektiivsete metaboliitide tootmist, millega kaasneb ka tugev kehakaalu kaotus. Vastupidiselt, 129Sv kehakaalu kaotus on mõõdukas ning põletikulist seisundit iseloomustab suurenenud proinflammatoorsete metaboliitide tootmine.

Teises artiklis näitasime, et Bl6 hiirtel esineb 24 h peale LPS-i manustamist ka hüpotermia. Põletikust tingitud hüpotermia põhjustab hüpometabolismi ja vastupidi, mis toetab ka esimeses artiklis saadud tulemusi. LPS põhjustas 129Sv hiirte ajus põletikulist seisundit, mida iseloomustas põletikuliste mikrogliia pinnamarkerite taseme tõus. Bl6 hiirtel oli LPS-i manustamise järgselt mikrogliia rakkude pinnal peamise koesobivuskompleksi (MHC) II molekulide ekspressioonitase oluliselt langenud. Klassikaliselt on MHC-II ekspressiooni indutseerimine üheks mikrogliia aktiveerimise tunnuseks põletikulises või patoloogilises kontekstis ning langus võib peegeldada kaitsvat reaktsiooni, mille eesmärk on vältida rakukahjustusi. See tähelepanek andis meile ajendi järgnevalt uurida muutusi MHC-I raja komponentide ekspressioonis. Lisaks klassikalisele antigeeni esitlemise funktsioonile reguleerivad MHC-I molekulid negatiivselt LPS-i poolt käivitatud põletikulisi reaktsioone. Näiteks toodavad MHC-I puudulikkusega hiired rohkem põletikutsütokiine vastusena LPS-ile ning on tundlikumad LPS-i pool põhjustatud letaalsuse suhtes. MHC-I klassi molekulid nõrgendavad LPS-i käivitatud põletikulisi reaktsioone ja kaitsevad hiiri sepsise eest (Xu et al., 2012). Meie tulemused näitasid, et LPS stimuleeris Bl6 hiirte ajus tugevama vastuse MHC-I raja komponentides nii geeni kui valgu tasemel

võrreldes 129Sv hiirtega. Teise artikli tulemused lubavad järeldada, et Bl6 hiirte immunokompetentsus on kõrgem võrreldes 129Sv hiirtega.

Kolmandas artiklis uurisime Bl6 ja 129Sv hiirte vastuvõtlikkust kõrge rasvasisaldusega dieedist põhjustatud metaboolsete häirete tekkele. 129Sv hiirtel põhjustas rasvane toit märkimisväärse kaalutõusu, liikumisaktiivsuse languse ning metaboliitide nihked sarnanesid muutustega, mis on omased inimese metaboolsele sündroomile. Lisaks üldisele liikumisaktiivsuse langusele põhjustas rasvane toit 129Sv hiirtel ka ärevuskäitumist. Rasvase toidu tarbimise järgselt oli 129Sv hiirtel kõrgenenud hargnenud ahelaga aminohapete tase ning langenud atsüülkarnitiinide, glütsiini, spermidiini ja t4-OH-proliini tase. Glütsiini langust ja hargnenud ahelaga aminohapete suurenenud taset on seostatud metaboolse sündroomi ning teise tüübi diabeedi tekkega. Hargnenud ahelaga aminohapete taseme tõusu peamiseks põhjuseks veres on katabolismi pärssimine rasv- ja maksakudedes, mis suunatakse skeletilihastesse, põhjustades rasvhapete akumuleerumist ja insuliiniresistentsust. Atsüülkarnitiinide langus võib peegeldada nende suurenenud kasutust triglütseriidide sünteesiks, mille näol talletatakse energia adipotsüütides rasvatilkadesse. T4-OH-Pro vähenemist on varem seostatud insuliini düsregulatsiooniga (Kenéz et. al., 2018). Kuna proliini hüdroksüülimiseks on vaja askorbiinhapet, on hüdroksüproliini peetud ka oksüdatiivse stressi kaudseks markeriks. Askorbiinhappe puudusest tulenev t4-OH-Pro langus võib põhjustada struktuurselt ebastabiilse kollageeni tootmist. Bl6 hiirtel põhjustas kõrge rasvasisaldusega dieet võrreldes 129Sv hiirtega laialdasemaid muutusi lipiidide profiilis. Vastupidiselt 129Sv hiirtele olid Bl6 hiired kaitstud dieedist põhjustatud kaalutõusu eest ning samuti ei põhjustanud rasvase toidu tarbimine muutusi nende liikumiskäitumises. Kolmanda artikli tulemused lubavad väita, et 129Sv hiireliin pakub paremaid võimalusi psühhiaatriliste häiretega seotud metaboolse sündroomi modelleerimiseks.

Käesoleva uuringu tulemused näitavad, et Bl6 hiired tulevad paremini toime nii põletiku kui kõrge rasvasisaldusega dieedi põhjustatud negatiivsete mõjudega. Seevastu 129Sv hiired on tundlikumad immuunaktivatsioonile ning suurema vastuvõtlikkusega metaboolse sündroomi tekkele, mis on mõlemad psühhiaatriliste häirete olulised tunnused. Kokkuvõttes järeldame, et 129Sv hiired sobivad psühhiaatriliste häiretega seotud endofenotüüpide modelleerimiseks ning nende mudelite edasine uurimine aitab paremini mõista psühhiaatriliste häirete kujunemist ja arengut.

ACKNOWLEDGEMENTS

There are so many to whom I owe immense gratitude. First and foremost, I would like to thank my main supervisor, mentor, academic mother, and dear friend Kersti Lilleväli, who has taught and supported me since the beginning of my academic journey when I was just a "naive student". Without your guidance, I would not be the scientist I am today. I look forward to the opportunity to work with you again on future projects. And thank you for keeping your promise that I would not have to count cells during my PhD studies.

I am sincerely grateful to my patient and enduring supervisor, Dr. Eero Vasar, whose guidance has been invaluable to me. Your leadership skills and ability to see the bigger picture have been invaluable in developing my project and setting it on the right path.

I am immensely grateful to my supervisor, Dr. Mihkel Zilmer, for the interesting conversations and advice throughout this project.

I am very grateful to the reviewers of this thesis, Monika Jürgenson and Martti Laan, for their valuable suggestions and constructive criticism, which helped to improve this thesis.

A heartfelt thanks to the many lab mates who have managed to work alongside me over the years, those who have gone before me, and those who are still going through similar experience.

I owe a great debt of gratitude to my parents, Riina and Andres. Even though I have not always made it easy for them, I appreciate their efforts to give me the best education possible.

And finally, I'm beyond grateful to my partner Kristjan. You are my most enthusiastic cheerleader and my best friend. Thanks for always having my back. Without you, this experience would have been very lonely!

ORIGINAL PUBLICATIONS

CURRICULUM VITAE

Name: Maria Piirsalu
Date of birth: September 28, 1988
Address: Ravila 19, 50411 Tartu, Eesti
E-mail: maria.piirsalu@ut.ee

Academic qualifications:

2016–... University of Tartu, Faculty of Medicine, Neurosciences, PhD
2014–2016 University of Tartu, Faculty of Science and Technology, Genetic engineering, MSc
2011–2014 University of Tartu, Faculty of Science and Technology, Genetic engineering, BSc
2007–2010 EBS High School

Professional experience:

2019–2020 University of Tartu, Faculty of Medicine, Institute of Biomedicine and Translational Medicine, Junior Research Fellow (0,50)

Dissertations supervised:

2021 Johanna Liis Udumets, MSc, "Comparative study of the expression of genes involved in MHC I in different brain structures of 129Sv and Bl6 mice in a lipopolysaccharide-induced neuroinflammatory model"
2020 Helen Paapstel, MSc, "Molecular characterization of glial cells in a neuroinflammatory model of Cx3cr1 GFP/+ mutant mouse line"
2019 Lakshmi Thoondee, BSc, "Molecular characterization of microglial populations in CX3CR1-GFP mutant mouse line in an LPS induced inflammatory model"

Professional self-improvement:

2020 International Symposium "Extracellular Vesicles in Pathophysiology: New advances in the development of diagnostic and therapeutic approaches for treating chronic diseases and cancer", Tartu, Estonia
2019 Dora Pluss short-term mobility financed by the European Regional Development Fund – support to participate in the conference "XIV European Meeting on Glial Cells in Health and Disease", Porto, Portugal
2019 Sony MA900 cell sorter training, Tartu, Estonia
2019 Intensive course "Neuropathology", Tartu, Estonia
2018 Intensive course "Microbiome", Tartu, Estonia
2018 Developmental Biology Minisymposium/Crash Course, Tallinn, Estonia
2018 Doctoral School of Clinical Medicine financial assistance to participate in a joint research project entitled "Adaptive microglial activation and

its association with behavioral changes towards chronic stress in mice", University of Helsinki.

2017 Workshop "Chronic inflammatory diseases: regulation by miRNAs and beyond", Tartu, Estonia

2017 Competence course in laboratory animal science, according to directive 2010/63/EU, Estonian University of Life Sciences

Publications:

Piirsalu, M., Taalberg, E., Jayaram, M., Lilleväli, K., Zilmer, M., & Vasar, E. (2022). Impact of a High-Fat Diet on the Metabolomics Profile of 129S6 and C57BL6 Mouse Strains. *International journal of molecular sciences*, *23*(19), 11682. https://doi.org/10.3390/ijms231911682

Piirsalu, M., Chithanathan, K., Jayaram, M., Visnapuu, T., Lilleväli, K., Zilmer, M., & Vasar, E. (2022). Lipopolysaccharide-Induced Strain-Specific Differences in Neuroinflammation and MHC-I Pathway Regulation in the Brains of Bl6 and 129Sv Mice. *Cells*, *11*(6), 1032. https://doi.org/10.3390/cells11061032

Kaare, M., Mikheim, K., Lilleväli, K., Kilk, K., Jagomäe, T., Leidmaa, E., **Piirsalu, M**., Porosk, R., Singh, K., Reimets, R., Taalberg, E., Schäfer, M. K. E., Plaas, M., Vasar, E., & Philips, M. A. (2021). High-Fat Diet Induces Pre-Diabetes and Distinct Sex-Specific Metabolic Alterations in Negr1-Deficient Mice. *Biomedicines*, *9*(9), 1148. https://doi.org/10.3390/biomedicines9091148

Piirainen, S., Chithanathan, K., Bisht, K., **Piirsalu, M**., Savage, J. C., Tremblay, M. E., & Tian, L. (2021). Microglia contribute to social behavioral adaptation to chronic stress. *Glia*, *69*(10), 2459–2473. https://doi.org/10.1002/glia.24053

Varul, J., Eskla, K. L., **Piirsalu, M**., Innos, J., Philips, M. A., Visnapuu, T., Plaas, M., & Vasar, E. (2021). Dopamine System, NMDA Receptor and EGF Family Expressions in Brain Structures of Bl6 and 129Sv Strains Displaying Different Behavioral Adaptation. *Brain sciences*, *11*(6), 725. https://doi.org/10.3390/brainsci11060725

Piirsalu, M., Taalberg, E., Lilleväli, K., Tian, L., Zilmer, M., & Vasar, E. (2020). Treatment With Lipopolysaccharide Induces Distinct Changes in Metabolite Profile and Body Weight in 129Sv and Bl6 Mouse Strains. *Frontiers in pharmacology*, *11*, 371. https://doi.org/10.3389/fphar.2020.00371

ELULOOKIRJELDUS

Nimi: Maria Piirsalu
Sünniaeg: 28. september 1988
Aadress: Ravila 19, 50411 Tartu, Eesti
E-mail: maria.piirsalu@ut.ee

Hariduskäik:

2016–...	Tartu Ülikool, Meditsiiniteaduste valdkond, Neuroteadused, PhD
2014–2016	Tartu Ülikool, Loodus- ja täppisteaduste valdkond, Geenitehnoloogia, MSc
2011–2014	Tartu Ülikool, Loodus- ja täppisteaduste valdkond, Geenitehnoloogia, BSc
2007–2010	EBS Gümnaasium

Töökogemus:

2019–2020	Tartu Ülikool, Meditsiiniteaduste valdkond, bio- ja siirdemeditsiini instituut, bio- ja siirdemeditsiini nooremteadur (0,50)

Juhendamised:

2021	Johanna Liis Udumets, MSc, "MHC I rajas osalevate geenide ekspressiooni võrdlusuuring 129Sv ja Bl6 hiirte erinevates ajustruktuurides lipopolüsahhariidi poolt indutseeritud neuroinflammatoorses mudelis"
2020	Helen Paapstel, MSc, "Gliia rakkude molekulaarne iseloomustamine neuroinflammatoorses mudelis Cx3cr1GFP/+ mutantses hiireliinis"
2019	Lakshmi Thoondee, BSc, "LPS-i poolt indutseeritud põletikureaktsiooni mõju CX3CR1-GFP mutantse hiireliini mikrogliia populatsioonidele"

Erialane enesetäiendus:

2020	Rahvusvaheline sümpoosium "Extracellular Vesicles in Pathophysiology: New advances in the development of diagnostic and therapeutic approaches for treating chronic diseases and cancer", Tartu, Eesti
2019	Euroopa Regionaalarengu Fondist finantseeritav Dora Pluss lühiajaline õpiränne – toetus osaleda stendiettekandega "XIV European Meeting on Glial Cells in Health and Disease" konverentsil
2019	Sony MA900 rakusorteri kasutamise väljaõpe, Tartu, Eesti
2019	Neuropatoloogia intensiivkursus, Tartu, Eesti
2018	Intensiivkursus "Mikrobioom", Tartu, Eesti
2018	Arengubioloogia minisümpoosium, Tallinn, Eesti
2018	Kliinilise meditsiini doktorikooli toetus välislähetuseks, ASTRA projekt PER ASPERA kaudu – toetus osaleda Helsingi Ülikoolis koostööprojekti "Adaptive microglial activation and its association with behavioral changes towards chronic stress in mice" raames.

2017 Intensiivkursus “Chronic inflammatory diseases: regulation by miRNAs and beyond”, Tartu, Eesti

2017 Katseloomateaduse kursus, vastavalt Euroopa direktiivile 2010/63/EU, Eesti Maaülikool

Teaduspublikatsioonid:

Piirsalu, M., Taalberg, E., Jayaram, M., Lilleväli, K., Zilmer, M., & Vasar, E. (2022). Impact of a High-Fat Diet on the Metabolomics Profile of 129S6 and C57BL6 Mouse Strains. *International journal of molecular sciences*, *23*(19), 11682. https://doi.org/10.3390/ijms231911682

Piirsalu, M., Chithanathan, K., Jayaram, M., Visnapuu, T., Lilleväli, K., Zilmer, M., & Vasar, E. (2022). Lipopolysaccharide-Induced Strain-Specific Differences in Neuroinflammation and MHC-I Pathway Regulation in the Brains of Bl6 and 129Sv Mice. *Cells*, *11*(6), 1032. https://doi.org/10.3390/cells11061032

Kaare, M., Mikheim, K., Lilleväli, K., Kilk, K., Jagomäe, T., Leidmaa, E., **Piirsalu, M**., Porosk, R., Singh, K., Reimets, R., Taalberg, E., Schäfer, M. K. E., Plaas, M., Vasar, E., & Philips, M. A. (2021). High-Fat Diet Induces Pre-Diabetes and Distinct Sex-Specific Metabolic Alterations in Negr1-Deficient Mice. *Biomedicines*, *9*(9), 1148. https://doi.org/10.3390/biomedicines9091148

Piirainen, S., Chithanathan, K., Bisht, K., **Piirsalu, M**., Savage, J. C., Tremblay, M. E., & Tian, L. (2021). Microglia contribute to social behavioral adaptation to chronic stress. *Glia*, *69*(10), 2459–2473. https://doi.org/10.1002/glia.24053

Podrini C., Cambridge E. L., Lelliott C. J., Carragher D. M., Estabel J., Gerdin A.-K., Karp N. A., Scudamore C. L., Ramirez-Solis R., White J. K., and Sanger Mouse Genetics Project (2013). High-fat feeding rapidly induces obesity and lipid derangements in C57BL/6N mice. Mamm Genome 24, 240–251. doi:10.1007/s00335-013-9456-0

Varul, J., Eskla, K. L., **Piirsalu, M**., Innos, J., Philips, M. A., Visnapuu, T., Plaas, M., & Vasar, E. (2021). Dopamine System, NMDA Receptor and EGF Family Expressions in Brain Structures of Bl6 and 129Sv Strains Displaying Different Behavioral Adaptation. *Brain sciences*, *11*(6), 725. https://doi.org/10.3390/brainsci11060725

Piirsalu, M., Taalberg, E., Lilleväli, K., Tian, L., Zilmer, M., & Vasar, E. (2020). Treatment With Lipopolysaccharide Induces Distinct Changes in Metabolite Profile and Body Weight in 129Sv and Bl6 Mouse Strains. *Frontiers in pharmacology*, *11*, 371. https://doi.org/10.3389/fphar.2020.00371

DISSERTATIONES NEUROSCIENTIAE UNIVERSITATIS TARTUENSIS

1. **Sirli Raud.** Cholecystokinin$_2$ receptor deficient mice: changes in function of GABA-ergic system. Tartu, 2005.
2. **Kati Koido.** Single-nucleotide polymorphism profiling of 22 candidate genes in mood and anxiety disorders. Tartu, 2005.
3. **Dzhamilja Safiulina.** The studies of mitochondria in cultured cerebellar granule neurons: characterization of mitochondrial function, volume homeostasis and interaction with neurosteroids. Tartu, 2006.
4. **Tarmo Areda.** Behavioural and neurogenetic study of mechanisms related to cat odour induced anxiety in rodents. Tartu, 2006.
5. **Aleksei Nelovkov.** Behavioural and neurogenetic study of molecular mechanisms involved in regulation of exploratory behaviour in rodents. Tartu, 2006.
6. **Annika Vaarmann**. The studies on cystatin B deficient mice: neurochemical and behavioural alterations in animal model of progressive myoclonus epilepsy of Unverricht-Lundborg type. Tartu, 2007.
7. **Urho Abramov.** Sex and environmental factors determine the behavioural phenotype of mice lacking CCK_2 receptors: implications for the behavioural studies in transgenic lines. Tartu, 2008.
8. **Hendrik Luuk.** Distribution and behavioral effects of WFS1 protein in the central nervous system. Tartu, 2009.
9. **Anne Must.** Studies on molecular genetics of male completed suicide in Estonian population. Tartu, 2009.
10. **Kaido Kurrikoff**. Involvement of cholecystokinin in chronic pain mechanisms and endogenous antinociception. Tartu, 2009.
11. **Anu Aonurm-Helm.** Depression-like phenotype and altered intracellular signalling in neural cell adhesion molecule (NCAM)-deficient mice. Tartu, 2010.
12. **Silva Sütt.** Role of endocannabinoid system and *Wfs1* in regulation of emotional behaviour: behavioural, pharmacological and genetic studies. Tartu, 2010.
13. **Mari-Anne Philips.** Characterization of *Myg1* gene and protein: expression patterns, subcellular localization, gene deficient mouse and functional polymorphisms in human. Tartu, 2010.
14. **Ranno Rätsep.** Genetics of psoriasis and vitiligo, focus on IL10 family cytokines. Tartu, 2010.
15. **Kairit Joost.** Selective screening of metabolic diseases in Estonia: the application of new diagnostic methods. Tartu, 2012, 143 p.
16. **Monika Jürgenson.** A complex phenotype in mice with partial or complete deficiency of the NCAM protein. Tartu, 2012, 117 p.

17. **Ene Reimann.** Description of the cytokines and cutaneous neuroendocrine system in the development of vitiligo. Tartu, 2012, 117 p.
18. **Jürgen Innos.** Behavioural, pharmacological and neurochemical characterisation of limbic system-associated membrane protein (LSAMP) deficient mice. Tartu, 2013, 113 p.
19. **Kaili Anier.** The role of DNA methylation in the development of cocaine-induced behavioural sensitisation. Tartu, 2013, 147 p.
20. **Maarika Liik.** Cognitive functioning, perceived cognition, subjective complaints and symptoms of depression in patients with epilepsy: neuropsychological assessment and spet brain imaging study. Tartu, 2014, 124 p.
21. **Sten Ilmjärv.** Estimating differential expression from multiple indicators. Tartu, 2015, 125 p.
22. **Paula Reemann.** The effects of microenvironment on skin cells. Tartu, 2015, 146 p.
23. **Tanel Visnapuu.** Pharmacological and behavioral characterization of the monoaminergic and GABA-ergic systems of Wfs1-deficient mice. Tartu, 2015, 107 p.
24. **Indrek Heinla.** Behavioural and genetic comparison of B6 and 129Sv mouse lines focusing on the anxiety profile and the expression of *Lsamp* gene. Tartu, 2016, 115 p.
25. **Liina Haring.** Cognitive functioning after first psychotic episode. Tartu, 2017, 146 p.
26. **Triin Tekko.** Neurodevelopmental Approach in the Study of the Function of *Wfs1* and *Lsamp*, Potential Targets in the Regulation of Emotional Behaviour. Tartu, 2018, 194 p.
27. **Alina Altpere.** Targeting of mechanisms of elevated anxiety in female Wfs1-deficient mice. Tartu, 2018, 98 p.
28. **Maarja Toots.** Pharmacological challenge in rodent models of Wolfram syndrome with emphasis on diabetic phenotype. Tartu, 2018, 114 p.
29. **Katyayani Singh.** Neuropsychiatric endophenotypes – focusing on IgLON adhesion molecules in the mouse brain. Tartu, 2019, 148 p.
30. **Kattri-Liis Eskla.** Therapeutic strategies for ischemia reperfusion injury. Tartu, 2019, 138 p.
31. **Hardo Lilleväli**. Hyperphenylalaninaemias and neurophysiological disorders associated with the condition. Tartu, 2020, 134 p.
32. **Roman Balõtšev**. Interaction between the immune and metabolic systems in different stages of schizophrenia spectrum disorders. Tartu, 2020, 164 p.
33. **Mari Urb**. DNA methylation in the predisposition, expression and abstinence of cocaine addiction. Tartu, 2020, 147 p.
34. **Liisa Leppik.** Alterations in metabolomic profile of lipids, amino acids and biogenic amines in the early course of schizophrenia spectrum disorders. Tartu, 2021, 173 p.
35. **Kadri Seppa.** The neuroprotective effect of GLP-1 receptor agonist liraglutide in a rat model of Wolfram syndrome. Tartu, 2021, 154 p.

36. **Akbar Zeb.** The novel mechanisms of Parkin-dependent mitophagy. Tartu, 2022, 146 p.
37. **Aleksandr Bregin.** Alterations of emotional behaviour induced by the genetic invalidation of the limbic system associated membrane protein (Lsamp) – potential implications for neuropsychiatric disorders. Tartu, 2022, 176 p.
38. **Jane Varul.** Different stress coping strategies of 129Sv and C57/Bl6 mouse strains – evidence from behavioural, pharmacological, metabolomics and gene expression studies. Tartu, 2022, 177 p.
39. **Maria Kaare.** The involvement of NEGR1 and LSAMP in the psychiatric disorders are mediated through monoaminergic neurotransmission and changes in the systemic metabolism. Tartu, 2023, 164 p.